2019-04-25

Novel Nanocomposites for the Treatment of Antibiotic-Resistant Bacteria in Water – Antibacterial Effects and Mechanisms

Soyoung Baek
University of Miami, bbangtacu@gmail.com

UNIVERSITY OF MIAMI

NOVEL NANOCOMPOSITES FOR THE TREATMENT OF ANTIBIOTIC-RESISTANT BACTERIA IN WATER – ANTIBACTERIAL EFFECTS AND MECHANISMS

By

Soyoung Baek

A DISSERTATION

Submitted to the Faculty

of the University of Miami

in partial fulfillment of the requirements for

the degree of Doctor of Philosophy

Coral Gables, Florida

May 2019

UNIVERSITY OF MIAMI

A dissertation submitted in partial fulfillment of
the requirements for the degree of
Doctor of Philosophy

NOVEL NANOCOMPOSITES FOR THE TREATMENT OF ANTIBIOTIC-RESISTANT BACTERIA IN WATER – ANTIBACTERIAL EFFECTS AND MECHANISMS

Soyoung Baek

Approved:

_____ Sung Hee Joo, Ph.D. Assistant Professor of Environmental Engineering	_____ James Douglas Englehardt, Ph.D. Professor of Environmental Engineering
_____ Helena Solo-Gabriele, Ph.D. Professor of Environmental Engineering	_____ Guillermo Prado, Ph.D. Dean of the Graduate School

_____
Naresh Kumar, Ph.D.
Associate Professor of Public Health

BAEK, SOYOUNG (Ph.D., Civil Engineering)
Novel Nanocomposites for the Treatment of Antibiotic-Resistant Bacteria in Water – Antibacterial Effects and Mechanisms (May 2019)

Abstract of a dissertation at the University of Miami.

Dissertation supervised by Professor Sung Hee Joo.
No. of pages in text. (179)

Recently, the presence of antibiotic-resistant bacteria in water is a major concern worldwide due to its adverse health effects. Conventional disinfection technologies, such as ultraviolet, ozone, and chlorine disinfection are currently used to inactivate antibiotic-resistant bacteria in water. Conventional disinfection technologies not only produce byproducts but also selectively promote the survival of antibiotic-resistant bacteria. Nanoparticles (NPs), even in a small amounts, have potential benefits as novel materials in terms of inactivating pathogenic bacteria due to their strong antibacterial effect. However, because of issues pertaining to leaching, mobility, and the cost of NPs, their applications for water treatment have not been pursued earlier. Therefore, this study seeks to understand the development of NPs for water treatment applications by using alginate coating to encapsulate NPs.

To study the development of NP-alginate beads, the antibacterial properties and toxicity mechanisms of different types of NPs (i.e., Industrial NPs, NPs derived from consumer products, and nanohybrids) were investigated on antibiotic-resistant bacteria (i.e., *E. coli* and *P. aeruginosa*). The study showed that the large surface area and dispersion of NPs enhanced the effect of antibacterial properties. ROS (reactive oxygen species)

produced by NPs was the primary mechanism for inactivating the antibiotic-resistant bacteria.

Based on the results of the effects of antibacterial properties and the mechanisms of NPs, novel nanocomposites for the removal of antibiotic-resistant bacteria in water were synthesized by encapsulating NPs in alginate-beads. NP-alginate beads were designed to prevent NP's leaching into the water, and to promote the antibacterial properties of NPs through dispersion and increased surface areas. The results showed that the NP-alginate beads inactivated up to 99.1% of antibiotic-resistant bacteria and the bacterial inactivation increased with the increasing dose of NPs.

In the current study, these NPs-alginate beads revealed efficacy with no by-product formed and proved cost-effective with just a small amount of NPs and are reusable in the treatment of antibiotic-resistant bacteria in water. Therefore, the alginate nanocomposites can be deemed as potential antimicrobial agents for water disinfection, and offer a new opportunity for a large-scale production for point-of-use treatment.

ACKNOWLEDGMENT

I would like to express my sincere gratitude to my advisor, Dr. Sung Hee Joo. Along with her professional guidance, charismatic mentorship, and endless support, her dedication has been instrumental in achieving my goals. Thank you for everything you provided during my entire Ph.D. period.

I would like to acknowledge my committee members, Dr. James Englehardt, Dr. Helena Solo-Gabriele, and Dr. Naresh Kumar for providing their valuable suggestions and individual efforts in helping me through this process. It has been a true pleasure to work with these terrific mentors. Dr. Pat Blackwelder and Dr. Michal Toborek also provided significant guidance and support during the development of this dissertation.

I am indebted to Dr. Chunming Su at U.S. EPA for BET surface areas analysis, Dr. Joshua Cohn at UM Physics Department for XRD analysis, Dr. Minseo Park and Mr. Min Khanal at Auburn University for Raman spectroscopy analysis, Dr. Suraneni Prannoy and Mr. Sivakumar Ramanathan for TGA analysis, and Dr. Pat Blackwelder at UM Rosenstiel School of Marine & Atmospheric Science for her assistance on SEM and TEM image analysis. This research was supported by the U.S. Environmental Protection Agency through the Office of Research and Development (Award: EP 17Z000237) and the National Center for Environmental Research Award Program (Award: SU839293).

I must also thank all my colleagues for their constant support, encouragement, and good friendship throughout my graduate career. They have truly made my time an enjoyable and memorable one in the lab.

Most importantly, I am profoundly grateful to my parents, who have been a constant source of love, support, and encouragement at all times for longer than I can remember. I can't thank you enough for encouraging me throughout this experience. Lastly, I thank my God, my good Father, for letting me through all the difficulties. I have experienced Your guidance day by day. You are the one who let me finish my degree. Thank you, Lord.

TABLE OF CONTENTS

LIST OF FIGURES

LIST OF TABLES

LIST OF ABBREVIATIONS

CNT - Carbon nanotube

CMC - Carboxymethyl cellulose

DLS - Dynamic light scattering

E. coli - *Escherichia coli*

EDS - Energy-Dispersive X-ray Spectroscopy

FT-IR - Fourier-transform infrared spectroscopy

GO - Graphene oxdie

NHs - Nanohybrids

NPs - Nanoparticles

P.aeruginosa - *Pseudomonas aeruginosa*

PVP - Polyvinylpyrrolidone

ROS - Reactive oxygen species

SEM - Scanning Electron Microscope

SiO_2 - Silica dioxide

TEM - Transmission Electron Microscope

TGA - Thermogravimetric analysis

TiO_2 - Titanium dioxide

T.pseudonana - *Thalassiosira pseudonana*

XRD - X-Ray Diffraction

ZnO - Zinc oxide

PUBLICATIONS

The following is a list of papers arising from this Ph.D. dissertation.

Journals

Baek, S., Joo, S. H., Blackwelder, P., Toborek, M. (2018) Effects of coating materials on antibacterial properties of industrial and sunscreen-derived titanium-dioxide nanoparticles on Escherichia coli. *Chemosphere*. 208 pp.196-206

Baek, S., Joo, S.H., Kumar, N., Toborek, M. (2017) Antibacterial effect and toxicity pathways of industrial and sunscreen ZnO nanoparticles on Escherichia coli. *Journal of Environmental Chemical Engineering*, 5 (3) p. 3024-3032

Baek, S., Joo, S. H., Toborek, M. (2018) Novel treatment of antibiotic-resistant bacteria by encapsulation of ZnO nanoparticles in an alginate biopolymer: Insights into treatment mechanisms. *Journal of Hazardous Materials*. (under review)

Baek, S., Joo, S. H., Su, C., Toborek, M. (2018) Antibacterial effects of graphene- and carbon-nanotube-based nanohybrids on Escherichia coli: implications for treating multidrug-resistant bacteria in water. *Journal of Environmental Management.* (under review)

Baek, S., Joo, S. H., Su, C., Toborek, M. (2018) In-vitro toxicity evaluation of ZnO/TiO_2-conjugated carbon nanotubes/graphene oxidebased nanohybrids on a Thalassiosira pseudonana marine diatom. *Ecotoxicology and Environmental Safety* **(**under review)

CHAPTER 1: INTRODUCTION

1.1.Study motivation and hypothesis

Recently, antibiotic-resistant bacteria, otherwise known as superbugs, have been detected in drinking water (Ahmed, Zhou et al. 2015). Antibiotic-resistant bacteria are known to cause severe illness and can easily infect populations; they are responsible for at least 2 million infections and 23,000 deaths each year in the U.S (CDC 2013). Generally, chlorine, UV, and the ozone process are commonly used to deactivate pathogenic microorganisms including antibiotic-resistant bacteria in water (Zheng, Su et al. 2017). Although disinfection processes such as chlorine, UV, and ozone are commonly used to inactivate harmful bacteria in water treatment facilities, they have limited effectiveness for the removal of superbugs (Rizzo, Manaia et al. 2013, Lupan, Carpa et al. 2017), since they require high treatment expenses and doses to inactivate superbugs (Johnson 2010, Öncü, Menceloğlu et al. 2011).

Chlorination is ineffective for some highly resistant waterborne pathogens, and also has a tendency to form carcinogenic disinfection by-products (DBPs) when chlorine is added to water (Dimapilis, 2018). Because some of water-borne bacteria have increased their resistance to available disinfectants, this leads to higher required disinfectant doses, and hence the formation of higher amounts of DBPs. Although fewer by-products are formed by ozonation, it cost more than chemical disinfection and can form the harmful bromate when ozone reacts with bromide ions in water. Chemical disinfectants commonly used by the water industry such as free chlorine, chloramines and ozone can react with various constituents in natural water to form DBPs, many of which are carcinogens. More than 600 DBPs have been reported in the literature (Krasner, 2006). Considering the mechanisms of DBP formation, it has been predicted that DBPs will be formed any time

chemical oxidants are used in water treatment. Like ozone treatment, UV treatment does not leave residue in treated water, hence, it offers no protection against re-infection in the distribution network. It is also reported that chlorine used in water and sewage can selectively promote the survival of antibiotic-resistant bacteria (Shrivastava, Upreti et al. 2004). For instance, sewage treatment facilities using chlorine may have the unintended consequences of encouraging the formation of other antibiotics in the discharged water drinking water, by selectively supporting the survival of antibiotic-resistant bacteria. Since the problem of antibiotic-resistance in water is being worsened worldwide, and superbugs have been found in water treatment plants (Ahmed, Zhou et al. 2015). Therefore, to provide safe and clean water, it is imperative to develop alternative treatment that can deal with antibiotic-resistant bacteria.

Nanotechnology is an emerging field of research, specifically in terms of developing novel materials for the removal of bacteria from water systems (Biswas and Bandyopadhyaya 2016, Kanakaraju, Ravichandar et al. 2017). Due to their high surface area to volume ratio and high reactivity, NPs contribute the antibacterial effect of NPs on microorganisms. In order to support the bacterial removal, several antibacterial mechanisms of NPs have been proposed, either through direct contact or internalization in cells. NPs cause their sequential deformation, rupture, and penetration into the cell (Kumar, Pandey et al. 2011), generate the reactive oxygen species (ROS), and release electrons (Srivastava and Kumar 2016). Considering these unique antibacterial properties of NPs, they could be used as a material to remove bacteria.

However, despite the numerous benefits associated with the use of NPs for water treatment purposes, the applications of NPs for the removal of antibiotic-resistant bacteria

have not been understood well due to leaching issue and mobilization of NPs in water suspension (Li, Xu et al. 2009). Recently, the use of polymeric material such as alginate and chitosan have been used as a host for encapsulation of NPs (Venkatesan, Lee et al. 2017), so that an encapsulation of NPs in alginate gel can immobilize NPs and prevent leaching issue. Some of the literature on nanocomposite alginate beads have shown that alginate nanocomposites are effective for the inactivation of bacteria by utilizing antibacterial properties of nanomaterials (Motshekga, Sinha Ray et al. 2018, Salama, Diab et al. 2018). However, the antibacterial effects of NPs and their mechanisms can be different according to particle size, solution pH, ionic strength, and presence of coating material. To develop NPs as materials which are optimized for inactivation bacteria in water, the toxicity properties of NPs and their antibacterial effects on biological systems should be well-known. For example, NPs derived from commercial product may be different from industrial-grade NPs because NPs derived from consumer products are commonly coated with a polymer or other NPs to enhance their surface area. Therefore, the antibacterial properties and toxicity mechanisms of different types of NPs (i.e., Industrial NPs, NPs derived from consumer products, and nanohybrids) should be investigated on antibiotic-resistant bacteria for their applications in water.

This hypothesis of this study is that the antibacterial properties of NPs contribute to treating antibiotic-resistant bacteria in water. Therefore, based on the antibacterial study of NPs and their antibacterial mechanisms on bacteria, the application of NPs for the treatment of antibiotic-resistant bacteria were developed and examined the effectiveness of the removal of bacterial from water.

1.2. Objectives and scope

Therefore, this study pursues the following aims:

To investigate the antibacterial effects and toxicity mechanisms of NPs, and develop nanocomposite-alginate beads for the removal of antibiotic-resistant bacteria in water.

This study will: a) investigate the antibacterial effect and toxicity mechanisms of different types of NPs (i.e., Industrial NPs, NPs derived from consumer products, and nanohybrids) and b) examine the effect of surface coating materials on antibacterial properties of NPs.

Based on the findings a & b, this study also aims to c) develop the application of NPs by using alginate beads to encapsulate NPs and d) examine the effects of synthesized nanocomposites-alginate beads on antibiotic-resistant bacteria and compare it with conventional chlorine treatment (byproduct, cost, and treatment efficiency).

CHAPTER 2: LITERATURE REVIEW

2.1. Industrial and Consumer product derived nanoparticles

Nanoparticles (NPs) are particles between 1 and 100 nanometers in size with a surrounding interfacial layer, which is fundamentally affecting all of its properties (Auffan, Rose et al. 2009). NPs have a greater surface area than larger particles, which causes them to be more reactive to some other molecules. It also means that when a given volume of material is made up of smaller particles, the surface area of the material increases. Therefore, as particle size decreases, a greater proportion of the particles are found at the surface of the material. Due to their unique physical properties, NPs are increasingly utilized in many fields, such as: medicine, manufacturing, materials, electronics, and environmental uses. The most prominent application of nanotechnology is in consumer products, such as: cosmetics, food packaging, and nano-foods (Mottier, Mouchet et al. 2017). For example, the use of NPs such as zinc oxide (ZnO) or titanium dioxide (TiO_2) in sunscreens provide enhanced UV protection because they reflect and scatter the UV radiation efficiently. Among NPs, zinc oxide (ZnO) NP is one of the most widely used NPs in consumer products. 70% of the annual global production of ZnO NPs is used in cosmetics, and the remaining 30% in paints and other materials (Piccinno, Gottschalk et al. 2012). TiO_2 NPs are also mainly used in personal-care products, coatings, cleaning agents, and paints, producing around 10,000 tons of TiO_2 NPs per year globally (Piccinno, Gottschalk et al. 2012, Weir, Westerhoff et al. 2012). Thus, both NPs are known to have antimicrobial effects because the photoactivity of NPs are promoting reactive oxygen species (ROS) under UV light, due to their wide band gap energy and electronic properties (Hariharan 2006, Baker, Tyler et al. 2014).

Recently, such wide and increasing NP production raises concerns regarding potential toxicity to living organisms through cell damages or ROS through photocatalytic mechanisms (Jeon, Kim et al. 2016, Leung, Xu et al. 2016). Emerging literature shows that the increasing use of NPs and their accumulation pose threats to public health and the environment (Weir, Westerhoff et al. 2012). The research studies the toxic properties of industrial NPs, such as ZnO, and TiO_2 NPs on bacteria cells (Liu, Liu et al. 2011, Ramani, Ponnusamy et al. 2013, Sodano, Gorgitano et al. 2016). A study found that a significant amount of NPs from sunscreen products can be released into the swimming water, and reactive oxygen species generated from NPs were present in public pools (Jeon, Kim et al. 2016). Jiang et al. reported that industrial ZnO NPs have strong antibacterial effects against *E. coli*, implicating the ROS generation in NPs played an important role in the antibacterial properties of NPs (Jiang, Zhang et al. 2016). Lin et al. investigated the antibacterial properties of industrial TiO_2 NPs to *E.coli* according to the particle size, and the antibacterial effects of TiO_2 NPs increased as the particle size decreased (Lin 2014). However, the toxicity levels and toxicity mechanisms of NPs from consumer products containing NPs are not fully understood.

2.1.1. Metal oxide nanoparticles and nanohybrids

Metal oxide NPs

Metal oxide NPs can be composed of a variety of diverse materials, including: titanium, zinc, cerium, silver, gold, silica, aluminum, and iron oxide. Among a number of metal oxide NPs, the OECD is interested in ZnO and TiO_2 NPs, as they are commonly used and their inherent properties (Baker, Tyler et al. 2014). These metal-based NPs are used for antimicrobial applications. The metal elements can have various properties, including:

metallic reactivity, semiconductor or catalysts depending on its size, shape, and coating. They can exhibit unique physical and chemical properties according to the metal elements that form different compounds. According to the literature, the global production quantity of ZnO NPs was estimated between 101-10,000 tons per year, and the production of TiO_2 NPs was higher than 10,000 tons (Piccinno, Gottschalk et al. 2012). The tiny size and high surface-to-volume ratio are the unique physical and chemical properties of nanomaterials that determine nanomaterial-induced toxicity. The size of NPs has a storing effect on their reactivity and NP size influences their interactions with microorganisms (Park, Bae et al. 2013, Shang 2014). Because of the tiny size of nanomaterials, they can easily penetrate cell membranes (Baek, Joo et al. 2018). The amount of cellular uptake decreases with the increase in particle size. Park et al (Park, Bae et al. 2013) demonstrated that particle size was a critical determinant of the intracellular distribution of silica and its induced ROS formation. Moreover, antibacterial or toxic effects increases as the size of NPs decrease.

Nanohybrids (metal oxide and carbon-based NPs)

Given the increasing production of nanomaterials of all types, the potential release of combined nanocomposites in the environment and theirs effects on the ecosystem are becoming a concern that needs to be addressed. Recently, the synthesis of two nanocomposites has been extensively studied to investigate more highly reactive photolysis. These studies show that combined nanocomposites provide not only a large surface area, but they also increase photo catalyst (Huang, Zang et al. 2014). When metal oxide NPs are combined with carbon-based NPs, these synthesized nanohybrids induce the dispersion of metal NPs and allow greater photocatlytic activity (Liu, Hu et al. 2012, Huang, Wang et al. 2015). Therefore, carbon-based NPs, such as graphene and carbon

nanotubes are combined with metal oxide NPs to enhance their physical and chemical properties in various fields, such as: energy storage, batteries, and biomedical applications (Hu, Huang et al. 2012, Stengl, Bakardjieva et al. 2013, Nosrati, Olad et al. 2017). Many researchers confirmed the enhanced photocatalytic properties of nanohybrids. Wang et al reported that the synthesis of ZnO NPs with GO nanomaterials enhances the antibacterial effect toward bacterial cells, due to its increased photocatalytic activity (Wang, Cao et al. 2014). Sui et al evaluated the antibacterial ability of synthesized ZnO-CNT (Sui, Zhang et al. 2013). Olad &Shakoori reported that the synthesis of TiO_2 and GO showed high photocatalytic activity under visible light (Nosrati, Olad et al. 2017). Zhang et al reported that the enhanced adsorption property of ZnO-GO composites causes electron transfer between ZnO and GO, and this electron transfer suppresses the recombination of electron-hole pairs (Chen, Zhang et al. 2013). The developments of nanohybrids have attracted interest about the toxicity of nanocomposites consisted of two different types of NPs, due not only to their potential applications, but also to the industrial effluents which can impact microorganisms in the environment. However, there has been insufficient studies regarding synthesized nanocomposites for their antibacterial effect and their toxicity mechanism.

2.2. The effects of coating materials on NPs

Properties of NPs derived from consumer products may be different from industrial grade NPs because NPs used for consumer products are often coated with stabilizers to prevent aggregation (Labille, Feng et al. 2010, Lewicka, Benedetto et al. 2011, Smijs and Pavel 2011, Jeon, Kim et al. 2016). NPs have a strong tendency to aggregate together compared to submicrometer particles due to their large surface area. This can be explained

by the DLVO aggregation theory (The DLVO theory is named after Derjaguin, Landau, Verwey, and Overbeek), as illustrated in Figure 2.1.

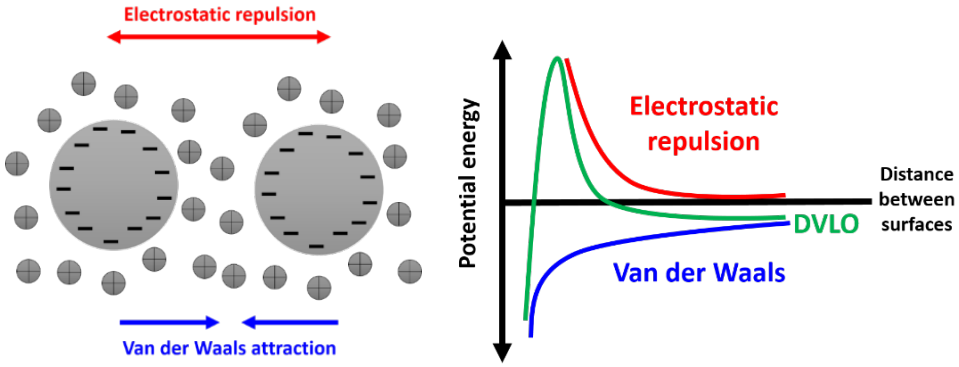

Figure 2.1. The DLVO theory of nanoparticle aggregation

The agglomeration is generally due to the Van der Waals attraction forces between NPs which can be counterbalanced by electrostatic and steric stabilization. Electrostatic repulsion can be achieved by the addition of charge to the NPs so that they can repel each other. Steric stabilization can be achieved by the adsorption of a thin layer of polymer onto the NPs surface to physically prevent the NPs from coming close enough to each other and cause agglomeration.

Generally speaking, the combination of both electrostatic and steric stabilization is termed electrosteric stabilization and can be achieved using polyelectrolytes (Li 2011, Othman, Abdul Rashid et al. 2012). Adsorption of polymer coating materials onto NPs can affect surface charge. Therefore, electrosteric stabilization can be achieved. Figure 2.2 illustrates NPs in absence and presence of coating materials. When the particles have same volume, NPs without coating materials have one large particle due to aggregation. However, NPs exposed to coating materials have several small particles with a higher surface area by dispersion each other. Coating materials play as stabilizers in NPs

suspension and aggregation is prevented by electrosteric repulsion so that surface area of NPs increases as their NPs size in suspension decreases (Dalai, Pakrashi et al. 2012).

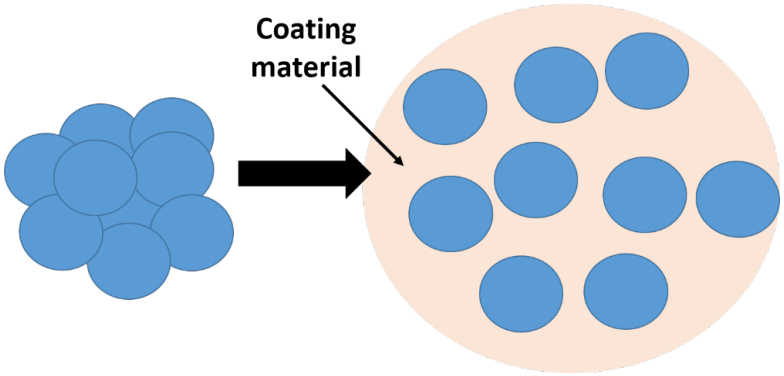

Figure 2.2. NPs in absence (left) and presence (right) of coating materials

Among organic coating materials, CMC (carboxy methyl cellouse) and PVP (polyvinylpyrrolidone, a neutrally charged polymeric coating material) are commonly used as coating materials of NPs in various consumer products such as food and personal-care products (Dalai, Pakrashi et al. 2012, Wang and Fan 2014). Stabilizers such as CMC and PVP have been found to modify the physicochemical properties of NPs, thereby affecting particle stability and mobility by electrosteric repulsion (Jafry, Liga et al. 2011, Dalai, Pakrashi et al. 2012). Among inorganic coating materials, silica (SiO_2) NPs are also one of the widely used coating materials in various commercial products to improve the surface area and photocatalytic activity of NPs (Nur 2006, Jafry, Liga et al. 2011). These coating components may interact with NPs, thereby changing their surface charge and mobility and affecting the interaction of NPs with organisms (Batley 2012).

The way coating materials affect NPs is reviewed as follows. Zhang et al. (2009) carried out an experiment investigating the stability of NPs, according to the addition of natural organic matters (NOM) and divalent cations, and the results showed that

aggregation of NPs, as the electrolyte concentration increased (Zhang, Chen et al. 2009, Li 2010). French et al. (2009) also reported that the addition of NOM induced the negative charge on the surface of NPs, consequently the NPs aggregation was reduced (French 2009, Zhang, Chen et al. 2009). Since the smaller size leads to increased surface area, NPs dispersed by coating materials may enhance the toxic effects by NPs dissolution in suspension or ROS generation. In addition, smaller size NPs by the effect of coating materials may be able to penetrate to cell membrane, which can cause cell damage or death.

2.3. Antibacterial effects of nanoparticles on antibiotic-resistant bacteria

Bacteria—as a fundamental component for ecological balance and a key factor of the bioaccumulation of NPs—have been used for many toxicological studies of NPs (Li, Lin et al. 2013). Recently, issues with antibiotic-resistant superbugs or disease-causing pathogens present in water systems have been reported (Zhu, Chang et al. 2010, Ma, Williams et al. 2013). Thus, the problem of antibiotic resistance in water is being heightened worldwide, and superbugs have been found in water treatment plants (Ahmed, Zhou et al. 2015). With the growing use of NPs, there has been an increasing interest in their antibacterial effects (Hajipour, Fromm et al. 2012). The use of nanomaterials (e.g., TiO_2, silver nanoparticles, carbon nanotubes) as antimicrobial disinfectants has shown high effectiveness, due to their large surface area and their enhanced chemical-biological characteristics. Toxicity mechanisms of NPs are determined differently according to whether or what extent they exhibit a biological response when interacting with cells and will also depend on the physicochemical characteristics of the NPs (such as the size, nature and chemical stability, surface coating, etc). There are three main antibacterial mechanisms of NPs on microorganisms as illustrated in Figure 2.3.

First, NPs themselves may be toxic. Direct contact or interaction with NPs can cause bacterial membrane damage and deformation of cells (Kiwi and Nadtochenko 2005, Romero-Vargas Castrillón, Perreault et al. 2015). When particles enter the bacterial cell, they attack the respiratory chain by interacting with essential enzymes that leads to bacterial inactivation. Compared to micro-particles, NPs interact with organisms much more easily.

Secondly, the toxicity mechanism of metal oxide NPs is their release of ions. Antibacterial effect of the metal oxide NPs in aqueous media is influenced by the amount of free metal ions in the suspensions and the antibacterial levels of free metal ions. The amount of free metal ions in the NPs suspensions may induce toxicity, but its mechanism is still not clear (Song, Zhang et al. 2010).

Lastly, NPs are generating reactive oxygen species (ROS), such as superoxide and peroxide, which contain oxygen showing chemical reactions (Fu, Hamzeh et al. 2015). Oxidative stress is one of the major causes of toxicity, due to interaction with cell structures. ROS from NPs could react directly with DNA and proteins, or could react with lipids (Li, Niu et al. 2014).

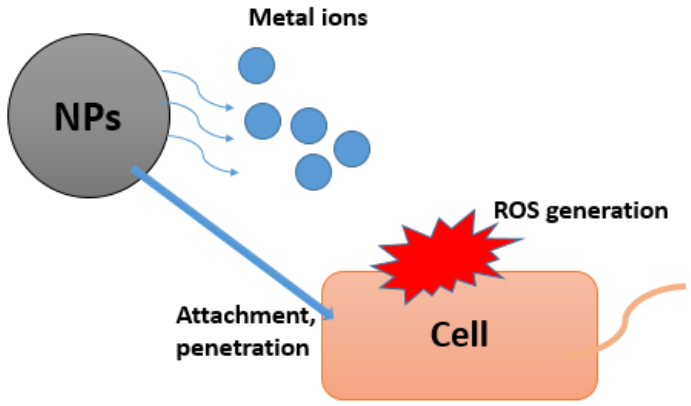

Figure 2.3. Toxicity mechanism of NPs on bacteria cells (Physical attachment, penetration / Release of metal ions / ROS generation)

2.4. Toxicity mechanisms

Nanomaterials (NMs) of varying chemical composition such as metal oxides and carbon-based NMs have been shown to induce oxidative stress (Baun, Hartmann et al. 2008). The key factors involved in NP-induced ROS include active redox cycling on the surface of NP due to transition of metal-based NP. The generation of reactive oxygen species (ROS), including superoxide anion ($O_2^{\cdot -}$), hydrogen peroxide (H_2O_2), peroxide (O_2^{2-}), hydroxyl radical ($\cdot OH$), and hydroxyl ion (OH^-), is the predominant mechanism leading to toxicity in cells, including DNA damage and cell motility (Metzler, Li et al. 2011). These excess radical productions from the surface of NPs induce an inflammatory process in the cells, affecting membrane lipids and altering the structure of DNA that could lead to cell death. Mechanisms of ROS generations are processed by electron transport in NPs. As illustrated in Figure 2.4, light energy absorption induces charge separation and excites electrons from the valence band to the conduction band. As excited electrons move

to the conduction band, holes are left in the valence band. (Qi, Cheng et al. 2017). Then, the photo-generated electrons and holes are reactive at the surface of NPs to facilitate reduction and oxidation reactions that generate ROS, including superoxide anion and hydroxyl radical. Then, ROS emerging on the photocatalytic surfaces attack infectious agents such as viruses and bacteria.

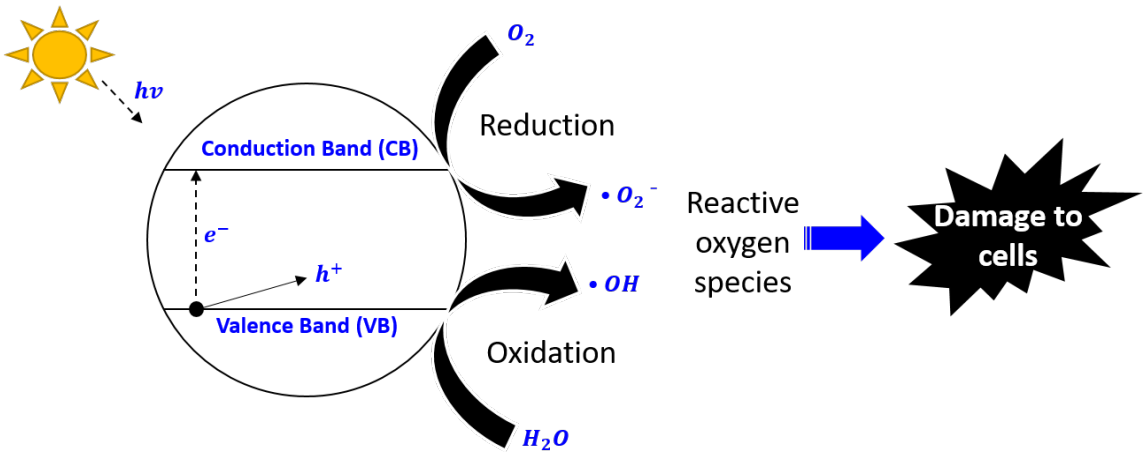

Figure 2.4. Schematic of ROS generation of metal oxide nanoparticles

For instance, ROS (e.g., H_2O_2, $^{\bullet}OH$, $O_2^{\bullet-}$) in metal oxide NPs suspensions are formed through the following processes (Sharma, Anderson et al. 2012, Dasari, Pathakoti et al. 2013):

$$ZnO\ /\ TiO_2\ NPs \rightarrow O_2 \quad (1)$$

$$O_2 + e^- \rightarrow O_2^{\bullet-} \quad (2)$$

$$O_2^{\bullet-} + H_2O \rightarrow {}^{\bullet}HO_2 + OH^- \quad (3)$$

$${}^{\bullet}HO_2 + {}^{\bullet}HO_2 \rightarrow H_2O_2 + O_2 \quad (4)$$

$$H_2O_2 + O_2^{\bullet-} \rightarrow O_2 + {}^{\bullet}OH + OH^- \quad (5)$$

As a result of the TiO_2 NPs or ZnO NPs excited by energy, the electrons and holes react with adjacent molecules (O_2, H_2O, OH^-), generation the formation of ROS ($O_2^{\bullet-}$,$^{\bullet}OH$, H_2O_2)

Photo-catalysis of metal oxide NPs (e.g., ZnO and TiO_2) depends upon the energy of incident photons, because they require a light or ultraviolet (UV) source to excite the surface. For instance, ZnO is a semiconductor with band gap energy of 3.37 eV, corresponding to a wavelength of 368 nm (Ma, Wallis et al. 2014). A photon with energy greater than 3.37 eV (wavelength less than 368 nm) has the potential to photoactivate the material and promote generation of ROS. Studies with bacteria have demonstrated that toxicity of ZnO NPs is substantially enhanced when natural sunlight is present due to photo-induced ROS generation (Adams, Lyon et al. 2006, Lipovsky 2009). For example, ROS generation of ZnO NPs was increased three fold in the presence of natural sunlight as compared to regular laboratory light or darkness. Similarly, the antibacterial activity of TiO_2 was also greater in the presence of light than in the dark (Adams, Lyon et al. 2006). These results indicate that ROS generation under sunlight or UV has great implications for the antibacterial effect on microorganisms in environment. However, it is reported that under ordinary room light with a total light intensity of 10 $\mu W/cm^{-2}$, the intensity of UV light, which is $\sim$1 $\mu W/cm^{-2}$, is sufficient to induce ROS in TiO_2 NPs (Fujishima 2000). Thus, a study (Lipovsky 2009) examined the amount of hydroxyl radicals formed from ZnO NPs suspensions as a function of wavelength of illumination. The level of oxy radicals was found to increase considerably when the suspension was irradiated with visible light at the range of 400-500 nm.

ROS generation of NPs is also related to size because smaller size induces high surface area and high surface reactivity of NPs, leading to the production of higher ROS generation (Angélique Simon-Deckers 2009, Raghupathi, Koodali et al. 2011, Shang 2014, François Perreault 2015). Previous studies have documented that smaller particle size promotes more photocatalytic activity of NPs, and increased ROS causes disorder in the cell membrane or cell death (Maness 1999, Adams, Lyon et al. 2006, Alrousan, Dunlop et al. 2009, Zhu, Chang et al. 2010, Love, Maurer-Jones et al. 2012, Leung, Xu et al. 2016). However, some studies have shown that size is not only the most influential factor of their toxicity, but toxicity is also affected by other factors such as: coating materials, shape, water chemistry, and existence of other NPs (Othman, Abdul Rashid et al. 2012, Lin, Li et al. 2014, Nosrati, Olad et al. 2017).

CHAPTER 3:

ANTIBACTERIAL EFFECTS OF NANOPARTICLES ON BACTERIA AND THEIR TOXICITY MECHANISMS[1]

[1] Baek, S., Joo, S.H., Kumar, N., Toborek, M. (2017) Antibacterial effect and toxicity pathways of industrial and sunscreen ZnO nanoparticles on Escherichia coli. *Journal of Environmental Chemical Engineering*, 5 (3) p. 3024-3032

3.1. Background

Nanoparticles (NPs) that possess versatile physicochemical properties have been advancing the frontiers of science, technology, medicine, and consumer products (Petros and DeSimone 2010, Espitia, Soares et al. 2012). Therefore, their production and consumption, especially in consumer products, are likely to increase significantly in future. Among NPs, zinc oxide (ZnO) NPs are the most widely used in consumer products. Their annual global production is 101-1,000 tons, about 70% of which are used in cosmetics and the remaining 30% in paints (Piccinno, Gottschalk et al. 2012). ZnO NPs are found in sunscreens and cosmetics because of their unique properties, including protection against UV rays, antimicrobial effects, and photoactivity by promoting reactive oxygen species (ROS) generation under UV light due to their wide band gap energy (3.2 eV) and electronic properties (Hariharan 2006, Baker, Tyler et al. 2014). Emerging literature shows that the increasing use of NPs and their accumulation pose threats to public health and the environment. Therefore, increasing interest has resulted in better comprehension on the toxicity of NPs (Kanel and Al-Abed 2011, Planchon, Ferrari et al. 2013, Arakha, Pal et al. 2015). NPs undergo change through their interaction with different environmental conditions. For instance, a study (Wang, Lin et al. 2016) showed that environmental conditions such as pH, ionic strength, and temperature values influence the surface area, charge, composition, shape, and morphology of ZnO NPs (Li, Zhu et al. 2011). Given these changes, the toxicity of NPs can vary with respect to their types, test organism species, and culture media Bacteria—as a fundamental component for ecological balance and a key factor of the bioaccumulation of NPs—have been used for many toxicological studies of NPs (Li, Lin et al. 2013). Recently, issues with antibiotic-resistant superbugs or disease-

causing pathogens present in water systems have been reported (Zhu, Chang et al. 2010, Ma, Williams et al. 2013), which could contribute to a deformation of the impact of NPs. Due to the toxicity of NPs, their interaction with microorganisms is a key factor in biomass decomposition and waste treatment systems (Li 2014).

With the growing use of NPs, there has been an increasing interest in their antibacterial effects(Hajipour, Fromm et al. 2012, Jiang, Zhang et al. 2016, Sarwar, Chakraborti et al. 2016). The use of nanomaterials (e.g., TiO2, silver nanoparticles, carbon nanotubes) as antimicrobial disinfectants has shown high effectiveness due to their large surface area and their enhanced chemical-biological reactivity (Kumar and Raza 2008, Bao, Zhang et al. 2011, Jung, Hwang et al. 2011, Nangmenyi, Li et al. 2011, Lee, Kim et al. 2014). However, the adequate level of NPs needed to act as a disinfectant has yet to be determined. Several toxicity mechanisms have been proposed, either through direct contact or internalization in cells that cause their sequential deformation, rupture, and penetration of NPs into the cell (Lin, Li et al. 2014), through the generation of ROS due to their interaction with electrons released from NPs (Kumar, Pandey et al. 2011), or through the release of metal ions (e.g. Zn^{2+}) with dissolution of NPs (Srivastava and Kumar 2016).

Along with the increase in the levels of environmental NPs, there has been an increase in research related to them; however, the ultimate fate, toxicity levels and toxicity mechanisms of NPs are not fully understood (Hegde, Brar et al. 2016). A recent study by Bondarenko et al. (Bondarenko, Juganson et al. 2013) suggests that the toxicity of NPs varies with respect to their physicochemical properties, dispersion state, concentration, and the physiological state of *E. coli* cells. Consequently, inconsistency in toxicity of NPs may

be primarily attributable to the types and concentrations of NPs and concentrations and types of bacterial cells (Baek and An 2011, Pagnout, Jomini et al. 2012, Manzo, Miglietta et al. 2013, Li, Niu et al. 2014, Pasquet, Chevalier et al. 2014).

Since we are directly exposed to NPs through consumer products and their (re)cycling in the environment, it is important to understand the toxicity of NPs extracted from these products. However, most studies rely on industrial-grade NPs to assess their toxicity on biological systems, largely because extracted ZnO NPs are not readily available. The paper will address this major gap in the literature by investigating the antibacterial effects of ZnO NPs extracted from a consumer product (sunscreen lotion) on *E. coli*, as it is the most widely studied model organism, and researchers will compare these results with those of industrial ZnO NPs used in the previous research (Pasquet, Chevalier et al. 2014, Leung, Xu et al. 2016, Padmavathy and Vijayaraghavan 2016). Since the findings of this paper are directly relevant to public health and the environment, these findings have the potential to guide policies to manage exposure to NPs in consumer products and the environment.

3.2. Materials and Methods

3.2.1. Preparation of ZnO NPs and suspension

Three different ZnO NPs were used for all the experiments: industrial ZnO NPs (IND); ZnO NPs extracted from industrial ZnO NPs (EXT); and ZnO NPs extracted from sunscreen, (SUN). The toxic profile of NPs extracted from actual nanoproducts may exhibit differences, possibly due to altered physicochemical properties and the various ingredients present in such products, which motivates us to investigate the toxicity kinetics and mechanisms behind industrial ZnO NPs. Industrial ZnO NPs (> 97% purity, < 50 ± 5 nm

nominal size, > 10.8 m^2/g surface area) were purchased from Sigma-Aldrich (St. Louis, MO). A popular sunscreen containing 5% ZnO and 4% octocrylene (Walgreens Clear Zinc Broad Spectrum SPF 50) was purchased from a local Walgreens store (Miami, FL). ZnO NPs were extracted from sunscreen with a modified method based on the literature (Nischwitz and Goenaga-Infante 2012).

The extractions of ZnO NPs from industrial ZnO NPs and sunscreen were prepared by a series of solvent extractions and deionized water extractions. Briefly, hexane (30 mL) was added to both industrial and sunscreen ZnO NPs (3 g), followed by sonication for 5 minutes and centrifugation at 4,400 rpm for 5 minutes. Supernatant was discarded and ethanol (30 mL) was then added to the solution and sonicated for 5 minutes. Afterwards, centrifugation at 4,400 rpm for 5 minutes was performed and ethanol was discarded. Deionized water (30 mL) was added, followed by centrifugation for 10 minutes at 3,000 rpm. This washing procedure was repeated twice and the final pellet was dried in an oven at 100 °C for 12 hours. All ZnO NPs suspensions were prepared using a sequential dilution in Luria Bertani (LB) broth (10 g/L tryptone, 5 g/L yeast extract, 5 g/L NaCl), beginning with 1280 mg/L of ZnO NPs for different concentrations of ZnO NPs suspension (20, 80, 320, 1280 mg/L), and a sonication probe was used for 1 minute for homogeneity. For quantification of ZnO NPs concentrations, the absorbance measurement of the specific optical densities at 395 nm wavelengths was performed, ranging from 0, 20, 80, 160, 320, 640, to 1280 mg/L of ZnO NPs; these resulted in a linear regression line ($R^2 = 0.97$).

3.2.2. Characterization of ZnO NPs

Physical and chemical properties of all three types of NPs were examined with the aid of BET (Brunauer, Emmett, and Teller) surface area analysis, scanning electron microscopy (SEM), energy dispersive spectroscopy (EDS), X-ray powder diffraction (XRD), and transmission electron microscopy (TEM). The surface area of the particles was measured from N_2-BET adsorption isotherms using a BET-surface area analyzer (Nova 2000e Surface Area and Pore Size Analyzer). XRD analysis was performed to characterize the crystal structure and confirm the chemical composition of the NPs extracted from consumer products. Microscope slides were coated with a 10-mm area of silica gel and loaded with industrial zinc oxide MNP powder and sunscreen consumer ZnO NPs powder. A Malvern Zetasizer Nano ZS90 analyzer (Malvern Instruments, Westborough, MA) was used to measure the zeta potential and hydrodynamic particle size (determined by dynamic light scattering) at 25 °C.

In order to characterize the surface morphology, elemental analysis, particle size distribution, and probing interactions of ZnO NPs with bacterial cells, SEM, EDS, and TEM analyses were performed. Samples were coated with palladium (Pd) in a sputter coater, and they were then imaged in a Philips XL-30 Field Emission SEM equipped with EDS. This enabled the visualization of ZnO NPs and *E. coli* morphologies in which bacterial cells were subjected to the fixation process. The control cells (ZnO NPs-free) and treated cells exposed to the ZnO NPs for 6 hours were suspended in 2% glutaraldehyde in a phosphate buffered saline (PBS) buffer overnight and washed three times with PBS buffer. Glutaraldehyde fixed bacterial cells were dehydrated in a graded series of ethanol (20-100%, three times) and dried in three changes of hexamethyldisilazane (HMDS) on

glass coverslips. After a complete outgas overnight, those were coated with Pd and the samples were then examined with a TEM (Philips CM 10, Eindhoven, Netherlands). Micrographs were used to obtain information regarding the average nanoparticle diameter, size distribution, and standard deviations using ImageJ software developed at the National Institutes of Health, USA.

3.2.3. *E. coli* DH5-Alpha cultivation and exposure of ZnO NPs suspensions

Transformation, the heritable modification of the properties of competent bacteria by DNA from another bacterial strain, was prepared by cultivating *E. coli* with MAX Efficiency DH5α™ Competent Cells (Invitrogen, CA). A plasmid with DNA resistant to ampicillin from another bacterial strain (foreign DNA) was introduced to the DNA of competent bacterium (host DNA) based on the transformation procedure guideline. All micro-centrifuge tubes were thoroughly pre-chilled on ice before use, and 5 µL of pUC19 control DNA was added to 100 µL of cells. The DNA samples were then incubated on ice for 30 minutes and heat-shocked in 42 °C water for 45 seconds, followed by placing the culture tube on ice for 2 minutes. The prepared culture tubes were placed in a shaking incubator at 250 rpm for 1 hour at 37 °C. Incubated *E. coli* was spread on LB agar plates containing ampicillin and incubated overnight at 37 °C. The *E. coli* colonies were cultured in LB broth (3 mL) for 12-14 hours in an incubator (MaxQ 4000, Thermo Scientific, NY) at 37 °C under continuous shaking at 225 rpm. A total of 100 µL of cultures was incubated in 100 mL of LB broth and the cultivation of bacteria was performed for 12 hours until the absorbance value reached 0.45 using measurement.

The cultivated cells were exposed to four different concentrations of ZnO NPs suspensions (i.e. 20, 80, 320, and 1280 mg/L) in LB broth at a final volume of 4 mL (OD_{600}

= 0.14). Three types of nanoparticles were used for antibacterial tests. *E. coli* was exposed to a ZnO NPs suspension for 6 hours in an incubator at 37 °C under continuous shaking at 225 rpm. A sample aliquot of 200 μL was added into a 96-well plate, and the optical density value was measured using a microplate reader (Spectra MAX 190, Molrecular Devices, CA) at 600 nm with an interval of 2 hours. The growth inhibition rate (%) (Fig. 3d) was also calculated using the following equation:

$$Inhibition\ rate\ (\%) = \left(1 - \frac{V_i}{V_o}\right) \times 100 \qquad \text{Eq. (1)}$$

By measuring the OD_{600} of the bacterial culture in the absence (V_o, control) and presence of different concentrations of ZnO NPs (V_i) at time 6, the inhibition rate (%) was estimated.

3.2.4. Assessment of ROS

To probe which mechanisms were responsible for the antibacterial effect, ROS generated by ZnO NPs were measured. The protocol of the ab113851-DCFDA cellular ROS detection assay kit (Abcam Inc, Toronto, ON, Canada) was used. The three types of ZnO NPs (IND, EXT, SUN) suspensions were exposed to the cultivated cells at 20 and 320 mg/L with shaking at 225 rpm for 6 hours in an incubator at 37 °C. The treated suspension cells were then collected in a conical tube and washed using PBS, followed by centrifugation. The pellet was re-suspended in 10 μM of diluted DCF-DA solution and incubated at 37 °C for 30 minutes under dark conditions. After washing the pellet with the buffer, it was re-suspended in 100 μM of PBS. The cells were loaded into a clear bottom 96-well microplate, and the plate was placed on a fluorescence plate reader (Gemini EM Molecular Devices, Sunnyvale, CA) at an excitation wavelength of 485 nm and at an emission wavelength of 535 nm.

3.2.5. Statistical analysis

All the tests were performed at least in duplicate. The statistical analysis was performed using the statistical student's *t*-test with Graph Pad Prism 3.0 (Graph Pad Software Inc., San Diego, CA). Experimental values were compared to their corresponding control values, and all data showed statistical significance at $p < 0.05$.

3.3. Results

3.3.1. ZnO NPs characterization

Characterization of ZnO NPs in the presence and absence of E. coli exposure was carried out using a BET surface area analyzer. The measured surface areas of industrial nano-ZnO and sunscreen derived nano-ZnO particles were 32.22 ± 0.97 m^2/g and 2.29 ± 0.47 m^2/g. The XRD spectra confirmed ZnO NPs from both industrial-grade materials and sunscreen (Fig. 3.1a); the EDS analysis results of three types of ZnO NPs in LB medium are shown in Fig. 3.1b. The zinc compounds used in this study were pure at the level of detection for EDS and were characterized by XRD. However, some potentially effective organic components may have been present, but were not detectable by the methods used in this study. All three types of ZnO NPs showed Zn as the primary element, which provides a basis for comparison of toxicity kinetics and mechanisms among the three types of ZnO NPs.

The SEM analysis results indicate that ZnO NPs in LB broth showed significant amounts of aggregation formed on the ZnO NPs surfaces (Fig. 3.1c). Compared to the control sample (bacteria with no exposure to ZnO NPs), significant deformation and morphological changes of bacterial cells were observed after exposure to all types of ZnO

NPs suspension (320 mg/L) (Fig. 3.1d). Aggregated NPs attached to cell surfaces result in cell damage caused by direct and indirect toxic effects (Lee, Kim et al. 2014). Destruction of cell membranes by ZnO NPs could result in cell penetration and DNA damage. As shown in the SEM images, those aggregates form floc of micron sizes in diameter, and this could contribute to the adsorbed NPs on cell surfaces, possibly affecting toxicity.

Analysis of particle size distribution of three types of ZnO NPs using TEM in conjunction with ImageJ software program showed average particle sizes of 12.7 nm (industrial ZnO NPs: IND), 15.7 nm (industrial extracted ZnO NPs: EXT), and 17.2 nm (sunscreen-extracted ZnO NPs: SUN) with Gaussian and Lorentz fitting curves. The particle size ranges were 2.4-96.3 nm (IND), 1.3-54.3 nm (EXT), and 2-342.8 nm (SUN) (Figs 3.2a-c, respectively). Hydrodynamic diameters of the three types of ZnO NPs were also measured. As shown in Fig. 3.2d, the particle sizes of ZnO NPs in LB broth were 113.3 nm (IND), 170.2 nm (EXT), and 223.4 nm (SUN), while zeta potential values were high, in the order of IND (-15.56 mV) > EXT (-14.86 mV) > SUN (-2.77 mV). The smallest particle size and higher zeta potential found in IND correspond to the highest surface area (32 m^2/g), indicating that smaller particle sizes (higher surface areas) correlate to higher stability. Additionally, the data suggests that aggregation occurred in the order of SUN > EXT > IND. Compared to ZnO powder, hydrodynamic diameter sizes of ZnO NPs suspensions revealed significant aggregation, forming larger sizes (Zhou and Keller 2010).

Aggregation of nanoparticles is influenced by surface charge and pH. While the release of zinc ions from ZnO NPs in aqueous media has been reported at pH levels below 6, causing electron transfer between ZnO NPs and a bacterial membrane that generates ROS from

cells (Bian, Mudunkotuwa et al. 2011), the PZC (point of zero charge) of ZnO NPs is known to occur between pH 8.7-10.3 (Pagnout, Jomini et al. 2012, Suganthi and Rajan 2012). Throughout these experiments, the pH ranges remained constant (pH 7.3-7.6) regardless of the types of ZnO NPs, which suggests relative stability above pH 7.0 and a low tendency for the release of Zn^{2+} (Kao, Chen et al. 2012).

(a)

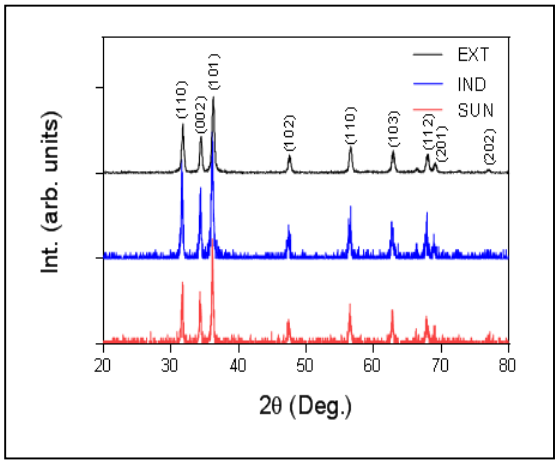

(b)

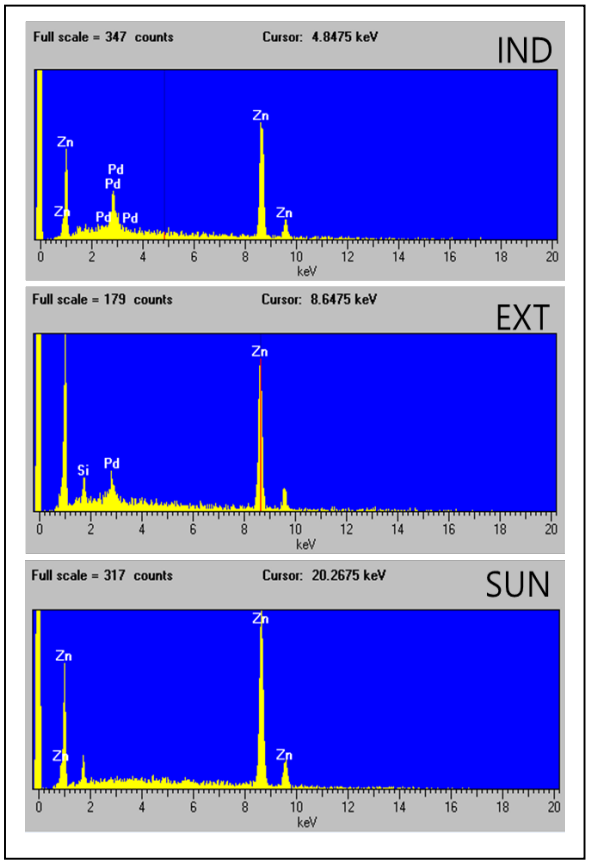

(c)

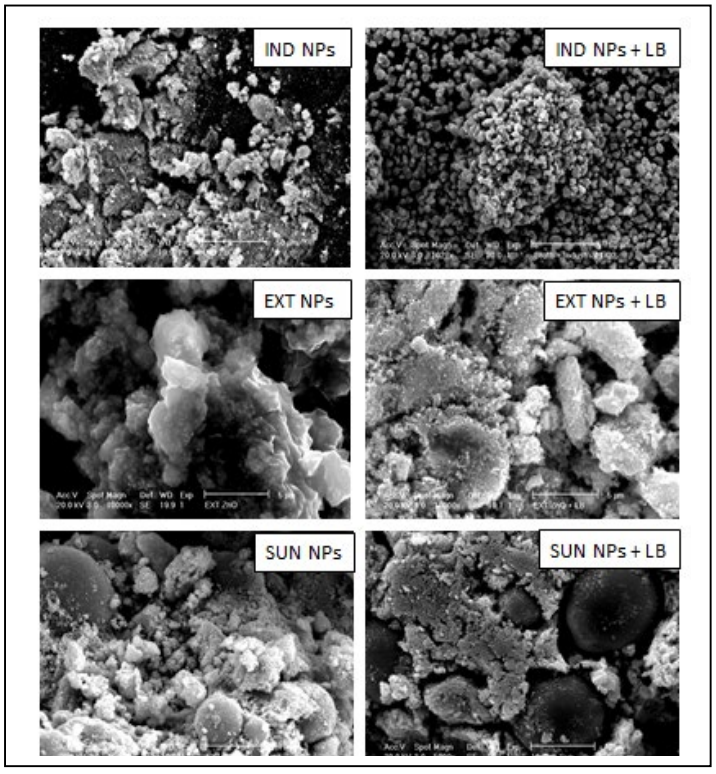

(d)

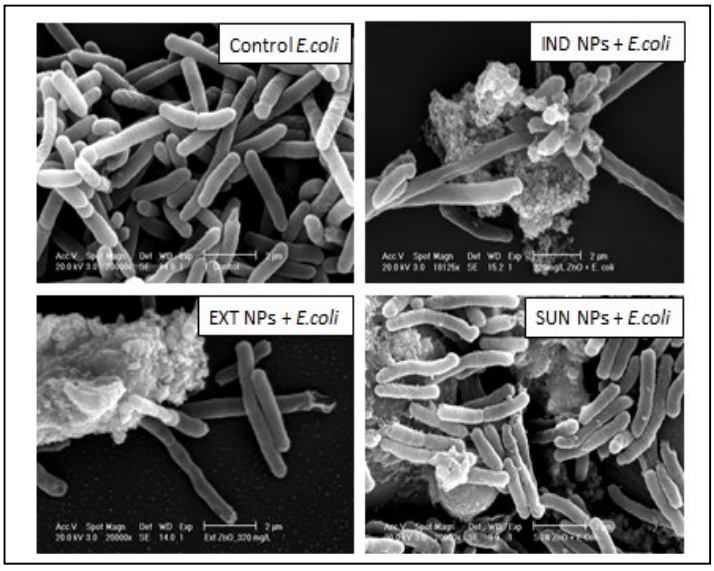

Figure 3.1. (a) XRD spectra of IND, EXT, SUN; (b) EDS spectra of IND, EXT, and SUN ZnO NPs in LB; (c) SEM images of three different ZnO NPs in the presence and absence of LB (scale bar: IND -50 µm, EXT-5 µm, SUN-10 µm); and (d) *E. coli* cells after exposure to three types of 320 mg/L ZnO NPs (scale bar: 2 µm) (IND: industrial ZnO NPs; EXT: ZnO NPs extracted from industrial ZnO NPs; SUN: ZnO NPs extracted from sunscreen).

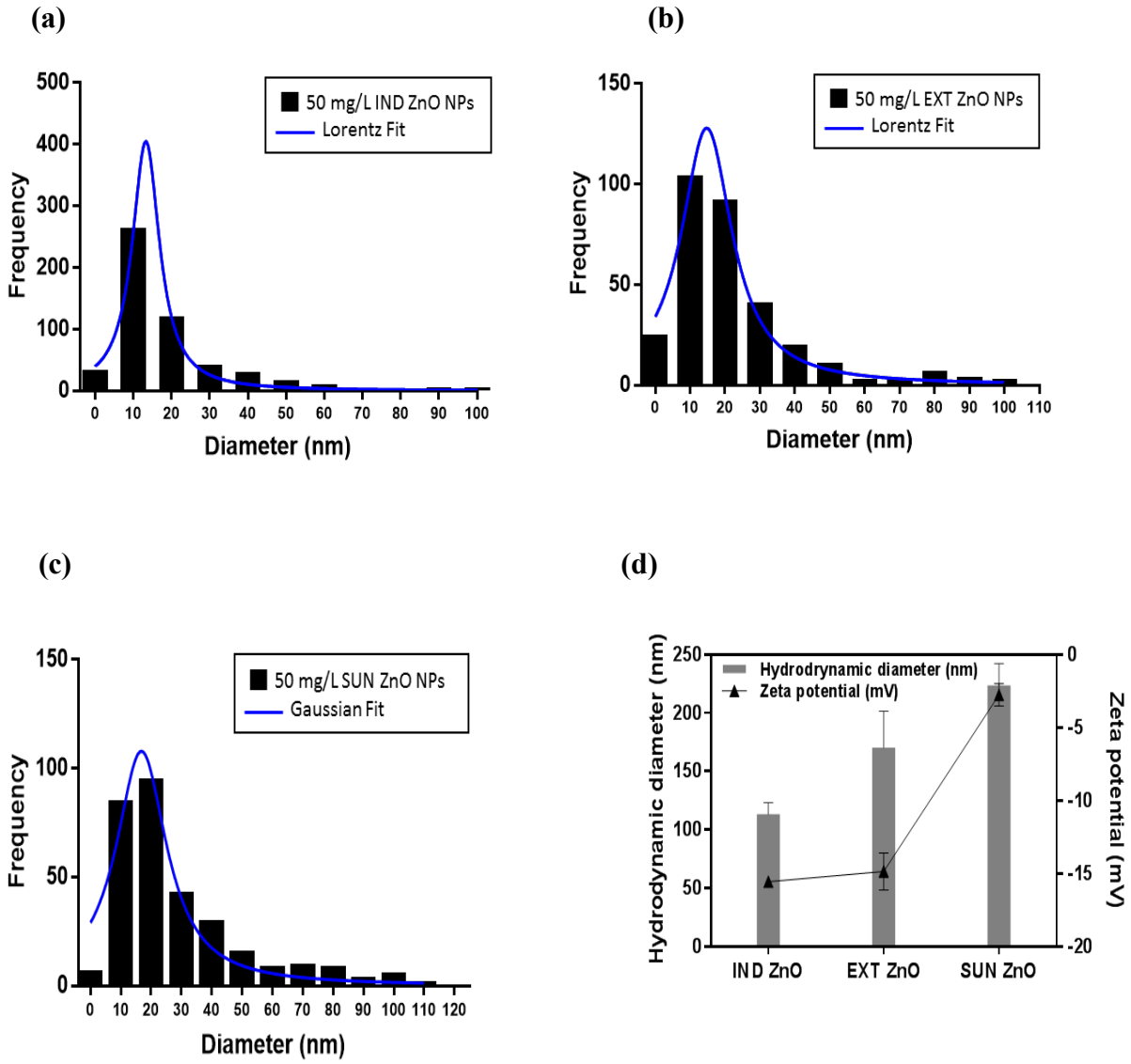

Figure 3.2. Particle size distributions of three types of NPs. Particle images were taken by TEM and particle size was analyzed by ImageJ software; (a) IND; (b) EXT; (c) SUN; and (d) hydrodynamic diameter determined by DLS and zeta potential of three types of ZnO NPs in LB broth (IND: industrial ZnO NPs; EXT: ZnO NPs extracted from industrial ZnO NPs; SUN: ZnO NPs extracted from sunscreen).

3.3.2. Concentration-dependent toxicity of ZnO NPs on *E. coli*

In this study, the relative antibacterial activity of cells was measured as a function of exposure duration, concentration, and type of ZnO NPs. The values of OD600 reflect bacterial growth after cells were exposed to the three different ZnO NPs over time (Fig. 3.3a-c). Control samples (Fig. 3.3a-c), which contained only bacterial cells (no ZnO NPs), did not exhibit any growth inhibition. However, as shown in Fig.3.3 a-c, when *E. coli* was exposed to ZnO NPs, bacterial growth decreased over time and the extent of cell viability was more significant as concentrations of ZnO NPs were increased. Interestingly, the overall growth inhibition was the most significant upon exposure to IND and the least pronounced from E. coli treated with SUN, indicating that ZnO NPs are not toxic at a lower concentration (20 mg/L), even though metal oxide material is known to be toxic. Above the concentration of 80 mg/L ZnO NPs, there appears to be a significant decrease of *E. coli* growth from IND and EXT, but SUN did not induce such a dramatic growth decrease unless ZnO NPs were used at 1280 mg/L. At this highest concentration of ZnO NPs, the OD600 values significantly decreased to 0.01 (IND) and 0.05 (EXT & SUN) from 0.2 (control).

These results suggest that the antibacterial effect increases at higher ZnO NPs concentrations and is influenced by particle sizes and surface coatings as well. As previously addressed, IND has the smallest particle size (the largest surface area) while SUN has the largest particle size; this larger size is associated with aggregation since the extraction removed all coating materials present in sunscreen. Interestingly, EXT, which was extracted from industrial ZnO NPs by the same extraction method conducted for SUN,

showed neither the highest nor the lowest antibacterial effect. This may indicate the presence of other ingredients (octocrylene, silica, ethylhexyl stearate, diisopropyl adipate, etc.) that prevent significant aggregation. Aggregation adhesion against cells may increase with increasing concentrations of ZnO NPs, which clearly explains the experimental results—i.e. increasing antibacterial effect at higher ZnO NPs concentrations over time.

At the lowest concentration (20 mg/L), there was no significant difference in the inhibition growth rates of bacteria among IND, EXT, and SUN (11.62, 11.63, and 11.71 %, respectively). However, the cell growth inhibition rate (%) at 6 hours reveals that there was a nine-fold increase of the growth inhibition rate from IND (20 to 1280 mg/L ZnO NPs). The same increase in concentration of EXT and SUN resulted in growth inhibition by seven- and six-fold, respectively. Thus, the growth inhibition rate (%) was proportional to ZnO NP concentrations and the antibacterial effect occurred in the order of IND > EXT > SUN (Fig. 3.3d). As indicated previously (characterization study, Figs. 3.1 & 2), the antibacterial effects of all three types of ZnO NPs (IND, EXT, & SUN) vary with respect to their sizes and aggregation phases. Based on our results, the toxicity of ZnO NPs is likely to vary with respect to the concentration, particle size, and type of ZnO NPs.

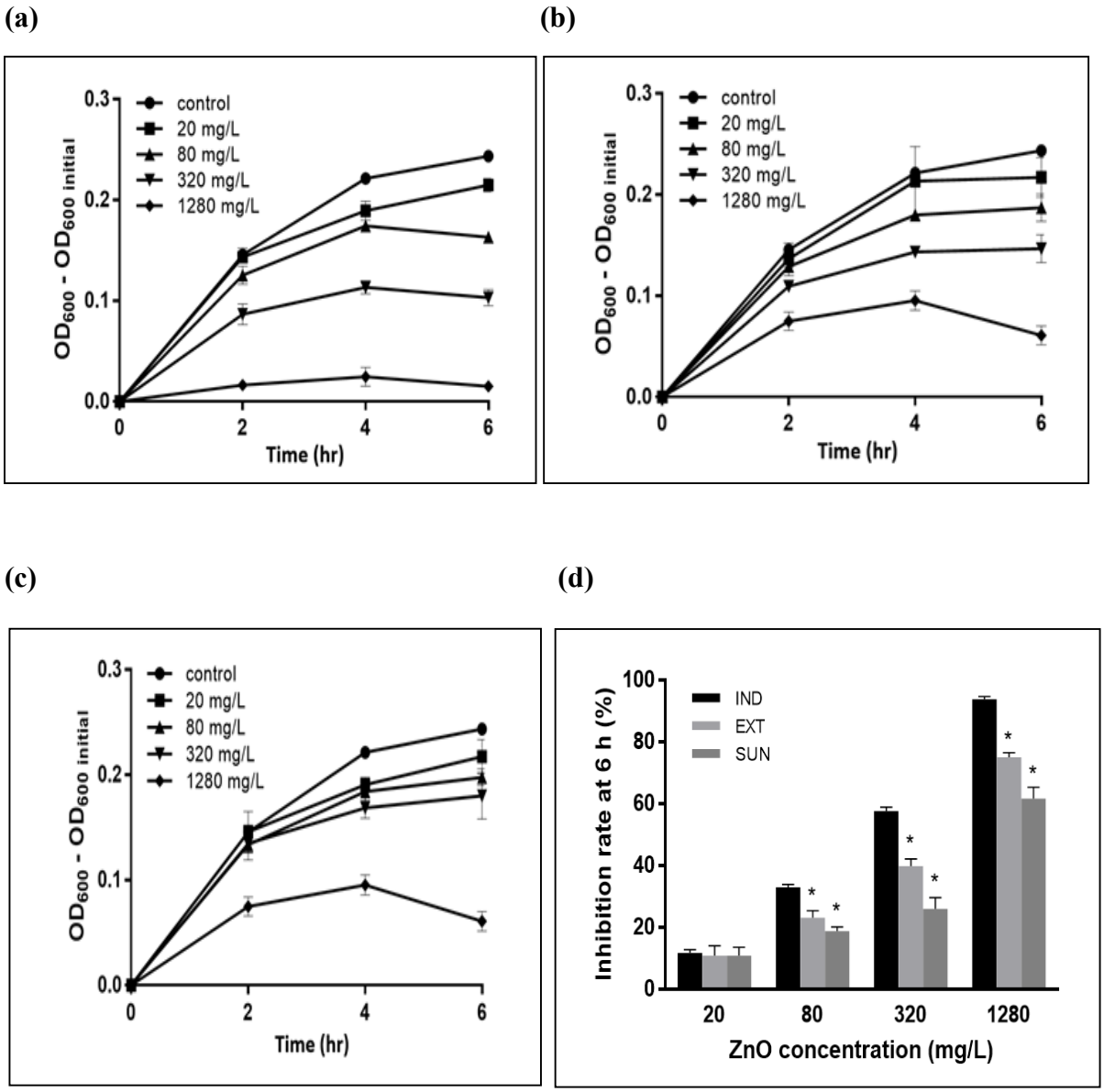

Figure 3.3. Growth curves of *E. coli* at different concentrations (control, 20, 80, 320, 1280 mg/L) of (a) IND; (b) EXT; and (c) SUN; and (d) growth inhibition rate (%) of *E. coli* after exposure to three types of ZnO NPs (20, 80, 320, 1280 mg/L) at 6 hours (IND: industrial ZnO NPs; EXT: ZnO NPs extracted from industrial ZnO NPs; SUN: ZnO NPs extracted from sunscreen).

3.3.3. ZnO NPs-induced ROS generation

While the antibacterial impact of ZnO NPs is attributed to the physicochemical properties of ZnO NPs, other toxicity mechanisms could also be involved. The reactive

oxygen species (ROS) produced by ZnO NPs may induce lethal stress levels in bacteria. Since superoxide and hydrogen peroxide serve as a substrate for hydroxyl radical formation through Fenton chemistry, this oxidative process can lead to cell injury and death, where hydroxyl radicals break down nucleic acids, carbonylated proteins, and peroxidative lipids. To this end, ROS generation of the bacterial cells in the presence and absence of ZnO NPs in LB broth was measured.

ROS released from the log phase of bacteria exposed to three types of ZnO NPs at two different concentrations (20 & 320 mg/L) was measured during exposure (Fig. 3.4). ROS were measured using DCF-DA, which penetrates the cells and is converted to 2',7' dichlorodihydrofluorescein (DCF) when the DCF-DA is oxidized by ROS. Fig. 4.1.4 shows ROS generation (as measured by fluorescence intensity) induced by exposure of three types of ZnO NPs to *E. coli* cells at the log phase over six hours. The ROS generation increased with the increase in the concentrations of ZnO NPs and duration of exposure, which is consistent with previous results on ZnO NP toxicity (Fig. 3.3).

Similarly, other studies have also reported increasing ROS generation by ZnO NPs as a function of concentration and exposure duration (Li, Niu et al. 2014). Increasing the concentrations of ZnO NPs may lead to a greater affinity for attaching onto the surface of *E. coli,* producing more ROS compounds, attacking DNA, producing chain breaks, and modifying carbohydrates (Suresh, Pelletier et al. 2013) Similarly, Kumar et al. observed a significant uptake of ZnO NPs by *E. coli*, which facilitated increasing ROS generation at higher concentrations of ZnO NPs (Kumar, Pandey et al. 2011). When *E. coli* were exposed to ZnO NPs from the beginning of the growth phase, the fluorescence intensity in 6 hours at 320 mg/L ZnO NPs occurred in the order of IND (86 a.u.) > EXT (63 a.u.) > SUN (34

a.u.) with the same trend repeating at other tested concentrations. When ZnO NPs were added in the stationary phase of bacterial growth (Fig 3.4b), fluorescence intensity was elevated by ~1.5 times as compared to the control; however, no significant differences between the three types of ZnO NPs were noted (e.g., IND (160 a.u), EXT (150 a.u.), SUN (140 a.u.) in 6 hours at 320 mg/L ZnO NPs). In both the log and stationary phases, toxicity was increased at higher concentrations and longer exposure times.

Overall ROS generation at the stationary phase of *E. coli* growth was higher than that at the log phase (Fig. 3.4b). These results suggest that for *E. coli* at the stationary phase, the highest level of metabolic products appears to produce more ROS, as the cell density is the highest and most *E. coli* strains appear to contain high amounts of plasmid (Zhao and Drlica 2014). Additionally, the amount of ROS generation may be more attributed to the fully-grown bacteria, which display a high bacterial concentration, rather than the interaction between ZnO NPs and the bacteria, given that ZnO NPs were only introduced after the colony of *E. coli* was fully grown. Thus, the proposed mechanisms evidenced by our study involve both physicochemical properties and ROS generation. However, it was also found that the extent of toxicity was correlated to the bacteria growth phases in conjunction with exposure duration. Fig. 3.5 shows the relative percentage of fluorescence intensity (accumulated ROS) of *E. coli* exposed to three different ZnO NPs for six hours as compared to control colonies, which were not treated with ZnO NPs. Comparing the relative ROS generation between the log phase and the stationary phase, the toxicity effect of ZnO NPs was more apparent at the log phase than at the stationary phase. Thus, the observed differences in the relative ROS generation rate could be attributed to the growth state. During exposure to ZnO NPs at the exponential phase, *E. coli* growth is inhibited,

reducing their doubling cells. As bacterial cells are treated with increased ZnO NP concentrations and exposure duration, the number of damaged cells will ultimately increase.

While the relative ROS generation at 20 mg/L of ZnO NPs was similar to the results from the control group regardless of type of ZnO NPs, this impact significantly increased at 320 mg/L (Fig. 3.5a). Again, IND (industrial ZnO) had the highest generation of ROS compared to the other types of ZnO NPs. Smaller particle sizes and higher concentrations of ZnO NPs produce more ROS, which can be attributed to its antibacterial behavior. Thus, when the concentration is the same, the ROS generation can be strongly affected on the surface area of ZnO NPs, which is related to their particle size. At the stationary phase, the relative ROS generation (accumulated ROS) was similar among the three types of ZnO NPs, concentrations, and exposure time (Fig 3.5b).

Although the quantity of ROS generation of *E. coli* was significantly high at the stationary phase, the relative ROS generation (%) was higher at the log phase than at the stationary phase. Our results suggest that ZnO NPs exhibit more antimicrobial activity on bacteria at the log phase as compared to the stationary phase. Indeed, bacteria at the log phase are likely to be vulnerable to NP-induced toxicity, leading to subsequent decomposition of cell membranes. Moreover, industrial ZnO NPs at the highest concentration (320 mg/L) of ZnO NPs showed a more detrimental impact than other types of ZnO NPs, possibly due to their having a larger surface area and smaller particle size.

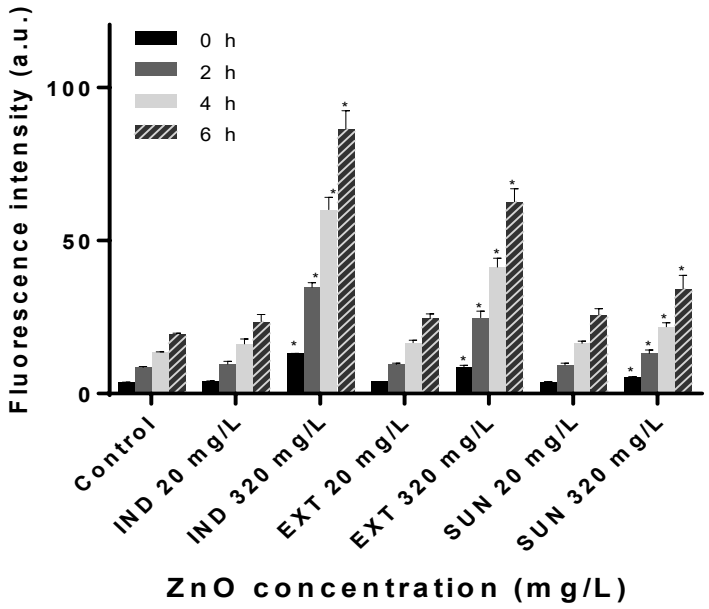

(A)

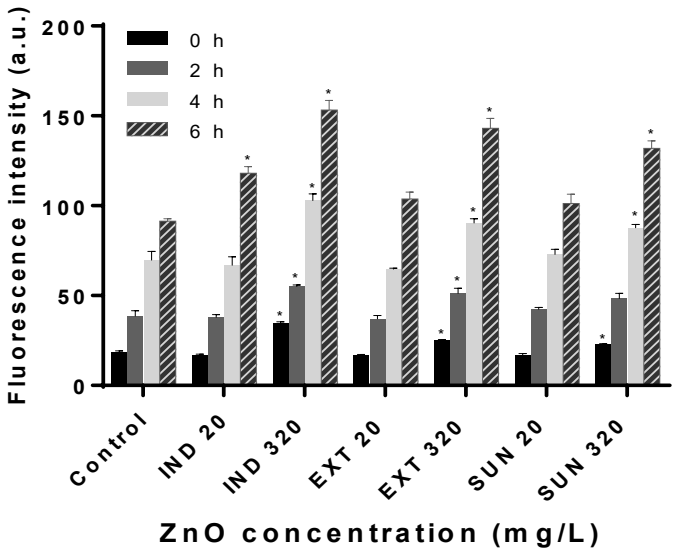

(B)

Figure 3.4. Fluorescence intensity (ROS generation) of three types of ZnO NPs (20 & 320 mg/L) after exposure to (a) *E. coli* cells at log phase and (b) *E. coli* cells at stationary phase over 6 hours (IND: industrial ZnO NPs; EXT: ZnO NPs extracted from industrial ZnO NPs; SUN: ZnO NPs extracted from sunscreen).

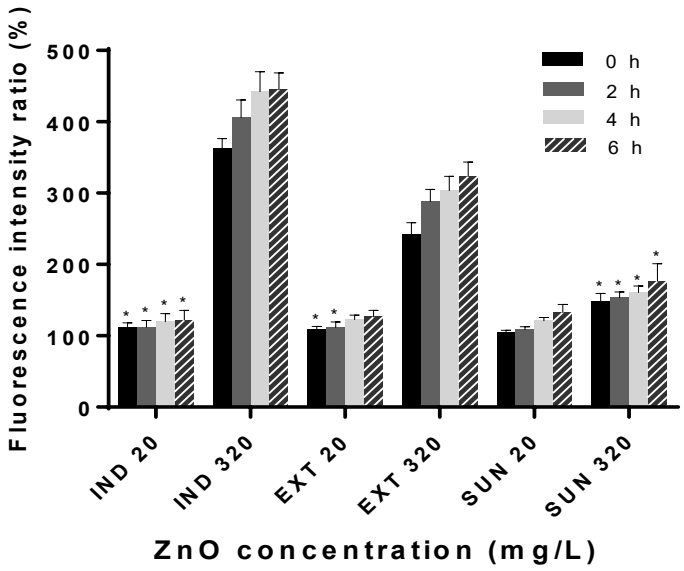

(A)

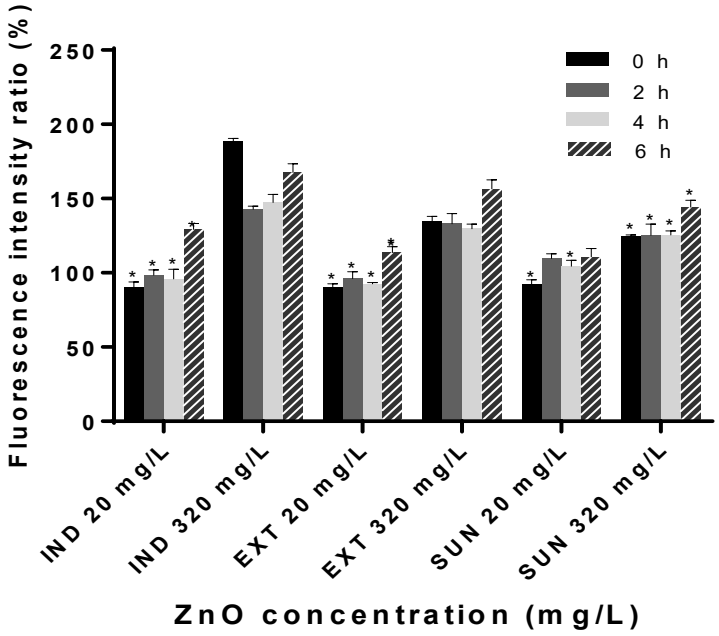

(B)

Figure 3.5. Relative ROS generation (%) (accumulated ROS generation (%)) estimated by subtraction of control cells (without NPs) induced by exposure of three types of ZnO NPs (20 & 320 mg/L) to (a) *E. coli* cells at log phase and (b) *E. coli* cells at stationary phase over 6 hours (IND: industrial ZnO NPs; EXT: ZnO NPs extracted from industrial ZnO NPs; SUN: ZnO NPs extracted from sunscreen).

3.4. Discussion and implications

Two important findings emerge from this research. First, the antibacterial effects of ZnO NPs vary significantly with respect to the concentration and particle size of NPs and exposure duration. Second, exposure to ZnO NPs results in an increase in the levels of ROS, and levels of ROS vary between the log (or growth) and stationary phases. While some of the findings from this study are consistent with the existing literature (Adams, Lyon et al. 2006, Zhang, Jiang et al. 2006, Raghupathi, Koodali et al. 2011) in that the antibacterial effect is influenced by the concentrations and particle sizes of NPs, this paper makes several novel contributions as well.

First, the physical and chemical characteristics of NPs extracted from a consumer product were different from the industrial-grade NPs. For example, the size of IND NPs was smaller than the NPs extracted from the consumer product tested in this research. Second, industrial NPs were more toxic than those from the consumer product tested in this study. However, at elevated concentrations, NPs extracted from the tested consumer product in our study also had significant antibacterial effects. Third, this research sheds light on the mechanism of the toxicity of ZnO NPs. As the concentration of NPs increases, they bind to the bacterial cells, which in turn damages the cellular molecular structure by internalization, resulting in a leakage of cytoplasmic contents with and without deformation of cell surfaces, and increases the production of ROS (Yamamoto 2001, Brayner 2006, Applerot 2009, Liu, He et al. 2009, Ma, Wallis et al. 2014).

Fourth, the effects of NPs at log and stationary phases were different. The reaction of the ZnO NPs surface with water promotes the transfer of electrons from the valence band to the conduction band, generating electrons and holes as carriers. When photons are

introduced to the system, they supply the required energy that causes electrons and holes to react with oxygen, hydroxyl, or water to form superoxide and hydroxyl radicals (Brayner 2008). However, ROS are also efficiently generated under dark conditions by the interaction of ZnO NPs with cellular components. For instance, ROS (e.g., H_2O_2, $^{\bullet}OH$, $O_2^{\bullet-}$) are formed in ZnO NPs suspensions through the following mechanisms, as suggested by Dasari et al.(Dasari, Pathakoti et al. 2013) and Sharma et al. (Sharma, Anderson et al. 2012).

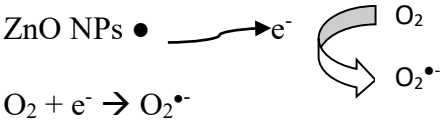

$O_2 + e^- \rightarrow O_2^{\bullet-}$

$O_2^{\bullet-} + H_2O \rightarrow {}^{\bullet}HO_2 + OH^-$

$^{\bullet}HO_2 + {}^{\bullet}HO_2 \rightarrow H_2O_2 + O_2$

$H_2O_2 + O_2^{\bullet-} \rightarrow O_2 + {}^{\bullet}OH + OH^-$

Our research suggests that the increase in ROS was significantly higher at the log phase than that at the stationary phase. However, the ROS generation ratio at the stationary phase of *E. coli* growth was higher than that at the log phase, suggesting that *E. coli* produces more ROS due to having the highest level of metabolism at the stationary phase, along with the highest cell density and more plasmid production. Finally, this research suggests that both physicochemical properties in NPs and ROS generation at different phases are important in understanding the toxicity of NPs.

The findings of our research have important implications for the environment, health, and medicine. First, the finding concerning the toxicity of NPs from consumer

products can guide policies for managing exposure to NPs, since most of our direct exposure to NPs occurs through consumer products. Moreover, NPs released into the environment (re)cycle in the absence of effective filtration systems. Therefore, it is important to regulate the production and consumption of NPs, especially in consumer products, due to their toxicity. Second, our findings could serve as a step-forward strategy in eliminating drug-resistant bacteria (or superbugs) by introducing NPs as a disinfectant or antimicrobial reagent at early stages of bacterial growth. Third, the presence of NPs can reduce the treatment efficacy of contaminants in biological wastewater processing units.

Once aggregated, nano-colloidal particles are treated by filtration at the wastewater treatment plant and can cause adverse effects on the filter because of their bio-toxicity, due to ROS generation in the presence of oxygen in system. For example, ROS (e.g. superoxide, hydrogen peroxide, hydroxyl radical) is generated through the reduction of oxygen to superoxide, the formation of hydrogen peroxide by the dismutation of superoxide anions, and then followed by the generation of hydroxyl radicals through the reduction of hydrogen peroxide. Otherwise, the hydroxyl radical can be fully reduced to water. Finally, NPs can also be used in medical devices and clinical settings, such as disinfectants and antibiotic coating to prevent microbes, which aligns well with the emerging need for alternative antibacterial agents in dental implants and medical devices with prolonged antibiotic properties.

Although this paper makes several important contributions and has important implications for the environment and human health, several limitations remain. First, the study was not conducted under UV light conditions. *E. coli* cells may generate more ROS

production under UV light, due to the impact of photons lowering the activation energy required for the oxidation reaction (Dasari, Pathakoti et al. 2013). Future research should be geared towards exploring the toxicity of NPs in more controlled settings.

Second, many factors can affect the mixture and aggregation of NPs, which can accelerate antibacterial effects in aquatic conditions. However, we were unable to fully homogenize NPs in the samples. Future research may consider applying a stabilizer or coating materials on the surface of NPs to achieve homogenous distribution (Zhou and Keller 2010, Tejamaya, Romer et al. 2012). Third, all experiments were conducted in a controlled setting, which constrains the scope of generalizability of these findings to real-world settings, including transport and fate of nanomaterials in the environment and their impact on human health and ecosystems. For example, the concentration of NPs is higher in soil than in water (Li, Mahendra et al. 2008, Crane and Scott 2012). Finally, we used single-cell bacteria, which further reduces the scope of generalizability of our findings to real-world settings, where bacteria are found in multispecies communities. Therefore, future research must be geared towards examining the effects of NPs on multispecies bacteria and/or animals.

3.5. Conclusions

In summary, among the three types of ZnO NPs, IND showed the highest toxicity, largely due to their decreased size with aluminum coating material, which is used as a dopant on ZnO NPs. Aluminum doped ZnO NPs that were stabilized allowed for a decrease in particle size compared to uncoated ZnO NPs (Suwanboon, Amornpitoksuk et al. 2008, Aimable 2010, Gomez, Bachelot et al. 2011). When the coating material of these NPs was removed, their toxicity declined because their size increased with aggregation. The

cytotoxicity caused by ZnO NPs induces inhibition of bacterial growth and facilitates ROS generation. In fact, our results indicate that ROS generation is one of the important causes of the toxicity effects of ZnO NPs on bacteria.

However, depending on the cell structure and characteristics of microorganisms, the antibacterial effects of NPs can vary, causing either direct destruction of bacterial cells or distortion of microbial surfaces. Optimization of the dosage of NPs for bacterial cells, proper application duration of NPs to bacteria at different growth phases, coating materials present in NPs, and long- or short-term antimicrobial behavior all warrant further investigation, which can guide strategies for treating microorganisms (such as superbugs to act as antibacterial agents) and management of NP exposure from consumer products and the environment.

CHAPTER 4:

EFFECTS OF COATING MATERIALS ON ANTIBACTERIAL PROPERTIES OF TITANIUM-DIOXIDE NANOPARTICLES[2]

[2] Baek, S., Joo, S. H., Blackwelder, P., Toborek, M. (2018) Effects of coating materials on antibacterial properties of industrial and sunscreen-derived titanium-dioxide nanoparticles on Escherichia coli. *Chemosphere*. 208 pp.196-206

4.1. Background

Growing employment of nanotechnology leads to increasing releases of nanoparticles (NPs) into the natural environment, causing unknown and unintended environmental effects (Hegde, Brar et al. 2016, Padmavathy and Vijayaraghavan 2016, Wang, Lin et al. 2016). Due to the versatile properties of NPs, including surface area, particle size, and quantum effects, NPs are widely used in commercial products (Jeon, Kim et al. 2016, Wang, Zhu et al. 2016). TiO_2 NPs are mainly used in personal-care products, coatings, cleaning agents, and paints, producing around 10,000 tons per year globally (Piccinno, Gottschalk et al. 2012, Weir, Westerhoff et al. 2012). Such wide and increasing productions also raise concerns regarding potential toxicity to living organisms (Jeon, Kim et al. 2016, Leung, Xu et al. 2016). NPs can negatively affect human health by targeting both the human host and its microbiomes.

Escherichia coli (E.coli), is widely used in laboratory for studying the toxicity of NPs, and cell-NP interaction because it is commonly found single cell bacteria in the intestines of animals and humans, and aquatic environment (Lin et al., 2014; Baek et al., 2017). Research has revealed increasing toxicity of TiO_2 NPs to *E. coli* at small particle sizes and large surface areas (Smijs and Pavel 2011). In addition, the degree of toxicity in *E. coli* was influenced by ionic strength and electrolytes that affect the aggregation of TiO_2 (Lewicka, Benedetto et al. 2011). As with other types of NPs, TiO_2 NPs are often coated with stabilizers to prevent aggregation (Labille, Feng et al. 2010, Lewicka, Benedetto et al. 2011, Smijs and Pavel 2011, Jeon, Kim et al. 2016). Thus, TiO_2 may be present in a bare or coated form of NPs in the aquatic environment (Dalai, Pakrashi et al. 2012). Engineered polymers or organic and inorganic substances may serve as coating material and act as

stabilizers for dispersal of colloidal NPs. Stabilizers have been found to modify the physicochemical properties of NPs, thereby affecting particle stability and mobility by electrosteric repulsion (Jafry, Liga et al. 2011, Dalai, Pakrashi et al. 2012) (Dalai, Pakrashi et al. 2012, Wang and Fan 2014), and resulting in altered interaction with organisms (Batley 2012).

According to the DLVO theory, NP aggregation is controlled by Van der Waals attractive and electrostatic double-layer forces (Hotze, Phenrat et al. 2010). Thus, stabilizers influence the properties of NPs by adsorption of coating materials through enhancing NPs' surface charge or presenting steric or electrosteric repulsion (Huynh and Chen 2011).

There is an impact of polymeric organic and inorganic matter coatings on TiO_2 NPs toxicity and biological effects on *E. coli*. In addition, providing insight into this mechanism is a goal since it is not fully understood (Li, 2011). Although interactions of TiO2 NPs with bacterial cells have been examined, the majority of these studies have been limited to toxicity impact in non-coated NPs.

The interaction between TiO_2 NPs and bacterial cells is influenced by the model coating materials. This approach enables us to evaluate the antibacterial impact of these coated NPs on *E. coli*, with further implications to the toxicity of NPs in the environment.

Among organic coating materials, CMC (carboxymethylcellulose) and PVP (polyvinulprrolidone) are both neutrally charged polymers and were chosen since they are commonly used in food-additive and personal-care products (Dalai et al., 2012; Wang and Fan, 2014). SiO_2 is another widely used coating material employed in various commercial products (e.g., sunscreen) to improve the photocatalytic activity of TiO_2 NPs (Nur, 2006;

Jafry et al., 2011). Previous studies have been performed on industrial SiO_2, including SiO_2 coated TiO_2 NPs (Jafry et al., 2011; Siddiquey et al., 2008). Since TiO_2 NPs are directly used for commercial products, it is important to understand to compare the toxicity of sunscreen-derived TiO_2. The extracted SiO_2-TiO_2 NPs from sunscreen, and industrial SiO_2-TiO_2 NPs were investigated to determine physicochemical characteristics of the NPs, and these nanotoxicity on bacteria was evaluated.

TiO_2 NPs coated with CMC and PVP (both neutrally charged polymers) materials, as well an inorganic coating (SiO_2), effect bacterial growth inhibition, ROS generation, and morphology as a function of exposure time and concentration.

4.2. Materials and Methods

4.2.1. Nanoparticle preparation

Industrial and sunscreen-derived TiO_2 NPs were used in all experiments. Industrial TiO_2 NPs (TiO_2, >99.7 % purity, <25 nm size, 45–55 m^2/g surface area, anatase), CMC (average MW: ~90,000), PVP (average MW: ~10,000), and silica NPs (SiO_2; >99.8% purity, <14 nm size, 175–225 m^2/g) were purchased from Sigma-Aldrich (St. Louis, MO). Commercially available sunscreen products containing TiO_2 NPs were purchased at a local drugstore in Miami, FL. The CMC- and PVP-coated TiO_2 NPs were prepared by dissolving 0.2 % (w/v) of CMC or PVP in deionized (DI) water using a magnetic stirrer for 12 hours. After complete dissolution, TiO_2 NPs were added to each solution and dispersed under sonication for 3 minutes.

To identify the effect of silica present in sunscreen on antibacterial properties of TiO_2 NPs, the TiO_2 NPs were extracted from the sunscreen product using a similar method as

described in the literature (Nischwitz and Goenaga-Infante 2012). Briefly, extractions of NPs were performed by a series of ethanol and DI water washes, followed by washing with hexane and subsequent sonication and centrifugation. After discarding supernatants, suspensions were washed in ethanol and DI water five times, and the pellet dried in an oven at 100°C for 12 hours. Industrial-grade SiO_2 and TiO_2 NPs were mixed in DI water and sonicated for 3 minutes. Prior to experimentation, all NP suspensions were subjected to dispersion using a sonication probe for 1 minutes.

4.2.2. Characterization of TiO_2 NPs

NP surface morphology, physicochemical properties, elemental analysis, and interactions with bacterial cells were examined. NP suspensions were analyzed using Energy Dispersive Spectroscopy (EDS), Field Emission Scanning Electron Microscopy (SEM, Philips XL-30 FEG), Transmission Electron Microscopy (JEOL 1400 TEM), Malvern Zetasizer Nano ZS90 analyzer, and Fourier-Transform Infrared Spectroscopy (FTIR). For SEM and TEM Control cells and NP-treated *E. coli* cultures were suspended in 2% glutaraldehyde in a phosphate-buffered saline (PBS) buffer overnight. The pellet was then washed three times with the PBS buffer. A series of graded ethanol at 20, 50, 70, 95, and 100% was used for dehydration in three changes of 5 minutes each. For SEM the samples were then dried in three changes of hexamethyldisilazane (HMDS) in plastic weigh boats. After outgas sing overnight, the samples were placed in a Cressington Sputter Coater and coated with palladium (Pd). They were then imaged in the Philips XL-30 Field Emission SEM equipped with an Oxford/Link EDS system.

To quantify average particle sizes and particle-cell interactions, TEM analyses were carried out. Cells were prepared as in the above described protocol for SEM. However, after the

last 100% ethanol wash cells were embedded in Spurr Resin. The blocks were then sectioned in a Porter Blum Ultramicrotome, placed on copper grids, and imaged in a Philips CM-10 TEM (Eindhoven, Netherlands) at the Miller School of Medicine TEM Core at the University of Miami.

Digitally acquired micrographs were analyzed using Image J software developed at the National Institutes of Health, USA to calculate average NP diameter, size distribution, and standard deviation. A Malvern Zetasizer Nano ZS90 (Malvern Instruments, Westborough, MA) was employed to measure the hydrodynamic diameter of particles in suspension using dynamic light scattering (DLS) at 25°C, and the zeta potential of the NPs in DI water.

For FTIR measurements, NP suspensions were made in DI water and dried using a fume hood overnight at room temperature. Using a Frontier series FTIR spectrometer by PerkinElmer (Frontier, Perkin Elmer, Norwalk, CT), 50-100 mg of the powdered TiO_2 sample was applied to the clean crystal surface so that the crystal was completely covered with sample before the force gauge was applied and the spectrum taken. The crystal was thoroughly cleaned between samples to ensure no cross contamination occurred. Before each measurement, a blank measurement was taken. Each sample was scanned four times, and the summation of its spectra was analyzed.

4.2.3. *E. coli* DH5-Alpha cultivation and cell-viability analysis

E. coli cultured for characterizing the NP-cell interactions was grown as follows. A pUC19 vector was transformed into Max Efficiency DH5α™ Competent Cells (Invitrogen, CA). The transformed cells were cultivated on Luria Bertani (LB) agar plates containing ampicillin. The *E. coli* colonies were incubated in bacterial culture tubes with LB at 37 °C

for 12–14 h in an incubator (MaxQ 4000, Thermo Scientific, NY). The growth inhibition of *E. coli* was assessed by exposing cultivated cells to different concentrations of TiO_2 NP suspensions (10, 50, 250 mg/L) for 6 h. A bacterial cell culture free of TiO_2 NPs was used as a control.

The growth inhibition of *E. coli* was measured by optical densities of UV-vis absorption at 600 nm (OD_{600}). *E. coli* were inoculated in LB and incubated for 12-16 h at 37 °C in an incubator with shaking at 225 rpm. The cultivated *E. coli* cells (with an OD_{600} of 0.45) were exposed to different concentrations (0, 10, 50, or 250 mg/L) of TiO_2 NP suspension in LB for 6h at 37 °C in an incubator at 225 rpm. Then, the aliquots of 200 μL were added into a 96-well plate, and OD_{600} was measured using a microplate reader (Spectra MAX 190, Molecular Devices, CA) with an interval of 2 h. The growth inhibition of *E. coli* was calculated as percentage of survived cells compared to control cells after 6 h of exposure. Samples were plated in triplicate, and all experiments were performed under sterile conditions.

4.2.4. Quantification of ROS generation

To measure the generation of ROS from TiO_2 NPs, a fluorogenic dye 2',7'-dichlorofluorescin diacetate (DCFDA) was used following the manufacturer's instructions (Abcam Inc, Toronto, ON, Canada). After diffusion into the cell, DCF-DA is deacetylated by cellular esterases to a non-fluorescent compound that is oxidized by ROS into 2', 7'-*dichlorofluorescein* (DCF). The method allows to assess hydroxyl, peroxyl and other ROS activity within cells. Briefly, cultivated cells exposed to different coating materials and TiO_2 NP concentrations were seeded in the 96-well plate (black color, clear bottom). The treated cells were washed with PBS, followed by an addition of the DCF-DA dye (10 μM)

to each well and incubation for 30 minutes at 37 °C. DCF fluorescence was detected by fluorescence spectroscopy with excitation and emission spectra of 485 nm and 535 nm, respectively.

4.2.5. Statistical analysis

All the experiments were performed in a triplicate. The statistical student's *t* test with Graph Pad Prism 3.0 analysis (Graph Pad Software Inc., San Diego, CA) was used for the statistical analysis. All the experimental values were compared to their corresponding control values and showed statistical significance at $p < 0.05$.

4.3. Results and discussion

4.3.1. Characterization of TiO_2 NPs with and without coatings

The shape, morphology, and size of industrial and sunscreen-derived TiO_2 NPs were analyzed using SEM and TEM in the presence and in the absence of coating materials (CMC, PVP, and SiO_2). As shown in Figure 4.1, spheres which were in some cases aggregated were observed in all samples. However, sunscreen-derived TiO_2 (SUN) NPs exhibited the largest particle size (up to 284 nm), (Table 1), which clearly indicates that the silica coating on TiO_2 resulted in a larger particle size and a uniform spherical shape. Industrial TiO_2 NPs (IND) in the absence of CMC or PVP showed significant aggregation with larger particle sizes and low zeta potential values.

In contrast, the presence of CMC or PVP significantly enhanced the stability of IND, as shown in the zeta potential values measured at pH 7, with substantial shape changes characterized by spherical particles and relatively smaller particle sizes of TiO_2 (Fig. 4.1A). Such substantial shape transformation by stabilizers has been found in other studies

(Othman, Abdul Rashid et al. 2012, Tejamaya, Romer et al. 2012). TiO_2 NPs have also been found to exhibit a fully dispersed and stabilized form in natural water containing organic materials (Planchon et al., 2013). In this study we found the particle size distributions measured by ImageJ revealed average sizes of 29.4 nm (IND), 16.3 nm (CMC+TiO_2), and 9.8 nm (PVP+TiO_2) (Table 1).

In colloidal suspension, the hydrodynamic diameters were on the order of IND (625.7 nm) > SiO_2 mixed with IND (594.5 nm) > IND mixed with CMC (547.1 nm) > SUN (335.7 nm) > IND mixed with PVP (206.6 nm). The difference in hydrodynamic diameters between CMC and PVP mixed TiO_2 suggests an adsorption effect related to the molecular weight of the stabilizers. For example, CMC that has a greater molecular weight and longer chains in comparison to PVP can adsorb more on the NP surfaces, thereby exhibiting stronger binding with the NPs. This can result in larger particle sizes. Short chain dispersants may be more effective in stabilizing NPs in suspension which has been shown in other studies (Liufu, Xiao et al. 2005, Othman, Abdul Rashid et al. 2012).

Images of TiO_2 NPs in the presence and in the absence of the coating materials reveal that in their absence TiO_2 NPs were aggregated (Figure 4.1B). Interestingly, silica-coated IND clearly showed the distribution of silica with bonded connection surrounding TiO_2 NPs. These bonded clusters appear to significantly aggregate in comparison with those in the presence of either CMC or PVP. TiO_2 and SiO_2 NPs appear to have interconnected to form individual spheres. A similar observation was made in the study in which silica NPs did not coat TiO_2 NPs (Jaroenworaluck, Sunsaneeyametha et al. 2006).

According to one study, increasing the amount of silica in coatings on TiO_2 NPs was not correlated to change in physical characteristics, e.g., forming individual amorphous spheres

(Jaroenworaluck et al. 2006). However, another study (Zhang, Shi et al. 2009) showed that increasing the number of silica NPs resulted in a notable dispersion effect of the NPs. In this study elemental analysis (EDS) composition of IND, IND mixed with silica, and SUN were performed. The results confirmed Ti purity, to the detection limit of the method, in IND as well as 60% Ti and 40% Si from SUN and IND mixed with silica NPs (Fig. 4.1C). It is proposed that the differences in morphology, size, zeta potential, and stability in the presence of coating materials (CMC, PVP, and SiO_2) may affect the antibacterial effect of TiO_2 as well.

Table 1. Zeta potential, hydrodynamic diameter (nm), and TEM particle size (nm) of TiO_2 NPs.

NPs	Zeta potential (mV)	Hydrodynamic diameter (nm)	Particle size (nm)
IND TiO_2	14.23	625.7	29.4
CMC+IND TiO_2	-61.5	547.1	16.3
PVP+IND TiO_2	-43.6	206.6	9.8
SiO_2+IND TiO_2	-15	594.5	29.6
SUN TiO_2	-14.8	335.7	284.5

(A)

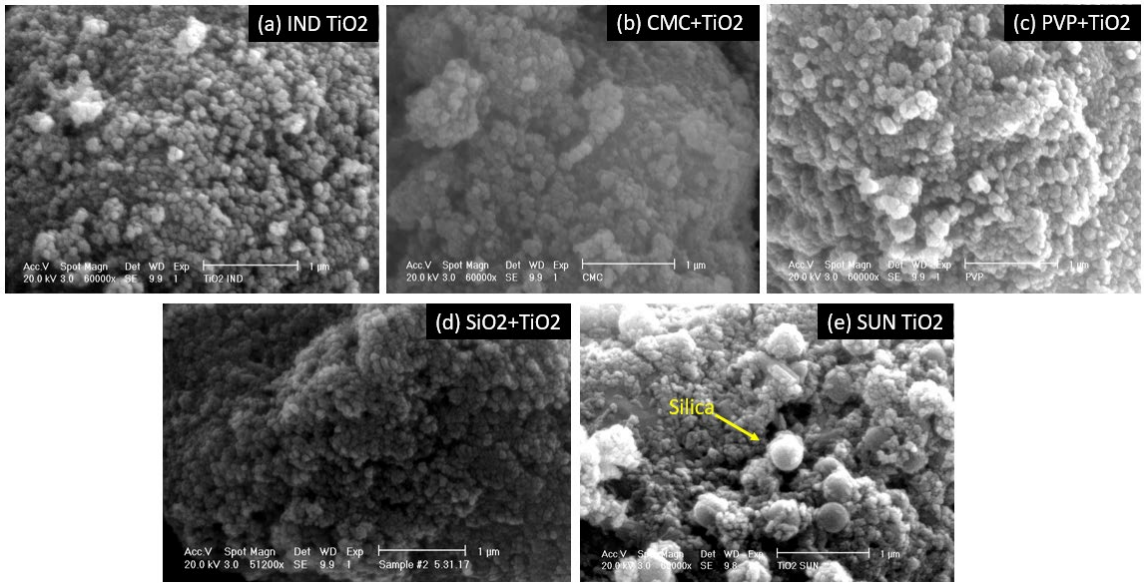
(a) IND TiO2
(b) CMC+TiO2
(c) PVP+TiO2
(d) SiO2+TiO2
(e) SUN TiO2
Silica

(B)

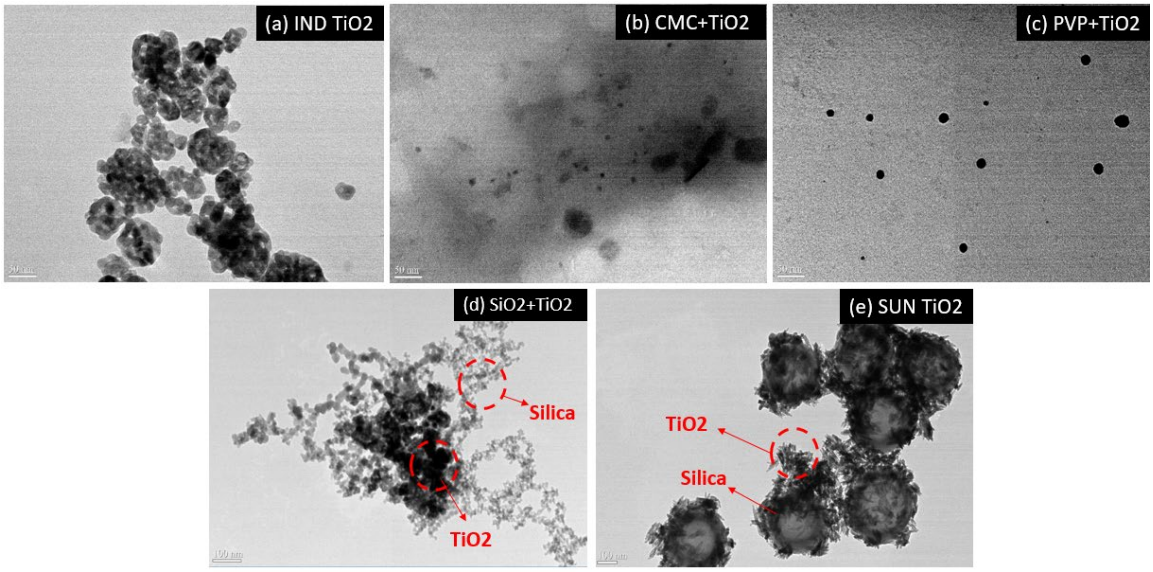
(a) IND TiO2
(b) CMC+TiO2
(c) PVP+TiO2
(d) SiO2+TiO2
(e) SUN TiO2
Silica
TiO2
Silica
TiO2

(C)

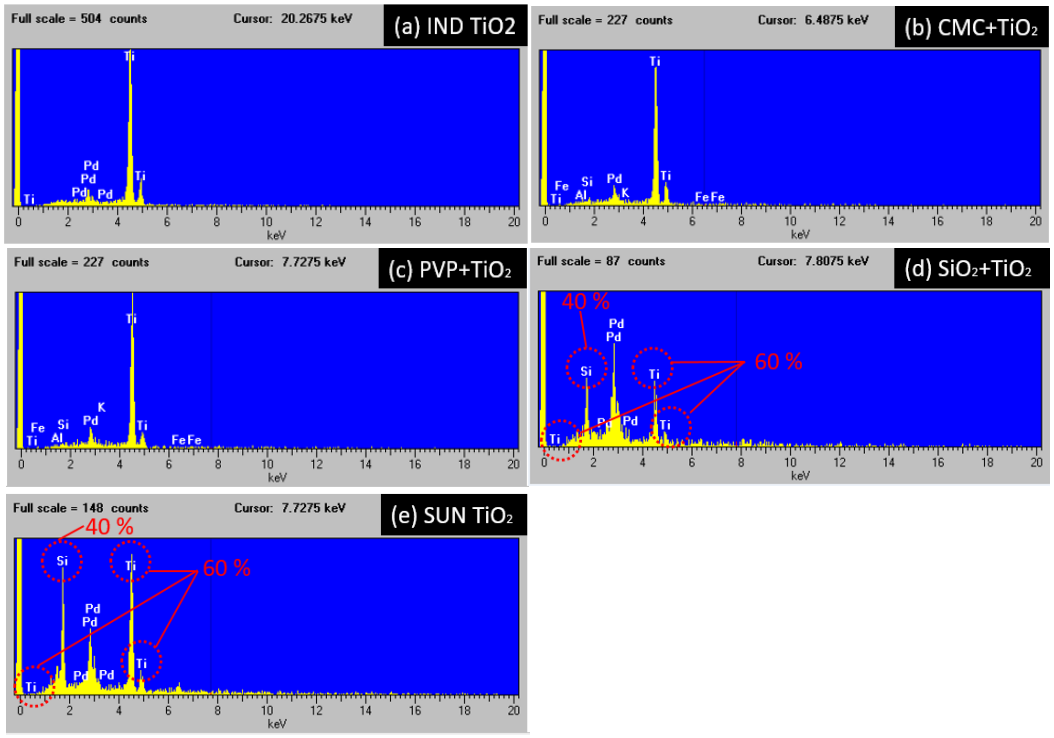

Figure 4.1. SEM (A) and TEM (B) images of 5 types of TiO_2 NPs: (a) IND TiO_2 (Industrial TiO_2 NPs), (b) CMC+IND TiO_2 NPs (Industrial TiO_2 NPs mixed with CMC), (c) PVP+IND TiO_2 NPs (Industrial TiO_2 NPs mixed with PVP), (d) SiO_2+IND TiO_2 NPs (Industrial TiO_2 NPs mixed with silica NPs), and (e) SUN TiO_2 NPs (Sunscreen-derived TiO_2 NPs); TiO_2 suspension concentration: 50 mg/L. EDS images of TiO_2 NPs (C) ; (a) IND TiO_2, (b) CMC+ IND TiO_2 NPs, (c) PVP+IND TiO_2 NPs, (d) SiO_2+IND TiO_2 NPs, (e) SUN TiO_2 NPs

4.3.2. The effect of coating materials on antibacterial properties of TiO_2 NPs on *E. coli*

The effect of commonly used coating materials (CMC, PVP, and silica) in consumer products on the antibacterial properties of TiO_2 NPs was investigated. *E. coli* was exposed to TiO_2 NPs for 6 hours and growth inhibition recorded as a function of time and concentration (Fig. 4.2a). Overall, bacterial growth was inhibited over time, and cell viability decreased significantly at the highest TiO_2 NP concentration (250 mg/L), and

similar growth inhibition was observed at lower concentrations. Above 50 mg/L of TiO_2 coated with PVP, a slightly higher antibacterial effect was evident compared to IND and CMC-coated TiO_2 NPs (Fig. 4.2a). At 250 mg/L of TiO_2 suspension, the coating materials (CMC and PVP) induced higher toxicity to *E. coli* with concentration-dependent increases. The greatest antibacterial effect was found in the order of PVP+TiO_2 > CMC+TiO_2 > IND. This order of toxicity appeared to correlate with particle sizes (IND > CMC+TiO_2 > PVP+TiO_2). Stabilizers such as CMC and PVP appear to increase the toxicity of TiO_2 due to smaller particle size of TiO_2. The attribution of smaller particle sizes to higher toxicity was also observed in other studies in which such an effect was revealed due to an increasing generation of ROS (Pagnout, Jomini et al. 2012, Lin, Li et al. 2014) or the degree of NP aggregation (Chowdhury, Cwiertny et al. 2012).

The antibacterial effect of TiO_2 on *E. coli* in the presence of silica was examined, and similar trends observed in Fig. 4.2a were found (Fig. 4.2b), namely increasing toxicity over longer time exposure and significant growth inhibition at the highest TiO_2 concentration (250 mg/L). Interestingly, a significant antibacterial effect (the lowest cell viability) from either SiO_2 mixed TiO_2 (SiO_2+TiO_2) or SUN at 250 mg/L of TiO_2 NPs was observed (Fig. 4.2b) with the order of SiO_2 coated TiO_2 > SUN > IND. This indicates that cell viability is influenced by the type of surface coating and particle sizes. Such bacteria inactivation by the presence of silica could also be due to increasing ROS.

According to one study, the catalytic activity of TiO_2 is particle size dependent, and the addition of silica NPs exhibited a scattering effect, which may then attribute to the TiO_2 particle size (Van Grieken et al. 2002). In another study (Jafry, Liga et al. 2011), TiO_2 NPs coated with silica exhibited higher toxicity than uncoated TiO_2 NPs, due to an enhanced

surface area of TiO_2 doped with silica NPs, resulting in increased adsorption and reactivity on cells. The slightly different toxicity between silica-coated IND and SUN could be due to their physicochemical characteristics. For instance, the significantly larger particle size observed in SUN (Fig. 4.1b) compared to the particle size in SiO_2-coated IND may have resulted in a slightly lower antibacterial effect. While the higher growth inhibition due to SUN compared to cell viability due to IND could be caused by the chemical composition effect in the presence of silica (e.g., complexation or adsorption of Si on TiO_2) rather than physicochemical properties of TiO_2.

(a)

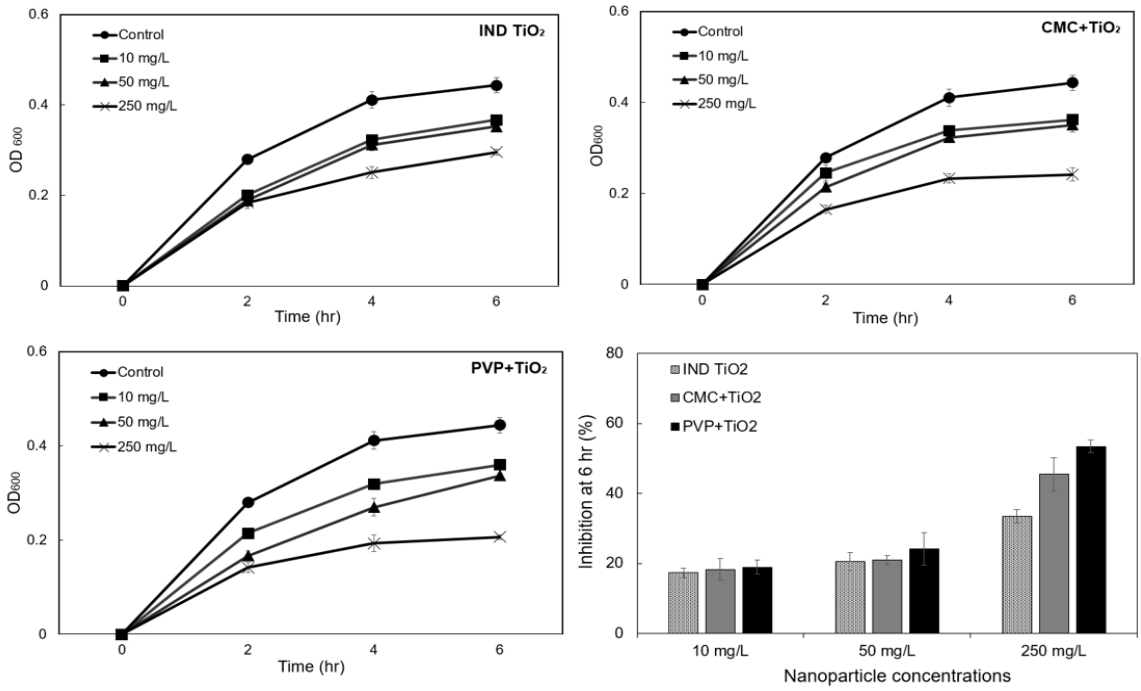

(b)

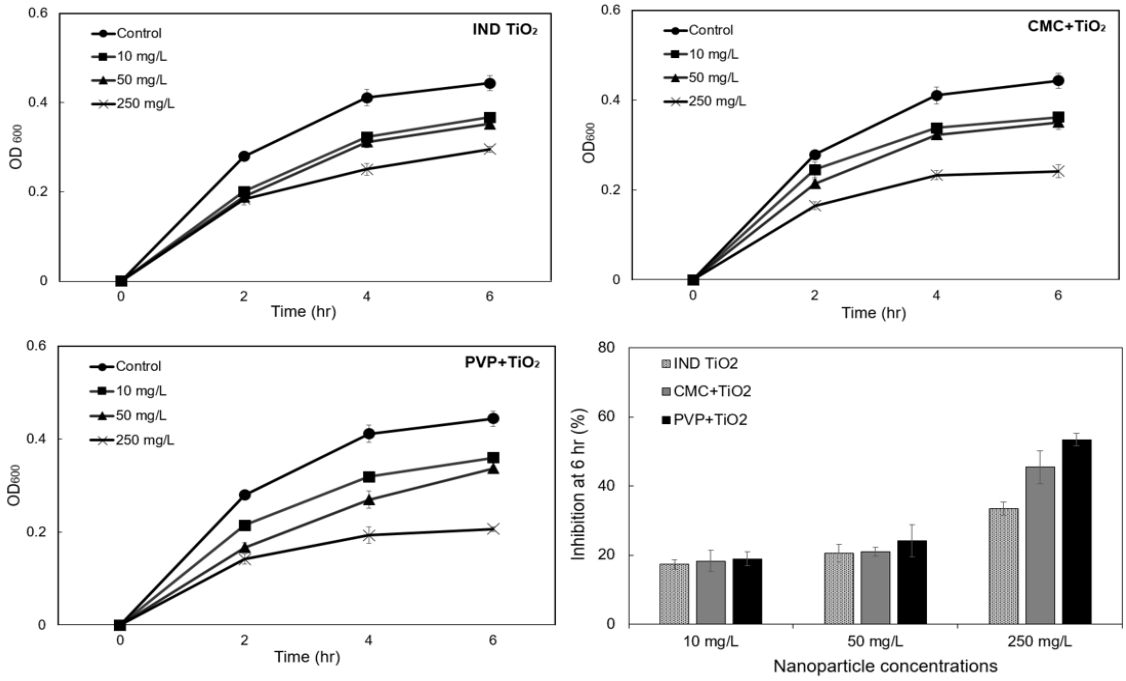

Figure 4.2. Growth curves of *E. coli* at different concentrations (control as well as 10, 50, and 250 mg/L) and cell-growth inhibition rate (%) of (a) TiO_2 NPs with and without organic coating materials: IND TiO_2 NPs, CMC+ IND TiO_2 NPs, and PVP+IND TiO_2 NPs, (b) TiO_2 NPs with and without inorganic coating materials; IND TiO_2 NPs, SiO_2+IND TiO_2 NPs, and SUN TiO_2 NPs derived from sunscreen.

4.3.3. Toxicity assessment of TiO_2 NPs in the presence and absence of coating materials

The release of ROS (hydroxyl, superoxide radicals, hydrogen peroxide, and singlet oxygen) occurs when TiO_2 absorbs UV light as a semiconductor, generating electrons and positively charged holes (h^+) (Carlotti, Ugazio et al. 2009, Gupta and Tripathi 2011). TiO_2 NPs are known not only to induce oxidative stress and DNA damage in *E. coli* cells but also regarding the effect of coating materials on their antibacterial effect on *E. coli*. To identify such an effect of coating materials, ROS generated from TiO_2 NPs was assessed

in the presence and in the absence of the coating materials under room-light conditions, after the exposure of TiO_2 NPs to *E. coli* over 6 hours. Overall, ROS generation appears to increase with concentration and exposure duration. Although toxicity effects were most significant in PVP-coated IND, followed by CMC-coated IND and IND, ROS generation was similar among the three types of TiO_2. These results suggest that CMC and PVP coating materials may react with ROS generated from TiO_2, scavenging ROS as per the following chemical reaction (Joo and Zhao, 2008):

$$^{\bullet}OH + CMC \rightarrow H_2O + CMC^{\bullet} \quad (1)$$

The pseudo-first-order rate constant is reported as 1×10^9 $M^{-1}s^{-1}$ (Wach et al., 2004). Interactions of TiO_2 NPs with stabilizers have been shown to inhibit ROS generation (Tuchina and Tuchin 2010). Other studies proposed the generation of ROS from NPs, and describe the interaction of NPs with cellular components (Hegde, Brar et al. 2016, Wang, Lin et al. 2016, Wang, Zhu et al. 2016). A study reported that polymer coatings blocked or eliminated the photocatalytic activity of TiO_2 NPs, thereby minimizing free radical formation on TiO_2 surfaces (Lee, Pernodet et al. 2007).

A similar observation was shown in other studies where the correlation between growth inhibition of treated *E. coli* and ROS generation was inconsistent (Kumar, Pandey et al. 2011, Dalai, Pakrashi et al. 2012). Instead of the ROS effect, particle size may have attributed to the toxicity. Kumar et al. (2011) confirmed that a significant uptake of TiO_2 NPs occurs on *E. coli* using electron microscopy, through the adhesion of aggregated NPs on surfaces of bacteria and subsequent changes in morphology (Kumar, Pandey et al. 2011). NPs may penetrate bacterial cell membranes and inhibit their metabolic enzymes (Pal, Tak et al. 2007).

Figure 4.3B shows ROS generation from IND, SiO_2-coated IND and SUN by measuring fluorescence intensity ratio (%) after exposure of TiO_2 to *E. coli* over 6 hrs. The results show significant generation of ROS from silica-coated IND at 250 mg/L of TiO_2. As indicated earlier, the toxicity was on the order of SiO_2-coated IND > SUN > IND, indicating that the greatest toxicity observed in SiO_2-coated IND could be due to a significant amount of ROS. The presence of silica appeared to increase the surface area and the band structure through the quantum-size effect and thus enhancing the photocatalytic activity of TiO_2 (Kim, Shul et al. 2005). The quantum-size effect, i.e. that the energy gap between the valence and conduction bands is enlarged as the particle size of TiO_2 decreases, was based on the band theory in quantum mechanics (Zhang, Shi et al. 2009). Increasing the band-gap energy of TiO_2 on the silica surface has been described in other studies (Kim, Shul et al. 2005, Park and Kang 2005, Zhang, Shi et al. 2009).

The lower ROS generation from SUN compared to that from SiO_2-coated IND could be due to the larger particle size shown in SUN. The generation of ROS is likely inhibited by either chemical compositions or larger particle sizes and surface areas of NPs (Xiong, Fang et al. 2011). Similarly, *E. coli* exposed to SiO_2-coated IND produced more ROS compared to SUN due to the smaller particle size observed in SiO_2-coated IND. As indicated in other studies and demonstrated in our work, the correlation between ROS generation and antibacterial activity is influenced by physicochemical properties and chemical composition of the coating materials (Park, Bae et al. 2013, Leung, Xu et al. 2016).

(a) **(b)**

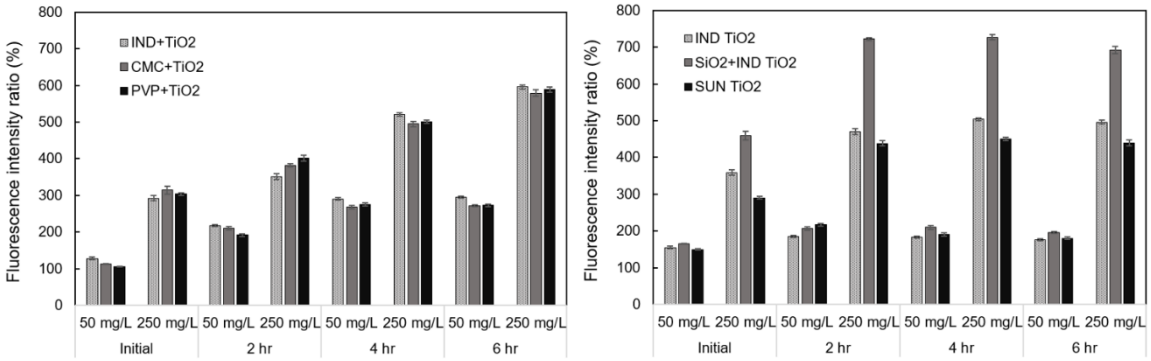

Figure 4.3. ROS generation assessment of five types of TiO_2 NPs (50 and 250 mg/L) by fluorescence intensity ratio (%) after exposure to *E. coli* over 6 hours in the presence of (a) organic coating materials and (b) inorganic coating materials.

4.3.4. Interaction between cells and NPs analyzed by SEM, TEM and FT-IR

To gain insight into TiO_2 antibacterial effects on *E. coli* related to the coating materials, SEM and TEM images of *E. coli* after exposure to TiO_2 NPs at different concentrations in the presence and in the absence of the coating materials were examined. Bacteria exposed to three types of TiO_2 NPs at 50 and 250 mg/L were examined in the SEM (Figure 4.4). At the high NP concentration (250 mg/L), more aggregated forms appeared, and more NP particles were attached to cells, whereas at the low concentration (50 mg/L), fewer aggregations were seen. Attachment of NPs to cell membranes and indications of damage, were particularly notable at the high concentration of TiO_2 NPs. Such marked cell disruption seen at high concentrations of NPs have also been found in other studies (Kim, Shul et al. 2005, Hegde, Brar et al. 2016, Leung, Xu et al. 2016).

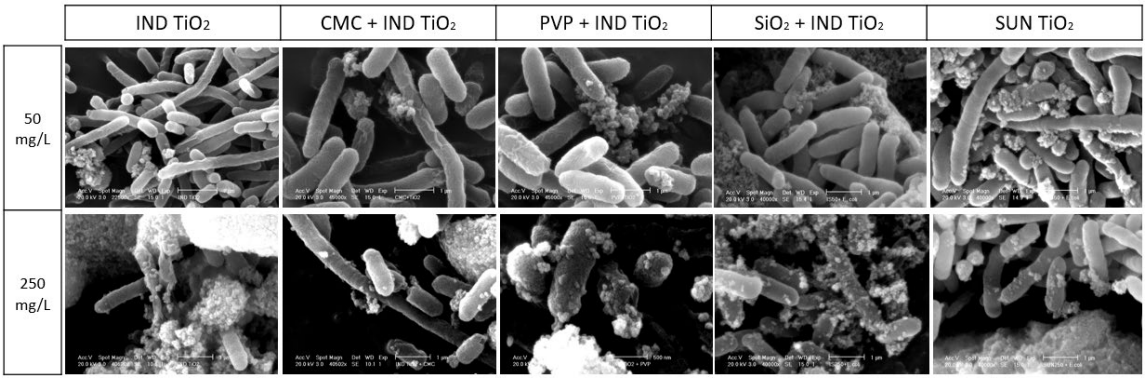

Figure 4.4. SEM images of *E. coli* after exposure to different TiO_2 NPs (in the absence and in the presence of organic and inorganic coating materials) in different concentrations: Industrial TiO_2 NPs, CMC+IND TiO_2 NPs, PVP+IND TiO_2 NPs, SiO_2+IND TiO_2 NPs, and SUN TiO_2 NPs derived from sunscreen at 50 and 250 mg/L concentrations.

It is possible that cell damage is caused by ROS generation, the antibacterial effect due to the interaction between NPs and cell membranes was found in the absence of ROS in a recent study (Leung, Ng et al. 2014). The ultrastructural relationships in fixed and sectioned bacterial cells after treatment with 250 mg/L of each material including, IND, CMC-coated IND, PVP-coated IND, SiO_2-coated IND, and SUN are shown in Figure 4.5. While IND-exposed cells showed significant adsorption of IND to the *E.coli* cells, several aggregated forms surrounded the cells (Figure 4.5A). In addition, some penetrated into the bacterial cells through intercellular interactions and were associated with cell damage (Figure. 4.5B).

CMC-coated IND (CMC+IND) showed aggregates in the cells through similar mechanisms to those in IND. These include adsorption of NPs on the cells, intracellular interactions between NPs and the cells, cell damage, and penetration of the NPs into the cells (Figures 4.5C and D). Some of the cells appeared dead with clear intracellular space, while some of the apparently living cells remained surrounded by NPs (Figure 4.5C). Significant numbers of dead cells observed in both CMC-coated IND and PVP-coated IND

could be associated with smaller particle sizes that enabled IND to cause more toxicity. Dead cells appeared to show leakage of cell contents (Figure 4.5D), and images support the antibacterial effect. These include lower toxicity from IND compared to that from CMC-coated IND and PVP-coated IND. Similarly, PVP-coated IND adhered to cell surfaces. Cells surrounded by NPs with transparent intracellular space were certainly dead, while other cells not in direct contact with the NPs remained intact (Figures 4.5 E and F).

Direct physical deformation such as membrane deformation and cell wall damage were observed in PVP-coated IND with black colors showing the adhesion of the NPs onto the cell surfaces. While intracellular interactions are not apparent in PVP-coated NP, more severe membrane damage occurred compared to those in CMC-coated IND and uncoated IND. Adsorption of NPs on cells may inhibit bacterial movement, causing cellular metabolic disturbance and cell death. Similar observations of the disruption of bacterial membranes are also found in other studies (Dalai, Pakrashi et al. 2012, Lin, Li et al. 2014, Leung, Xu et al. 2016, Wang, Lin et al. 2016). Coating materials may facilitate more interactions on the bacteria surfaces, and ROS generated from the NPs may result in disruption of the bacteria cell membranes (Lin, Li et al. 2014). Studies reveal that interactions between cells and NPs vary depending on the NPs composition, coating materials, and model organisms used (Xiong, Fang et al. 2011, Batley 2012).

In contrast, images of the ultrastructure of sectioned bacteria cells treated with 250 mg/L of SUN and SiO_2-coated IND did not exhibit cell attachment (Figure 4.5, G~J). Although they appeared to form aggregates, NPs were not attached to the bacteria membranes (Figure 4.5 G–H). Similarly, larger aggregates of NPs around the cells were observed from SUN, but the NPs were not interacting with the cells (Figure 4.5 I–J). Such large SUN aggregates

indicate their relatively large particle size, which is consistent with results from TEM particle-size distribution analysis. Notably, while CMC+IND and PVP+IND induced cell distortion, internalization, and membrane damage, the presence of silica (either SiO_2-IND or SUN) did not cause penetration of NPs into the bacterial membrane.

(a)

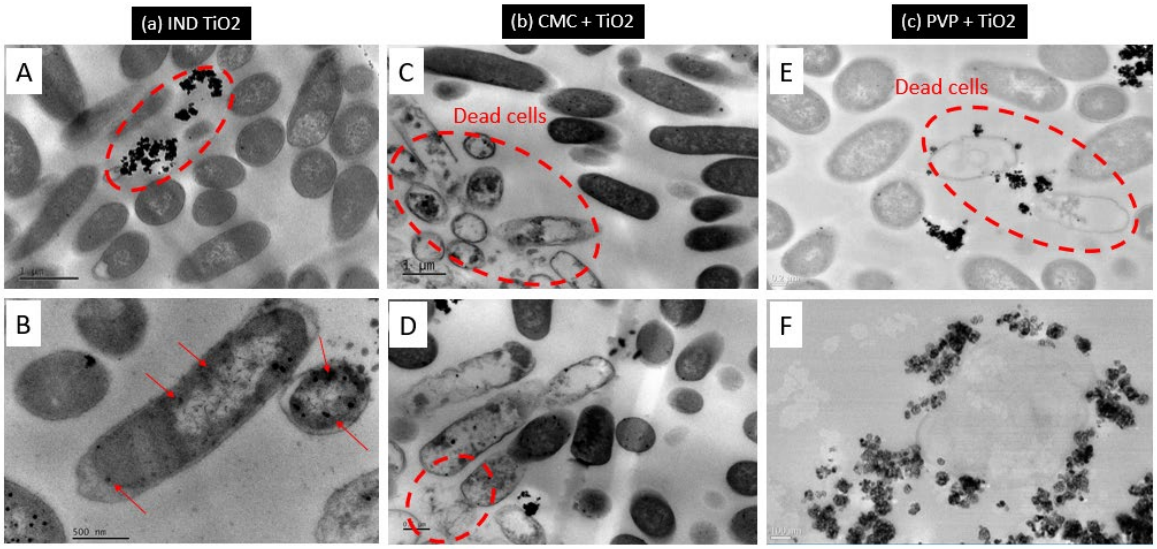

(b)

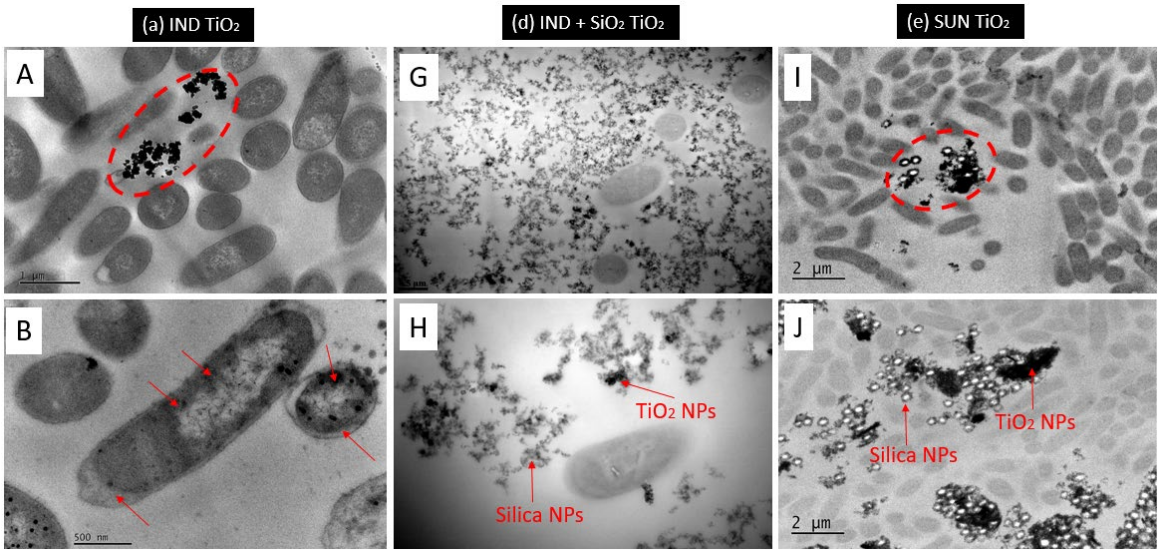

Figure 4.5. *E. coli* ultrastructure (TEM) after exposure to three different TiO_2 NPs (a) in the absence and in the presence of organic coating materials: IND TiO_2 NPs, CMC+IND TiO_2 NPs, and PVP+IND TiO_2 NPs, (b) in the absence and in the presence of inorganic coating materials: IND TiO_2 NPs, SiO_2+IND TiO_2 NPs, SUN TiO_2 NPs derived from sunscreen at 250 mg/L of NP concentration.

FTIR spectroscopy was employed to gain insight into chemical interactions with NPs. The FTIR patterns of TiO_2 NPs with organic coating materials (CMC and PVP; Figure 4.6a) and silica (Figure 4.6b) were examined. As shown in Fig. 4.6a, IND, CMC-IND, and PVP-IND had similar patterns without notable peaks. The broad band at approximately 650–800 cm^{-1} was attributed to the absorption peak of Ti–O, confirming the presence of TiO_2 in all the samples (Mirabedini, Mirabedini et al. 2011, Guo, Wang et al. 2013, Zhang, Shi et al. 2014, Cai, Liu et al. 2015, Wu, Liao et al. 2017). Fig. 4.6 (b) shows absorption peaks of Si-O-Si at 1,081 cm^{-1} from SiO_2-coated IND and at 1,016 cm^{-1} from SUN, respectively, due to the presence of silica in solution (Feng, Zhang et al. 2015, Wang and Chen 2015). Another absorption peak of Ti-O-Si at 924 cm^{-1} occurred in SUN. Other studies have described the formation of Ti-O-Si bonds, which are related to the photocatalytic activity between 910 and 960 cm^{-1}. As shown in Figure 4.5b, TiO_2 NPs were evenly distributed in the presence of SiO_2 NPs. This suggests silica is a catalyst that increases hydrophobic properties of NPs, thus enhancing the reactivity of TiO_2 by stabilizing its particles (Rasalingam, Peng et al. 2014).

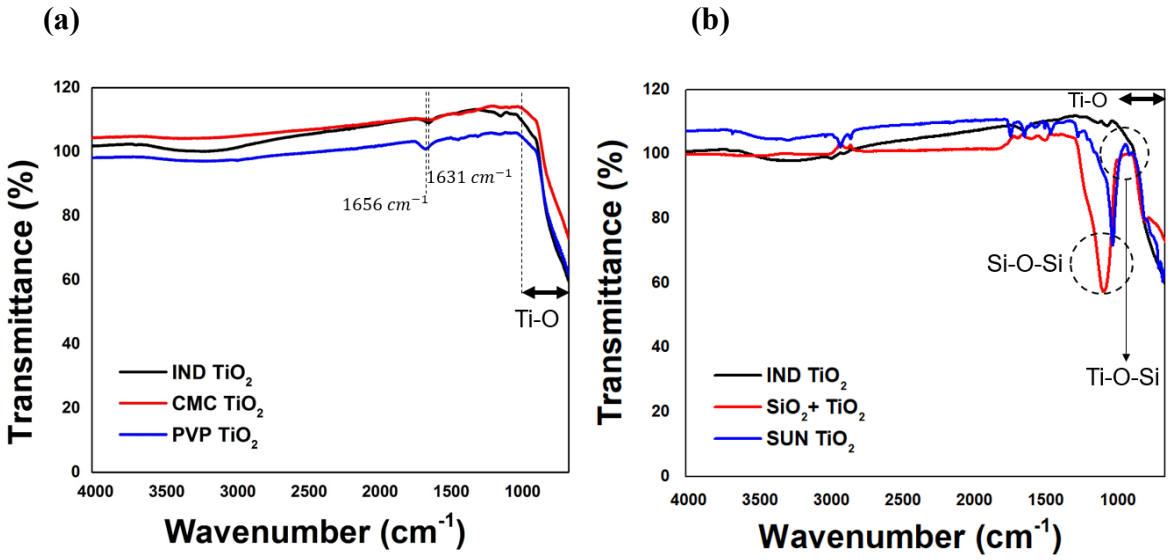

Figure 4.6. FTIR spectra of TiO_2 NPs (a) in the absence and in the presence of organic coating materials (CMC and PVP): IND, CMC-coated IND, and PVP-coated IND, (b) in the absence and in the presence of inorganic coating materials: IND, SiO_2-coated, IND, and SUN.

4.4. Conclusions

In summary, the addition of coating materials such as CMC, PVP and silica were found to prevent significant TiO_2 aggregation through dispersion. Such stabilizers changed physicochemical properties (particle sizes and zeta potential) of TiO_2 NPs. Although CMC- or PVP-coated TiO_2 NPs produced stable TiO_2 suspension, with a cluster size smaller than that of uncoated TiO_2 NPs, there was no difference in ROS generation between uncoated and coated TiO_2 NPs, indicating possible scavenging of ROS by CMC and PVP. Coated TiO_2 is related to significant cell death through interactions with bacteria membranes and/or penetration into the cells. This finding is consistent with culture results showing significant growth inhibition of *E. coli* due to CMC-IND or PVP-IND at the highest concentration of TiO_2 NPs. Significant antibacterial growth inhibition was observed in silica-coated IND and SUN but not in uncoated IND at the highest concentration of TiO_2

NPs. However, in contrast to CMC- and PVP-coated IND, substantial ROS generation was observed in silica-coated IND, notably at the highest concentration of IND. This may be due to the increasing reactivity of TiO_2 NPs due to stabilization by silica.

These findings have implications to the development of nanoproducts that use coating materials This is because 1) the types of coating materials affect the stability and the reactivity of TiO_2 NPs, 2) smaller more stable particle sizes exhibit higher toxicity, and 3) silica-coated TiO_2 has a more significant antibacterial effect than that of CMC- or PVP-coated TiO_2 NPs. Additional future research needs to evaluate the accumulation of NPs in microorganisms using different types of coated TiO_2 nanoproducts under well-controlled environmental conditions. These include controlled exposure time series experiments, variability in exposure media, UV radiation, temperature, and co-existing contaminants that may contribute to synergistic microorganism growth inhibition.

CHAPTER 5:

ANTIBACTERIAL EFFECTS OF NANOHYBRIDS AND THEIR TOXICITY MECHANISMS ON ANTIBIOTIC-RESISTANT BACTERIA[3]

[3] Baek, S., Joo, S. H., Su, C., Toborek, M. (2018) Antibacterial effects of graphene- and carbon-nanotube-based nanohybrids on Escherichia coli: implications for treating multidrug-resistant bacteria in water. *Journal of Environmental Management.* (under review)

5.1. Background

Nanomaterials, due to their unique mechanical and catalytic properties and electrical conductivity, have been widely applied for manufacturing industrial products, with an exponential potential increase of nanomaterials, particularly ZnO, TiO_2, carbonaceous nanomaterials, silver, and iron in the future (Klaine 2008); (Batley 2012, Jeon, Kim et al. 2016). Metal oxides, particularly ZnO and TiO_2, are commonly exploited in cosmetics, paints, coatings, and solar cells because of their photocatalytic properties (Wang, Lin et al. 2016). Similarly, two commonly used nanomaterials graphene oxide (GO) and carbon nanotubes (CNTs) are found in various industrial applications. For instance, GO—a monolayer of carbon atoms that are packed into a two-dimensional structure—is chemically modified with oxidizers on graphene with a large number of oxygen bonds to be used as a dispersant in water (Wenbing Hu 2010, Wang, Cao et al. 2014). Such unique properties enable GO to provide a large active site with other metals through both electrostatic and coordinate approaches (Wang, Cao et al. 2014). CNTs, primarily consisting of carbon, have been widely used, especially in plastics, catalysts, batteries, electronic components, aircrafts, and automotive industries, in photocatalytic applications because of their effectiveness in catalyzing materials (Akhavan, Azimirad et al. 2011) and to design semiconductor materials for the synergetic combination of their unique electrical and structural properties (Das, Abd Hamid et al. 2014).

Thus, there is an increasing concern about the release of nanomaterials in the environment, and very few materials are released as single-type nanoparticles; rather, materials exhibit a heterogeneous form, including nanohybrids in the environmental media (Klaine 2008,

Weir, Westerhoff et al. 2012, Wang, Lin et al. 2016). Several studies have found that nanoparticles affect aquatic organisms through toxicity causing mechanisms, including reactive oxygen species (ROS) generation, release of metal ions, and disruption of the cell membrane (Kumar, Pandey et al. 2011, Batley 2012, Lin, Li et al. 2014). Despite a number of reports on toxicity effects of nanomaterials (Wang, Zhu et al. 2016, Baek, Joo et al. 2018, Choi, Kim et al. 2018), few studies have investigated antibacterial effects of nanohybrids. Combined nanocomposites are found to not only offer a large surface area but also increase the photocatalytic effect (Huang, Zang et al. 2014). Given recently emerging concerns about multidrug-resistant bacteria detected in water (Jerome, 2016) and drug-resistant contaminated surface water, especially after a hurricane (Guarino, 2017), it is imperative to explore antibacterial effects of nanohybrids and develop a cost-effective and safe treatment application of nanomaterials to minimize risks associated with such contaminants in water. This study aims to (1) characterize four types of synthesized nanohybrids (NHs) using *scanning electron microscope* (SEM), *transmission electron microscope* (TEM), Fourier-transform infrared spectroscopy (FT-IR), and thermal gravimetric analysis (TGA), thereby identifying antibacterial properties and changes in physicochemical characteristics of NHs, (2) identify antibacterial effects of ZnO/TiO_2-conjugated GO- and CNT-based nanohybrids, and (3) explore mechanisms attributable to antibacterial effects of NHs on *Escherichia coli* (DH5α, a multidrug-resistant coliform bacterium). *E. coli* (DH5α) was selected since it is the foundation of aquatic ecosystems (van Elsas, Semenov et al. 2011) and one of *aquatic* indicator organisms, yet it is classified as one of multidrug-resistant coliform bacteria (Tetz et al., 2012; Molina-Aja et al., 2002; Kedzierska et al., 1999).

5.2. Materials and Methods

5.2.1. Materials

Single Layer Graphene Oxide (GO, >99% purity, bulk density of 0.26 g/cm^3, diameter of 1~5 μm, thickness of 0.8~1.2 nm, Hummers' method) was supplied by ACS Material (CA, USA), and carbon nanotube, multi-walled (MWCNT, >98% purity, 6-13 nm (O.D) × 2.5-20 μm (L)) was purchased from Sigma-Aldrich (MO, USA). $ZnCl_2$ (>99.99%) and zinc nitrate hexahydrate ($Zn(NO_3)_2 \cdot 6H_2O$, >98%) for ZnO nanocomposite synthesis, and titanium oxysulfate solution ($TiOSO_4$, ~15 wt%, 99.99%) for TiO_2 nanocomposite synthesis were purchased from Sigma-Aldrich (MO, USA).

5.2.2. Synthesis of NHs

ZnO-GO nanohybrid was synthesized following the previous literature (Fu, Jiang et al. 2018). 50 mg of GO was dispersed into 100 mL of DI water under ultrasound for 1 h. Then, the GO solvent was centrifuged with 4000 rpm, and 5 mmol of $Zn(NO_3)_2 \cdot 6H_2O$ was added with pH adjusted to 8 using ammonia water. After sonication, the mixture was autoclaved and heated at160 °C for 10 h. The mixture was separated by centrifugation and washed with DI water and the ZnO-GO was obtained after being dried under vacuum at 60 °C for 24 hours.

ZnO-CNT were synthesized following the previous literature (Wang, Xia et al. 2008). Nitric acid (80%) were added to multi walled carbon nanotube at 80 ℃ for 4 hours and then washed with DI water several times. $NH_3 \cdot H_2O$ solution slowly added into the $ZnCl_2$ solution under stirring, then the white precipitate disappeared to form $Zn(NH_3)_4^{2+}$. Then, CNTs were solution were soaked in to this solution for 48 h, and centrifuged. The obtained

products were dried at 70 ℃ in vacuum oven, and then calcined at 300 °C for 4 hours at an atmosphere of nitrogen.

TiO_2-GO was prepared following the previous literature (Stengl, Bakardjieva et al. 2013). Ammonium hydroxide solution (10%) was added slowly into 100 ml of 1.6 M $TiOSO_4$ under constant stirring at temperature of 0 ℃ in ice bath until a homogeneous mixture reached pH 8.0. The white precipitate was obtained by filtration and mixed with 100 ml of 15% hydrogen peroxide solution. After yellow solution of titania peroxo complex was obtained, 50 mg of GO was dispersed in water using sonicator and added into the yellow solution of titania peroxo complex. Next, the mixture was annealed at a heated mantle in a round bottom flask with a reflux cooler at 100 ℃ for 48 hours. Finally, the resultant product was filtered off and dried at 105 ℃ for 10 hours.

TiO_2-CNT were synthesized following the previous literature (Huang, Zang et al. 2014). 50 mg of multiwall carbon nanotube (MWCNT) was added in to a 100 mL of $TiOSO_4$ (0.01M) solution, and 1 ml of H_2SO_4 (0.2M) under ultrasound. Then the suspension was refluxed in a thermostatic water (80 °C) for 72 hours, ad suspension was dispersed for 10 min every 6 hours to avoid the agglomeration of MWCNTs.

5.2.3. Nanoparticles characterization (SEM, TEM, EDS, FT-IR, TGA)

The morphologies, elemental analysis, and the nanostructure of the particles were characterized with Field Emission Scanning Electron Microscopy (SEM, Philips XL-30 FEG), Energy Dispersive Spectroscopy (EDS), and Transmission Electron Microscopy (JEOL 1400 TEM).

For SEM preparation, a small sample of each particle was coated with a thin (20 nm) coating of Pd in a Cressington Sputter coater. Samples were then placed in a FEI XL-30 Field Emission Scanning Electron Microscope and imaged at several magnifications. For SEM preparation of control and experimental *E. coli* cultures, each was preserved according to the following protocol. Cultures were initially fixed in 2% glutaraldehyde in PBS buffer. Samples were then rinsed 3 times for 5 min each in PBS buffer, and dehydrated 3 times for 5 min each in a graded series of ethanol (20, 50, 70, 95, and 100%). Following dehydration, samples were dried in 3 changes for 5 min each in HMDS. Samples were allowed to outgas overnight, placed on stubs, and coated as outlined above.

EDS in SEM particulate samples were examined at various magnifications and X-rays collected using scan speed 2 at working distance of 10 mm. The elemental spectra produced were then saved and subjected to semi-quantitative analysis using the EDS software to collect relative elemental percentages present. An Oxford EDS system fitted on the SEM was used for this analysis.

Samples for TEM were diluted and a drop of the solution placed on a copper grid and allowed to air dry. The samples were then imaged at several magnifications and imaged in a Philips CM-10 TEM (Eindhoven, Netherlands) at the Miller School of Medicine TEM Core at the University of Miami. Cell cultures were prepared as described above for SEM until after the final dehydration step. After dehydration in 100% ethanol, samples were placed in molds containing spur embedding resin and polymerized for 3 days at 60 ℃. Following polymerization, the blocks were sectioned using a Porter Blum MT2 ultramicrotome fitted with a diamond knife, and sections were then floated onto grids and imaged.

Fourier transform infrared (FT-IR) spectra was used to identify the different functional groups that are present in nanocomposites by measuring the vibrational frequencies of the chemical bonds. The sample powders were ground and compressed into a pellet whose spectra in the 600-4000 cm^{-1}, and measured with Perkin Elmer Frontier FTIR (MA, USA).

The decomposition behavior of the NHs was analyzed by thermos gravimetric analysis (TGA) using a TGA55 (DE, USA). About 20-30 mg of the sample was loaded on a pan and the temperature was ramped at the rate of 10 ℃ per minute from ambient to 1000 ℃ in an inert atmosphere which has been purged with nitrogen.

5.2.4. *E. coli* cell cultivation and cell viability analysis

The antibacterial properties of the NHs were evaluated on *Escherichia coli* bacteria. *E. coli* colony was cultivated with MAX Efficiency DH5α Competent Cells (Invitrogen, CA). *E. coli* cells were incubated in culture tube containing 4 mL of LB broth at 37 ℃ under shaking at 225 rpm for 14 h. A 100 µL of cell suspension was incubated in 1 L flask containing LB broth at 37 ℃ under shaking at 225 rpm for 14 h. The cultivated cells were exposed to 4 different types of NHs (NHs) suspensions (i.e. 10, 100, and 300 mg/L) in 4 mL of LB broth. *E. coli* exposed to NHs suspension were incubated at 37 ℃ under shaking at 225 rpm for 6 h. A sample was taken every 2 h into a 96-well plate and the optical density (OD_{600}) was measured at 600 nm with a microplate reader (Spectra MAX 190, Molecular Devices, CA). The ratio of *E. coli* cells growth inhibition (%) was calculated as percentage of survived cells compared to control cells after 6 h of exposure. Samples were plated in triplicate, and all experiments were performed under sterile conditions.

5.2.5. ROS detection

Cellular Reactive Oxygen Species (ROS) generation was quantitated by using DCFDA cellular ROS detection assay kit (Abcam Inc, Toronto, ON, Canada). The assay uses the cell reagent 2',7' –dichlorofluorescin diacetate (DCFDA), and a fluorogenic dye that measures hydroxyl, peroxyl, and another ROS activity within the cell. *E. coli* cells exposed to 4 different NHs suspension was collected in a conical tube and washed by centrifugation in PBS. The cells were resuspended in the diluted DCFDA solution and incubated at 37 ℃ for 30 minutes in the dark. The antioxidant *N*-acetyl cysteine (NAC) was used to investigate the effect of ROS scavenger to confirm the toxicity mechanism. NAC has been commonly used as an ROS inhibitor by promoting production of antioxidant enzymes or providing precursor for glutathione synthesis (Ma, Wallis et al. 2014). To do this, cell cultures were pretreated with and without NAC (0.5 and 2 mM) and exposed to 100 mg/L of NHs for 72 h. Then, cells in presence and absence of NAC were transferred into clear bottom 96-well microplate after washed by centrifugation with PBS buffer. DCF was detected by fluorescence spectroscopy with maximum excitation and emission spectra of 485 nm and 535 nm in the presence of buffer.

5.2.6. Statistical analysis

All of experiments were performed at least in triplicate. The statistical analysis was performed using the statistical student's *t*-test with Graph Pad Prism 3.0 (Graph Pad Software Inc., San Diego, CA), all data were examined of statistical significance at $p < 0.05$.

5.3. Results and discussion

5.3.1. Characterization of NHs

The formation of ZnO and TiO_2 and their compounding with the CNT and GO has synthesized simultaneously in the hydrothermal process. Nanosized materials were found in all NHs samples in SEM, and TEM images, and demonstrating that NHs have been successfully synthesized (Figure 5.1). ZnO-GO images (Fig. 5.1A) showed that ZnO nanoparticles aggregated occasionally, and large aggregated clusters covered the surface of big smooth plate formed GO sheet. Irregular agglomerate dispersions can be seen around the GO sheet, and TEM image of ZnO-GO (Fig. 5.1B) also provided existence of ZnO NPs on GO surface. Images C and D in Figure 5.1 illustrate synthesized TiO_2-GO. Nanosized TiO_2 NPs clusters have formed along the side between GO sheets, and it seemed to have contact between the surface of GO sheet and TiO_2 NPs in Figure 5.1D. However, the aggregated size of TiO_2 onto the GO was seen to be larger and less dispersed compared to ZnO-GO, although TiO_2 aggregation were still observed with nano-sized. From the morphological images, it is observed that the high surface area and morphology of GO sheets effectively promoted the dispersion of metal oxide NPs on it. Thus, almost all the ZnO NPs are uniformly distributed on the GO sheet compared to TiO_2-GO. Figure 5.1E, G showed the CNT coated with ZnO, and TiO_2 NPs respectively. Both ZnO, and TiO_2 NPs were well dispersed onto the CNT, and CNTs act as substrates for the ZnO and TiO_2 NPs crystallites (Byrappa, Dayananda et al. 2008). However, it can be observed that metal oxide NPs loaded on CNTs are more aggregated each other compared to metal oxide NPs loaded on GO sheets. Thus, TiO_2 NPs on CNTs had bigger aggregation cluster than that of ZnO NPs on CNTs which is similar to above results with GO sheet (Fig. 5.1H). Figure 5.1F, and

1H showed that TEM images of CNT decorated by spherical ZnO NPs, and rod-shaped TiO_2 NPs respectively. The surface of ZnO-CNT shows ZnO NPs are fixed in aggregated structure of CNT (Upasani, Sreekumar et al. 2017). For TEM image of TiO_2-CNT (Fig 5.1H), it can be found that TiO_2 NP is made through the self-assembly of rod shape of TiO_2 NPs. Aggregations of GO based nanocomposites onto ZnO and TiO_2 seemed to have more reactive sites and dispersed uniformly than CNT based nanocomposites due to its flat shape, and considerable portion of metal oxide nanoparticles onto GO compared to CNT.

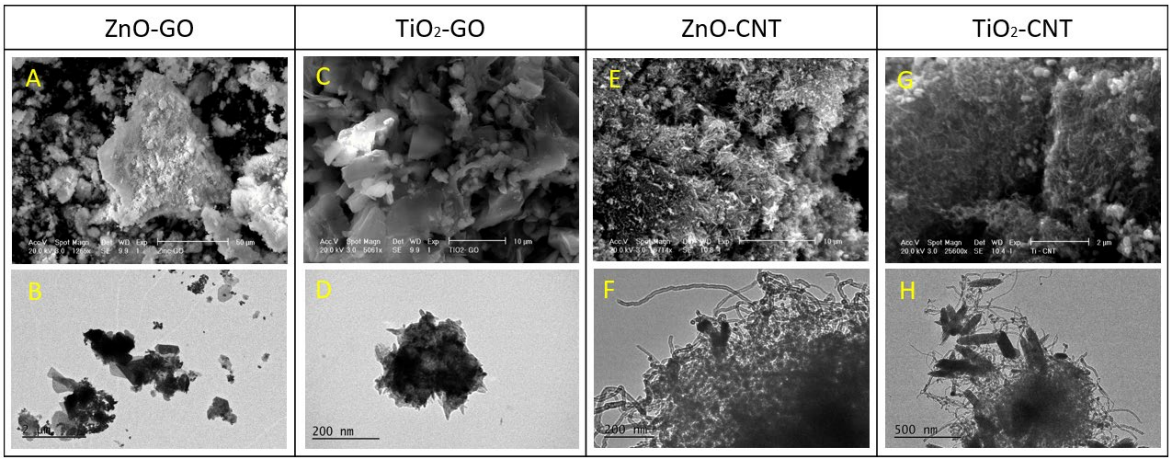

Figure 5.1. SEM and TEM analysis of 4 types of NHs

Figure 5.2(A) shows the Raman spectra of pure nanoparticles (GO, CNT, ZnO, and TiO_2) and nanocomposites (ZnO-GO, ZnO-CNT, TiO_2-GO and TiO_2-CNT). The vibration peaks of TiO_2 are presented at 398 cm^{-1}, 519 cm^{-1}, and 641 cm^{-1} indicating the presence of the TiO_2 anatase phase in all of these samples. The 430 cm^{-1}, and 580 cm^{-1} peaks are corresponding to wurtzite ZnO structure (Zamiri, Rebelo et al. 2014). The G band is the Raman spectrum of graphene based materials, and it typically shows the peak around 1580 cm^{-1}. The D band peak around 1350 cm^{-1} corresponds to disordered carbon or defective graphitic structure introduced to the crystalline structure (François Perreault 2015, Karaolia,

Michael-Kordatou et al. 2018). The intensity of the D band in CNT based material is more significant or higher than that of D band in GO based material. This suggests CNT based nanocomposites, such as; ZnO-CNT and TiO_2-CNT have more unstable and deficient structural than GO based nanocomposites, such as; ZnO-GO and TiO_2-GO (Karaolia, Michael-Kordatou et al. 2018).

Figure 5.2(B) indicates the decomposition behavior of NHs by thermos gravimetric analysis (TGA). A major weight loss of ZnO–GO is observed at 800 ℃, indicating 20% of weight loss caused by the combustion of carbon. According to a previous study, GO has low temperature stability and loses most of its mass when heated (Hsiao, Ma et al. 2013). Mass losses are due to decomposition of oxygen-containing function groups on GO to CO, CO_2 and H_2O and the thermal decomposition of the GO structure. A previous study analyzed GO-silica nanosheet and confirmed that a silica nanosheet acted as a protective layer that prevents oxidation degradation (Hsiao et al., 2013). The data suggest that ZnO and TiO_2 protect GO since ZnO and TiO_2 are far more thermally stable. Various forms of adsorbed water and partial degradation of GO resulted in initial mass loss of ZnO–GO until 200 °C and further mass decrease.

However, since TiO_2 is not as protective as the ZnO, the GO part of TiO_2–GO degraded continuously until 600 ℃. At 600 ℃, GO was completely degraded, with only TiO_2 left. TiO_2–GO had approximately 50% mass loss, suggesting that 50% of the material was GO. According to a study by Bom (2002), CNTs tend to decompose and lose most, if not all, of their mass at 500 ℃, while our study indicates that TiO_2 has a significant degree of stability compared to CNTs, as indicated by only a slight mass loss, most likely adsorption until 400 ℃. Upon decomposition, the sample remains stable until 800 ℃. More free water than

adsorbed water is found in ZnO–CNT, as indicated by the sharp drop in mass loss until 100 ℃. Yet, protecting metal oxides on CNT is still apparent as indicated by slow degradation over a larger temperature range. Both ZnO–CNT and TiO_2–CNT are likely to contain around 20% or less CNT based on the total mass loss.

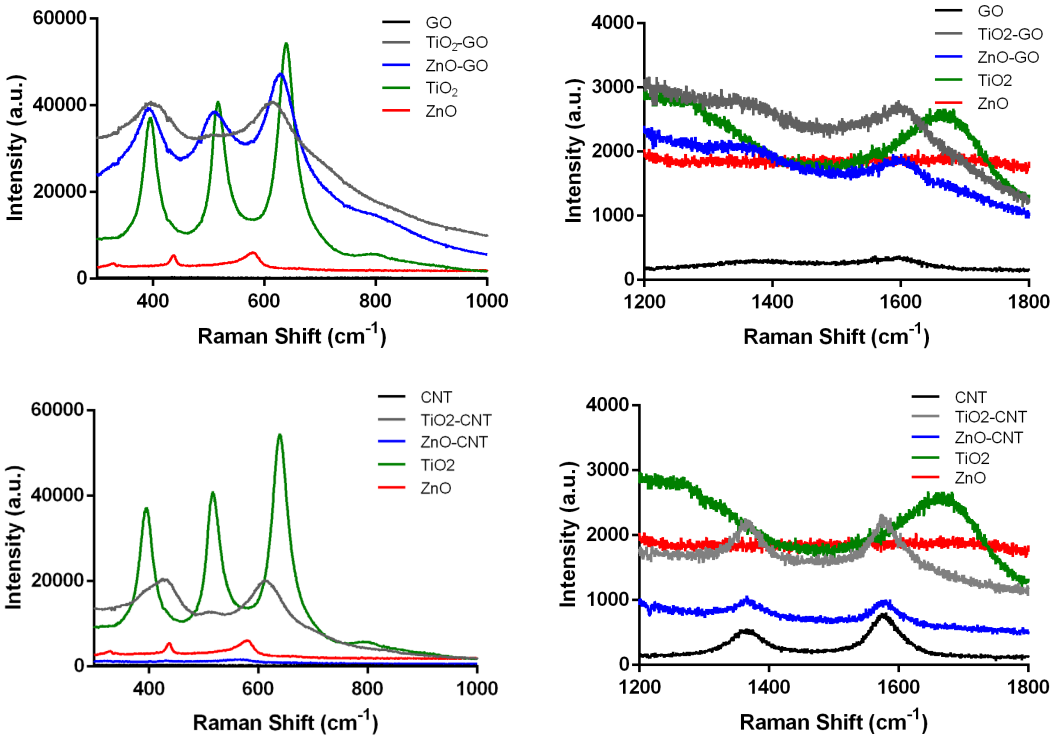

(A)

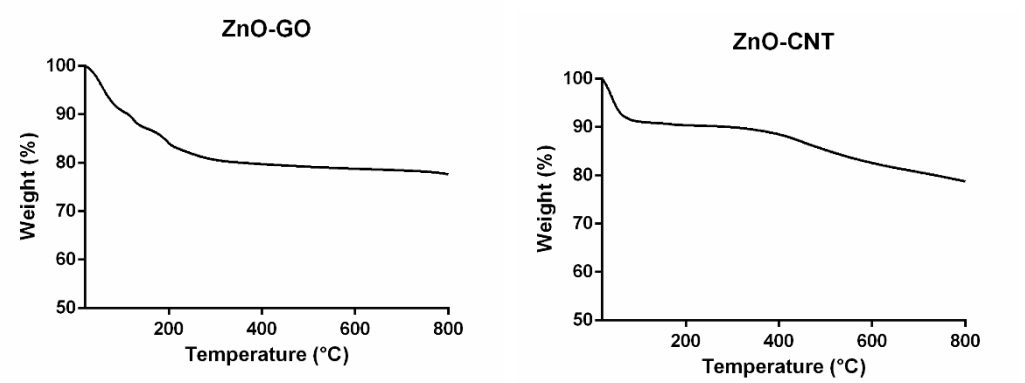

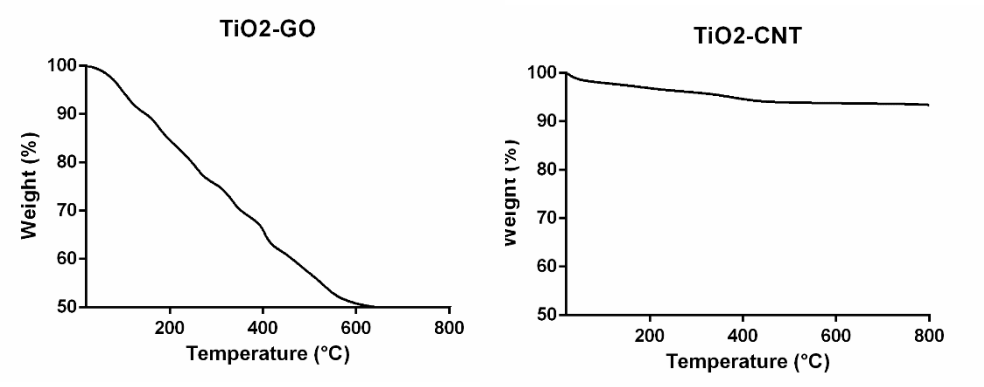

(B)

Figure 5.2. (A) Raman and (B) TGA analysis of 4 different types of NHs

5.3.2. Antibacterial effect of NHs on *E. coli*

To investigate the toxicity assessment of 4 different NHs suspension on *E. coli,* the antibacterial test was conducted by calculating the number of cells using OD_{600}. Four composites with different concentrations were tested in order to investigate composite effect on the antibacterial activities, and control study was performed with NHs free suspension. Figure 5.3A shows the growth curve of different NHs concentrations on *E. coli* for 6 hours. For all NHs suspension, clear concentration-response relationships were observed, and bacterial growth curve was inhibited over time for 6 hours except for concentrations at 20 mg/L. It shows that there is no antibacterial effect on *E. coli* cells which is exposed to concentration of NHs less than 20 mg/L. The effective concentration of the ZnO-GO for antibacterial showed above 20 mg/L, and ZnO-GO showed strongest antibacterial activity compared to other NHs. Along with the increase of the concentration of NHs, the growth of *E. coli* was inhibited severely. After 2 h exposure with ZnO-GO of 300 mg/L, the cell activity significantly deceased and these cells growth curve showed much slower than other cells exposed to 20, and 100 mg/L of ZnO-GO. ZnO-GO showed

significantly great antibacterial effect by suppressing the *E. coli* cell viability leading to 71.9 % of growth inhibition after 6 h exposure. The cell activity exposed to ZnO-CNT was also gradually reduced over time, and their cell viability showed more active than ZnO-GO exposed cells with 35.2% of growth inhibition after 6 h exposure. However, the cell viability exposed to various concentrations of TiO_2-GO was almost similar with control cell growth rate except for 6 h exposure. It is found that the antibacterial effect increased and showed significant trend by elapsing the time. The antibacterial effect of TiO_2-CNT exposed *E. coli* also increased by elapsing the time. This indicate that as the exposure time increases, the growth of cells exposed to high concentrations is markedly diminished. To determine the toxicity effect of the types of NHs on bacteria, growth inhibition rate was observed after 6 h exposure (Fig.5.3B). At the lowest concentration (20 mg/L), there was no inhibition growth rate of bacteria for 4 types of NHs. However, the growth inhibition rate was proportional to concentrations of NHs, and ZnO based NHs were more toxic than TiO_2 based NHs. The toxicity effects of ZnO-GO and ZnO-CNT were evident at 100 mg/L with showing 26.9, and 23.5% of growth inhibition rate respectively, while the toxicity of TiO_2-GO and TiO_2-CNT was not as clear as ZnO based NHs leading to 8.3, and 6.1% of growth inhibition rate. As the concentration increased from 100 mg/L to 300 mg/L, the toxicity of ZnO-GO was significantly higher than that of ZnO-CNT. When GO and CNT are synthesized with ZnO NPs, the toxicity of GO is greater than that of CNT. However, TiO_2-GO and TiO_2-CNT showed similar growth inhibition rate on *E. coli* cells according to the concentration. Therefore, the greatest antibacterial effect among 4 different types of NHs was found in the following order of ZnO-GO followed by ZnO-CNT then, TiO_2-CNT and TiO_2-GO both showing a similar antibacterial effect (The growth inhibition rate of

TiO_2-GO and TiO_2-CNT was 8.3, and 6.1% at 100 mg/L, and 23.2, and 33.4% at 300 mg/L, respectively). This difference in toxicity response between TiO_2-GO, and TiO_2-CNT might be brought from differences of cell physiology, metabolism, degree of contact, agglomeration state (Adams, Lyon et al. 2006, De Angelis, Barone et al. 2013). This growth inhibition rate results confirmed that ZnO NPs were observed more antibacterial effect than TiO_2 NPs when they were synthesized with GO, and CNT respectively. This finding that ZnO NPs exhibited higher toxicity to bacteria than TiO_2 NPs is due to high solubility of ZnO (Adams, Lyon et al. 2006, Aruoja, Dubourguier et al. 2009, Dasari, Pathakoti et al. 2013).

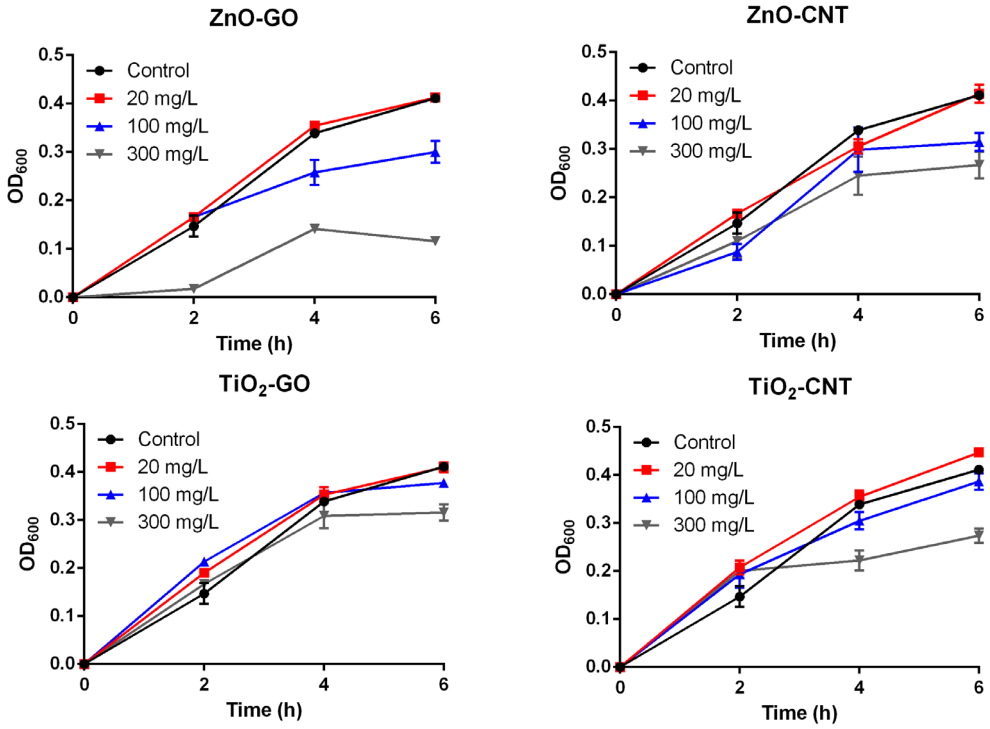

(A)

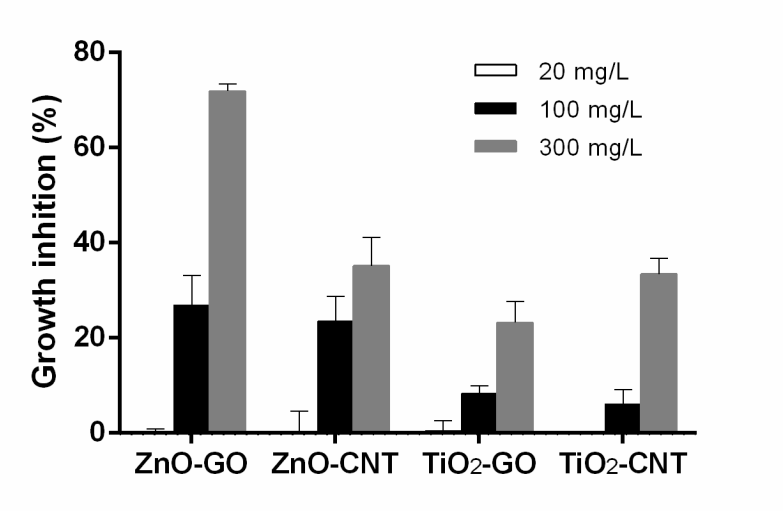

(B)

Figure 5.3. Antibacterial effect of 4 different types of NHs on *E. coli* (A) growth curve, and (B) growth inhibition at 6 h

5.3.3. ROS generation

Antibacterial activity of NHs can be attributed to the production of reactive oxygen species (ROS). When light energy absorption induces charge separation, nanocomposite produces pair of electrons and holes. Then, excited electron and hole carriers move to the surface of nanocomposite, and they facilitate oxidation and reduction reactions which generate ROS such as superoxide, hydrogen peroxide, hydroxyl radical etc. It has been known that doping, or coupling with other semiconductors such as carbon materials enhances photocatalytic activity of nanocomposite (Qi, Cheng et al. 2017).

To assess the antibacterial effect by ROS, oxidant-sensing fluorescent DCF-DA was used to investigate the ROS level of ZnO-GO, ZnO-CNT, TiO_2-GO, and TiO_2-CNT NHs on *E. coli* cells and compare its ROS generation. ROS generation of *E. coli* exposed to 4 types of NHs increased significantly by increasing in concentration (20-300 mg/L) and exposure

time (Fig. 5.4). Thus, the relationship between ROS and antibacterial activity was determined by the pretreatment of cells with NAC (N-acetyl-L-cysteine) to investigate whether the antioxidant mainly influence to the toxicity effect of NHs (0.5 and 2 mM). Compared to the untreated cells with NAC, treated cells with NAC exposed to ZnO-GO produced almost same or less fluorescence intensity with cells exposed to 20 mg/L of ZnO-GO indicating that NAC prevented by ROS from 300 mg/L of ZnO. Thus, cells treated with higher concentration of NAC (2 mM) produced less ROS compared to lower concentration NAC (0.5 mM). Cells treated to NAC (0.5 mM) produced slightly less ROS than cells without NAC in ZnO-CNT. However, it was observed that ROS generation from 300 mg/L of ZnO-CNT significantly decreased at higher concentration of NAC (2 mM) compared to lower NAC concentration. As NAC concentration increased from 0.5 mM to 2 mM, ROS generation from NAC treated cells decreased. This is because the capacity of NAC may have been overwhelmed by the increase of accumulated ROS generation according to the amount of NAC (Ma, Wallis et al. 2014). Likewise, the addition of NAC to TiO_2-GO was also observed to reduce the fluorescence intensity at concentration 2 mM, while ROS generation from 0.5 mM of NAC showed almost similar value with cells that untreated with NAC. In case of TiO_2-CNT, there was no significant difference of ROS generation depending on the NAC concentration or in presence of NAC. Given that the ability of NAC inhibit the ROS induce, this may indicate that the toxicity induced by TiO_2-CNT is the least compared to other NHs. From these results, the antibacterial activity of 4 different NHs is correlate with the amount of ROS generation in presence of NAC. This results may have been responsible for the toxicity mechanisms of NHs on bacteria could be primarily due to ROS generation. Furthermore, the present findings demonstrated that

the addition of NAC significantly inhibited the ROS induced by NHs in *E. coli* cells. Overall, the results showed that the fluorescence intensity according to exposure time was great in the order of ZnO-GO>ZnO-CNT>TiO_2-GO>TiO_2-CNT which is similar trend with growth inhibition results (Figure 5.3). *E. coli* cells treated with ZnO-GO in absence of NAC showed the ROS generation increased to 1.90 times for 20 mg/L, 1.93 times for 100 mg/L, and 2.32 times for 300 mg/L when the nanocomposite concentration increased from 2 h to 6 h. This results indicate that the rate of increase of the ROS generation over time is also high as the concentration increases. Similarly, Baek et al. (Baek, Joo et al. 2017) observed antibacterial effect of ZnO on *E.coli*, growth inhibition and ROS generation increased with the increase in the concentration and duration of exposure. Fluorescence intensity of NHs indicates that ZnO-GO modified nanocomposites could produce most photocatalytic antibacterial effect on *E. coli* cells among 4 different nanohybrid materials, and ZnO produce more ROS compared to that with TiO_2. Previous studies showed the toxicity effect excreted by ZnO is greater than TiO_2 due to the oxidative stress (Adams, Lyon et al. 2006, Kumar, Pandey et al. 2011). Angelis et al. suggested that interaction between cells and NPs produce different cellular ROS production for ZnO NPs and TiO_2 NPs, and agglomeration state of NPs was observed to influence the interaction with cells (De Angelis, Barone et al. 2013). Thus, the agglomeration structure could affect the quenching of both holes and free hydroxyl radicals, because aggregate size and structure influenced reaction probability either electrons or holes on particle surfaces (Jassby, Farner Budarz et al. 2012). Based on the antibacterial properties of nanoparticles, ROS can attribute to cell deformation and rupture because ROS such as peroxide,

superoxide, and hydroxyl radicals react with organic biomolecules, including lipid, carbohydrates proteins, and DNA (Dizaj, Lotfipour et al. 2014).

Previous study showed that GO can improve not only the dispersity of nanoparticles, but also active sites for functionalization when GO is combined with metal oxide including ZnO, and TiO_2 (Huang, Wang et al. 2015). High surface area of GO enhance the dispersion of metal nanoparticles and allow greater photocatalytic activity (Liu, Hu et al. 2012). Zhang et al reported that enhanced adsorption property of ZnO-GO composites causes electron transfer between ZnO and GO, and this electron transfer suppresses the recombination of electron-hole pairs (Chen, Zhang et al. 2013). Karaolia et al. showed that *E. coli* exposed to TiO_2-GO resulted in reduction of CFU concentration of cells around 31% and suggested that ROS is the main influencing factors for inactivating of the damaged cells by the contact of the catalyst with the bacterial (Karaolia, Michael-Kordatou et al. 2018). Moreover, the synthesized TiO_2-GO composites was shown to remove antibiotic-related microcontaminants in urban wastewater effluents under solar radiation (Karaolia, Michael-Kordatou et al. 2018).

ZnO-CNT also showed that photocatalytic activity increased as exposure time and concentration increased (Figure 5.4). CNT has known that enhances exposure of active sites and improves the dispersion of photocatalysts, and it has long distance of shuttling electrons blocks the recombination of photo-generated e^- and h^+ pairs (Qi, Cheng et al. 2017). When ZnO-CNT or TiO_2-CNT absorbs the light energy, the photo-generated electrons are transferred from valence band (VB) to conduction band (CB) within metal oxide NPs, and leave holes in VB as illustrated in figure 5.5. In the absence of the CNT, most of e^- and h^+ charges recombine quickly without doing any chemistry activity (Yuan

Yao 2008). Therefore, this electron separation is reducing electron-hole pair recombination and increasing photocatalytic activity (Qi, Cheng et al. 2017, Karaolia, Michael-Kordatou et al. 2018). Ahmadi et al. investigated the removal of TC by using TiO_2-CNT nanocomposite, and reported that increasing the amount of TiO_2 on the surface of CNT produced more pairs of electron/hole are produced and TC removal efficiency is increased (Ahmadi, Ramezani Motlagh et al. 2017). By adjusting the ratio of nanomaterials, effective sorption and photocatalytic activity can be different. Song et al. investigated that TiO_2-CNT ratio over 1.5% was leading to less effective sorption and photocatalytic activity due to significant aggregagtion on the surface of CNT (Song, Chen et al. 2012). However, increase in TiO_2 NPs may block the adsorption sites of CNT and decreased overall adsorption capacity on the surface of CNT (Zhang, Zhang et al. 2011, Das, Abd Hamid et al. 2014).

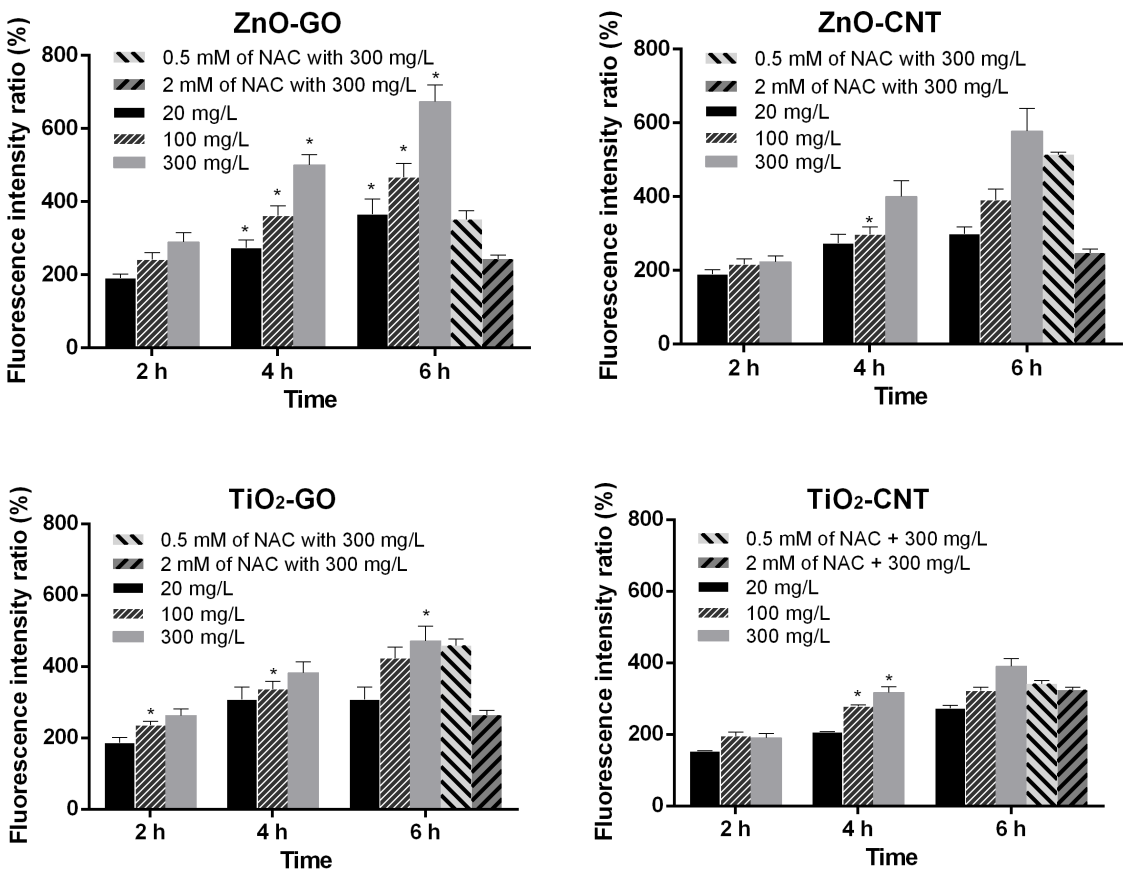

Figure 5.4. The amount of ROS release from *E. coli* exposed to 4 different types of NHs over time

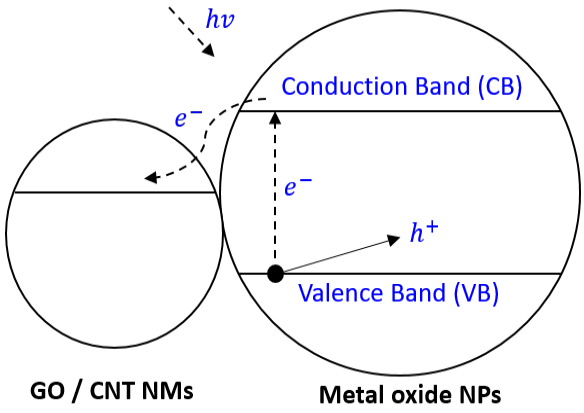

Figure 5.5. Schematic of proposed mechanism for enhanced photocatalysis of NHs

5.3.4. SEM and TEM analysis between *E.coli* cells and NHs

Depending on the materials used in toxicology study, antibacterial effect and ROS generation showed different results. Since physical interaction between NHs composites and cells can perform various, the distribution of NHs was characterized by SEM and TEM observation. To understand the interaction of NHs with *E. coli* cells, the surface morphologies of NHs after exposed to cells for 6 hours were examined. The SEM results show that *E. coli* exhibited attaching, or covering the surface of NHs (Fig. 5.6). Some of the bacteria cells were observed to have collapsed and damaged membrane (Fig. 5.6E), and cell morphologies changed from rod shape to globular shape that appears in the pre-death stage. SEM images in the first line of figure 5.6 indicates that the NHs changed the morphology of *E. coli* which may induce the growth inhibition of cells, and death. To further confirm the interaction between NHs and cells, TEM images were taken through the cross section examination of *E. coli* cells. Cells that were exposed to ZnO-GO were attached on the GO sheet (Fig. 5.6A), and observed that cell membrane is damaged and cut. Cells exposed to TiO_2-GO look healthier compared to the ZnO-GO exposed cells, and TiO_2-GO nanoparticles were much more aggregated than ZnO-GO (Fig. 5.6C&D). Figure 5.6B showed that there are some physical interactions between GO sheets and bacterial cells. Bacterial cells may be involved in the edge of GO, and ZnO NPs are attached on the surface of cells. TEM image of TiO_2-GO is observed that nanocomposite is adhering to the cell surfaces but not observed disruption of bacterial membrane directly by penetration (Fig. 5.6D).

Stoimenov et al. reported that the electrostatic attachment of ZnO NPs to the surface of cells induces bacteria death by initiating disorganization of the cell membrane (Stoimenov

2002). Wang et al. reported that the direct contact of ZnO NPs with the cell damages cells membrane, and wrapping of the ZnO-GO composites prevents the bacteria from nourishing themselves from the medium (Wang, Cao et al. 2014). Previous studies have proposed that physical interaction between GO sheet and cell layers was found to damage cells due to membrane piercing into bacterial cells or slicing the cell by GO, but *E.coli* cells has shown that the interaction of GO in contact with *E,coli* cells are mostly repulsive (Tu, Lv et al. 2013, Mao, Guo et al. 2014, Romero-Vargas Castrillón, Perreault et al. 2015). Thus, GO sheet size also can affect the antibacterial effect. Smaller size of sheet was found to have more antibacterial through oxidative mechanisms due to the higher defect density as GO size decrease (François Perreault 2015). However, larger GO sheets can induce a higher antibacterial effect by attributing to the capacity of larger sheets to cover bacterial cells and prevent proliferation of cells (Liu, Hu et al. 2012). Antibacterial properties of GO can be still present although the sheets are contacting with the surface of the cells (Mangadlao, Santos et al. 2015). Many studies indicated that layer types of GO showed the antimicrobial properties, rather than physical interaction of GO sheet with cells (Hui, Piao et al. 2014). These studies propose that contact or direct piercing of the membrane by GO sheets is essential for the antibacterial activity of GO.

ZnO-CNT nanocomposite looks like a mass of tangles each other around *E. coli* cells, and it is attaching around the cell membrane (Fig. 5.6E&F). TEM images of *E. coli* after exposure to ZnO-CNT are observed that the cell membrane of the bacteria was damaged by direct contact of CNT, but there is no penetration of CNT into the cells (Fig. 5.6F). TEM images of *E. coli* after exposed to TiO_2-CNT for 6 h showed that there is no direct interaction between cells and TiO_2-CNT nanocomposite (Fig. 5.6H). It is observed that

TiO_2-CNT nanocomposites are aggregated each other, but single particle does not appear to stick to the surface of the cells. These CNT clusters were observed in other study (Yang, Mamouni et al. 2010), it is observed that short CNT (<1 μm) does not interact with cells by their edge. However, the longer CNTs (1-5 μm) showed wrapping on bacterial cells, and individual CNTs can be seen interacting with cells at the edge of CNT. In other study, it was confirmed that there was no internalization of CNT into bacteria cell, even though bacteria wall was deeply associated with CNT (Angélique Simon-Deckers 2009).

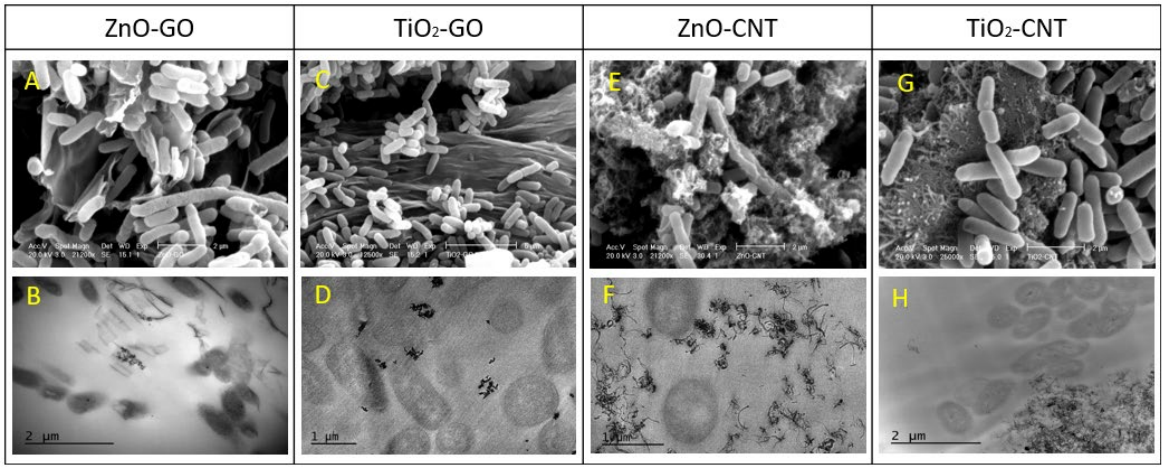

Figure 5.6. SEM, and TEM images of 4 different types of NHs after exposed to *E.coli* for 6 h

5.3.5. FT-IR

The characteristic FT-IR spectra provided the investigation of the interaction between NHs in Figure 5.7. The FT-IR spectra of GO, ZnO-GO, and TiO_2-GO nanocomposites are shown in Figure 5.7A. The IR peaks of oxygen containing functional groups at 1725 cm^{-1}, 1150 cm^{-1}, and 1180 cm^{-1} are assigned to C=O, C-OH, and C-O stretching vibrations, respectively. The peak at 1630 cm^{-1} is attributed to the C=C, and the

IR spectrum of ZnO presented peak in the range of 650 cm^{-1} associated with Zn-O. The intensity of O-H peak for GO decreased significantly in ZnO-GO and TiO_2-GO composites associated with the oxygen functional groups were dramatically eliminated (Liu, Yang et al. 2017, Rajeswari and Prabu 2017). Thus, decreased peaks in ZnO-GO indicates the further reduction of GO and attachment of ZnO NPs onto the GO nanosheet (Rajaura, Sharma et al. 2017). The strong peaks around 500-900 cm^{-1} are attributed to the stretching vibration of Ti-O-Ti and possibly to Ti-O-C bonds (Karaolia, Michael-Kordatou et al. 2018). The IR spectra of CNT, ZnO-CNT, and TiO_2-CNT nanocomposites are shown in Figure 5.7B. The spectrum of CNT showed no clear peaks at 500-4000 cm^{-1} (Nguyen and Shim 2015). The spectrum from ZnO-CNT and TiO_2-CNT also showed O-H, C-H, C=O, C=C, and C-O peaks. The peaks corresponding to Ti-OH and Ti-O-Ti groups showed in 1300 cm^{-1}, and 550 cm^{-1}, respectively (Yuan, Hung et al. 2017), and the peak around 500-550 cm^{-1} is attributed to the ZnO vibration (Upasani, Sreekumar et al. 2017).

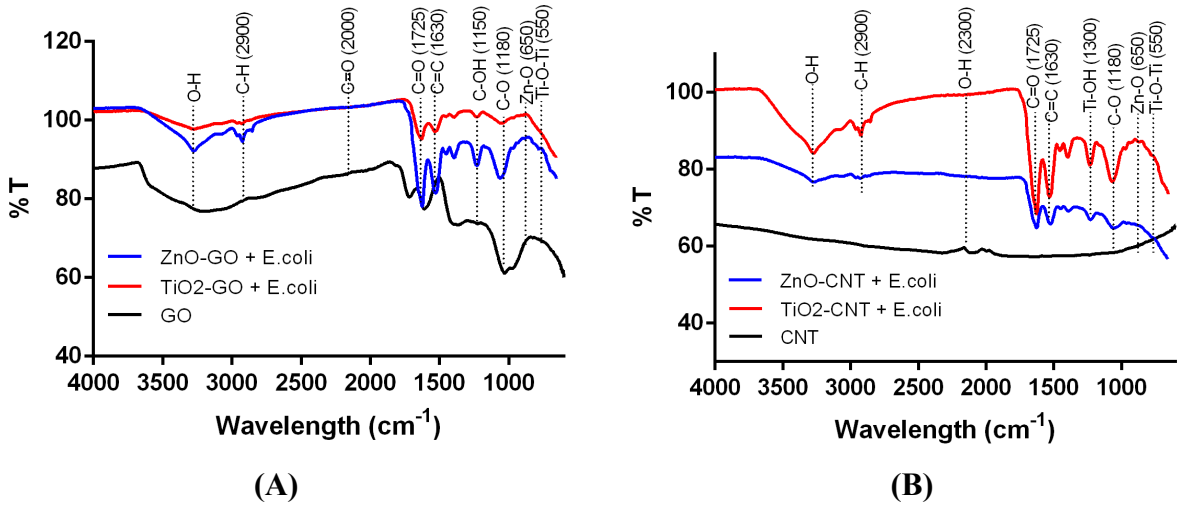

Figure 5.7. FT-IR analysis of 4 different types of NHs with and without *E. coli* cells

5.4. Conclusions

The antibacterial properties of four types of NHs (GO-based vs. CNT-based ZnO/TiO_2) on *E. coli* were most significant in ZnO-GO, followed by those in ZnO–CNT and TiO_2–CNT ≈ TiO_2–GO. It was discovered that GO acts as a substrate to increase dispersion of metal oxides (ZnO/TiO_2) with a sheet-shaped morphology. Antibacterial activities of the NHs indicated both dose and exposure-time dependency, which was consistent with growth inhibitions of the bacterial cells and ROS generation. Among four NHs, NHs that containing ZnO revealed higher toxicity to *E. coli* than those containing the TiO_2 component. Both GO and CNT increased the dispersion of metal-oxide NPs through increasing ROS generation by suppressing the recombination of electron–hole pairs. Although the SEM and TEM images revealed that GO based NHs had more attachment on the bacterial surface, CNT-based NHs significantly aggregated each other without interaction with cells. Further results indicate that GO-based NHs had a better interaction with ZnO through dispersion and significant enhancement of antibacterial effects in comparison to CNT-based NHs. The FT-IR analysis suggests formation of considerable functional groups on the surfaces of NHs, as compared to the bare carbon materials. Among four hypothesized mechanisms, ROS generation and physicochemical property changes were found to be the primary antibacterial mechanisms, as confirmed from quantification of ROS generation and sharp morphology changes that induced damages on cell membranes. Although this study was primarily focused on antibacterial mechanisms among four types of NHs, the results are significant in terms of designing new antibacterial treatment methods, especially for multidrug-resistant bacteria detected in water to protect the environment and public health. The NHs could also be applied as an alternative method

to conventional chlorine disinfection technology, especially for controlling regrowth of persistent microorganisms in water. Further studies would be necessary to develop point-of-use water treatment technology, especially under solar energy to facilitate photocatalytic properties of NHs, for controlling emerging contaminants of concern, such as the recently emerging multidrug-resistant bacteria in water.

CHAPTER 6:

IN-VITRO TOXICITY EVALUATION OF NANOHYBRIDS ON A MARINE DIATIOM[4]

[4] Baek, S., Joo, S. H., Su, C., Toborek, M. (2018) In-vitro toxicity evaluation of ZnO/TiO_2-conjugated carbon nanotubes/graphene oxidebased nanohybrids on a Thalassiosira pseudonana marine diatom. *Ecotoxicology and Environmental Safety* **(**under review)

6.1. Background

The use of nanoparticles (NPs) is increasing and becoming widespread in various fields, such as medicine, electronics, water purification, cosmetics, and manufacturing (Piccinno, Gottschalk et al. 2012). Among NPs, metal-oxide NPs such as ZnO and TiO_2 are the most abundant NPs in water (Minetto, Volpi Ghirardini et al. 2016). The production of nanohybrids (NHs) consisting of metal-oxide NPs and carbon-based nanomaterials has increased because NHs can be applied to improve surface area and catalytic efficiency of NHs (MamathaKumari, Praveen Kumar et al. 2015). The recent growth of the nanotechnology industry has raised concerns about the fate and potential hazards of NPs in water ecosystems, since NPs could end up in significant accumulation in the aquatic environment through their manufacturing process, product use, and disposal (Hotze, Phenrat et al. 2010, Love, Maurer-Jones et al. 2012, Suresh, Pelletier et al. 2013, Chen, Zhou et al. 2018).

Properties of NPs in aquatic systems may exhibit different behaviors through aggregation and precipitation and interact with aquatic microorganisms such as algae (Joo, Knecht et al. 2016, Baek, Joo et al. 2018). In aquatic environments, algae play a critical role in producing basic nourishment in all water bodies and in self-purification of organic contaminants in natural waters (Wilkie 2002, Cardinale 2011). Studies have revealed the toxicity effect of metal-oxide NPs on algae, and the ROS generation of NPs was suggested as a primary toxicity mechanism (Suman, Radhika Rajasree et al. 2015, Hou, Wu et al. 2018, Middepogu, Hou et al. 2018, Morelli, Gabellieri et al. 2018) . The ROS generated by TiO_2 and ZnO nanoparticles may oxidize organic contaminants and can cause fatal

damage to microorganisms by disrupting or damaging cell DNA or structures (Peng, Palma et al. 2011). Given that different types of NPs are released into water, released metal-oxide NPs can react or interact with other NPs and form nanohybrids (NHs) due to the NPs' large surface area and high reactivity. Besides, the toxicity effect of NPs in aquatic systems has been made for single-NP types of nanomaterials rather than NHs that consist of two different types of NPs (Wang, Zhu et al. 2016, Freixa, Acuna et al. 2018, Hu, Wang et al. 2018, Rajput, Minkina et al. 2018). To the best of our knowledge, in the recent literature, there is no study on the toxicity of NHs to marine microalgae.

Given various responses of algae species to exposure to heterogeneous nature of NPs (Galletti, Seo et al. 2016, Karimi, Sadeghi et al. 2018) and algae as a primary producer of food chains to higher consumers (animals/humans), it is imperative to explore the potential ecotoxicity of nanohybrids on algae species. Thus, the present study aims to (1) investigate *in vitro* ecotoxicity effects of NHs (ZnO–GO, TiO_2–GO, ZnO–CNT, and TiO_2–CNT) on *T. pseudonana*, a species of marine-centric diatoms chosen as a model for diatom physiology studies widely distributed throughout entire marine food chains (Armbrust 2004); (2) explore the toxicity mechanisms caused by the selected NHs, and (3) specifically link how differently characterized NHs influence algal growth inhibition, reactive oxidative stress, and cell morphology changes.

6.2. Materials and Methods

6.2.1. Materials

Graphene oxide was purchased from ACS Material (CA, USA) (GO; a single-layer of more than 99% purity, 0.26 g/cm^3 bulk density, 1–5 µm diameter, and 0.8–1.2 nm

thickness according to Hummers' method). A multi-walled carbon nanotube was supplied by Sigma-Aldrich (MO, USA) (MWCNT; more than 98% purity, 6–13 nm (O.D.) × 2.5–20 μm (L)). Chemicals such as zinc nitrate hexahydrate ($Zn(NO_3)_2 \cdot 6H_2O$; >98% purity), $ZnCl_2$ (>99.99% purity) for ZnO nanocomposite synthesis and a titanium oxysulfate solution ($TiOSO_4$; ~15 wt.% and 99.99% purity) for TiO_2 nanocomposite synthesis were obtained from Sigma-Aldrich (MO, USA).

6.2.2. Fabrication of four types of NHs

A hydrothermal process was used for the synthesis of four types of nanohybrids. A literature method (Stengl et al., 2013) was used for synthesis of TiO_2–GO as follows. Under constant stirring at the temperature of 0 ℃ in an ice bath, an ammonium hydroxide solution (10%) was added slowly into 100 mL of 1.6 M $TiOSO_4$, thereby forming a homogeneous mixture at pH 8.0. A white precipitate was obtained and then filtered by a vacuum pump and mixed with 100 mL of a hydrogen peroxide solution (15%). The obtained titania peroxo complex solution with a yellow color was mixed with 50 mg GO in water using a sonicator. The mixture was heated in a heating mantle with a reflux cooler at 100 °C for 48 h, and the resultant product was taken by being dried in the oven at 105 °C for 10 h. The TiO_2–CNT nanohybrid was synthesized by applying the following method (Huang, Zang et al. 2014). Multi-walled carbon nanotubes (MWCNTs: 50 mg) were mixed with 100 mL of a 0.01 M $TiOSO_4$ solution. Then, 1 mL of H_2SO_4 (0.2M) was added to the mixture under ultrasound sonication. A reflux of the mixed suspension was made in thermostatic water (80 °C) for 72 h, and the suspension was dispersed for 10 min every 6 h to avoid agglomeration of nanomaterials.

Regarding the synthesis of the ZnO–GO nanohybrid, 50 mg GO was dispersed into a 100 mL deionized (DI) water in an ultrasonic bath for 1 h (Fu, Jiang et al. 2018). The GO solvent was centrifuged at 4,000 rpm, and 5 mmol of $Zn(NO_3)_2 \cdot 6H_2O$ was added to ammonia water at pH 8, followed by autoclaving and heating of the mixture at 160 °C for 10 h. Centrifugation for separation, washing with DI water, and drying of the synthesized ZnO–GO under a vacuum at 60 °C for 24 h were carried out. ZnO–CNT synthesis was fabricated by addition of nitric acid (80%) to a multi-walled carbon nanotube (MWCNT) at 80 °C for 4 h and then washed several times with DI water(Wang, Xia et al. 2008). Then, a $ZnCl_2$ solution was mixed with a $NH_3 \cdot H_2O$ solution slowly under stirring. After $Zn(NH_3)_4^{2+}$ was formed and the white precipitate disappeared, the CNT solution was soaked into a $Zn(NH_3)_4^{2+}$ solution for 48 h. Then, the resultant products were dried at 70 °C in a vacuum oven and calcined at 300 °C for 4 h in atmospheric nitrogen.

6.2.3. Physicochemical properties of NHs

Characterization (physicochemical properties) of the four types of NHs was performed using Field Emission Scanning Electron Microscopy (FE SEM; Philips XL-30 FEG), Energy Dispersive Spectroscopy (EDS), JEOL 1400 Transmission Electron Microscopy (TEM), and Perkin Elmer Frontier Fourier Transform Infrared Spectroscopy (FT-IR) (MA, USA). First, in regard to SEM preparation, cultures were placed in 2% glutaraldehyde in a phosphate-buffered saline (PBS). Samples were rinsed three times for 5 min each in the PBS buffer, then dehydrated in a graded series of ethanol to 100%, and dried in hexamethyldisilazane. After being outgassed overnight, samples were coated with Pd in a sputter coater and imaged using an XL-30 field emission SEM. High-resolution TEM (HR-TEM) images were taken using a Philips CM-10 TEM (Eindhoven,

Netherlands) at the Miller School of Medicine TEM Core at the University of Miami. Aqueous samples were then drop-casted onto a carbon grid and let to air-dry before being scanned. The vibrational frequencies of the chemical bonds were measured to identify the different functional groups in nanocomposites using an FT-IR analysis. A pellet of the sample powders was measured with Perkin Elmer Frontier FTIR (MA, USA) after the sample powders were ground and compressed in the 600–4,000 cm^{-1} range.

6.2.4. Cell viability analysis with *T. pseudonana*

The *in vitro* toxicity evaluation of the NHs on *T. pseudonana* was carried out as follows. The algal cell in the marine medium was obtained by the University of Texas at Austin. According to the information provided by the supplier, the marine diatom (unicellular and brackish with centric cells) has shells made of silica. Artificial seawater containing an f/2 medium was used for culturing algal cells, and incubation at 12 h:12 h (light:dark) cycle was completed with a Verilux VT 10 (5,000 lx white light). Guillard's method was used for making artificial sea water (Guillard 1975), and UV absorbance was measured to determine the algal growth using a Beckman Coulter DU 720 spectrophotometer. Five points of calibration indicated the peak absorbance of *T. pseudonana* at 670 nm (linear with $R^2 = 0.9991$). The diatom cells were exposed to four different nanohybrid suspensions in culture tubing under the same temperature and light and incubated for 72 h. Algal cells were measured with UV absorbance at 0 h, 24 h, 48 h, and 72 h. The growth inhibition rate of algae was calculated to measure the extent of toxicity of NHs compared to that of the control.

6.2.5. Analysis of ROS detection

Photocatalytic activity of the algal cell was measured by fluorescence intensity using a Spectramax Gemini EM Microplate Reader (Molecular Devices, CA). A DCF-DA (2',7'–dichlorofluorescin diacetate) cellular-ROS-detection assay kit (Abcam Inc, Toronto, ON, Canada) was used to dye hydroxyl and peroxyl within the diatomic cells. Cells were exposed to four different nanohybrid suspensions for 0 h, 24 h, 48 h, and 72 h under illuminated conditions using a lamp. At each time point, cells were collected in a conical tube and washed by centrifugation in PBS. The washed cells were suspended in the diluted DCF-DA solution and incubated at 37 °C for 30 min in the dark. After they were washed by centrifugation with PBS buffer, the cells were transferred into a clear-bottom 96-well microplate. The detected DCF by fluorescence spectroscopy indicated a maximum excitation at 485 nm and emission spectra at 535 nm in the presence of the buffer. The photocatalytic activity of different NHs was examined with antioxidant *N*-acetyl cysteine (NAC), a ROS scavenger, to evaluate the toxicity mechanism between NHs and cells (Chen, Lin et al. 2014). NAC prevents toxicity caused by ROS through directly scavenging ROS or promoting production of antioxidant enzymes (Ma, Wallis et al. 2014). Our hypothesis is that the addition of NAC reduces the ROS generation of NHs. To measure this, cells were pretreated with 0.5 and 2 mM of NAC, and fluorescence intensity was measured at 72 h.

6.2.6. Statistical analysis

All experimental conditions were run in triplicate. The statistical analysis was performed using the statistical Student's *t*-test with Graph Pad Prism 3.0 (Graph Pad Software Inc., San Diego, CA); all data indicated statistical significance at $p < 0.05$.

6.3. Results and discussion

6.3.1. Physicochemical properties of NHs

The formation of metal oxides (ZnO and TiO_2) and their compounding with the CNT and GO were verified using SEM and TEM (Fig. 6.1). As illustrated in Figs. 6.1A and 6.1B, aggregated ZnO NPs were dispersed irregularly on GO, with clusters covering the surface of GO sheet plates, suggesting enhancement of dispersion by GO sheets. When TiO_2 was conjugated with GO, aggregated clusters were observed between GO sheets (Figs. 6.1C and 6.1D).

Byrappa, Dayananda et al. (2008) argued that CNTs act as substrates for the ZnO and TiO_2 NPs, thus causing dispersion of metal-oxide NPs onto the CNTs. However, they found metal-oxide NPs loaded on CNTs to have more aggregation with each other compared to those loaded on GO sheets. ZnO NPs were observed to have spherical shapes on CNT (Fig. 6.1F), and TiO_2 NPs had rod shapes (Fig. 6.1H). Thus, TiO_2 NPs on CNTs formed more aggregation clusters than those due to ZnO NPs on CNTs (Fig. 6.1H). According to a recent study, whereas a fixed aggregation structure of ZnO NPs on ZnO–CNT is found, TiO_2 NP in TiO_2–GO is found to have a rod shape and self-aggregation(Upasani, Sreekumar et al. 2017).

(A)

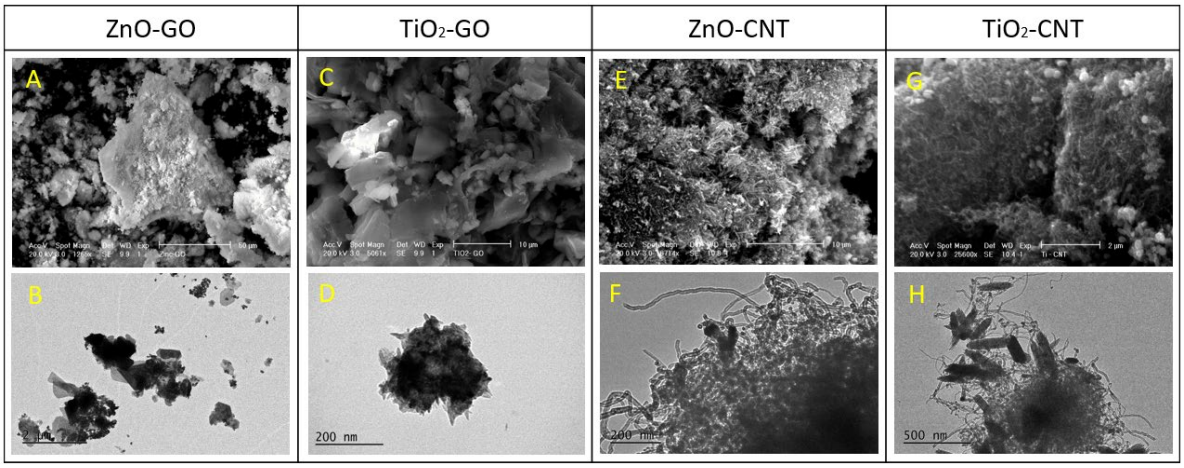
ZnO-GO
TiO2-GO
ZnO-CNT
TiO2-CNT
A
B
C
D
E
F
G
H
200 nm
500 nm

(B)

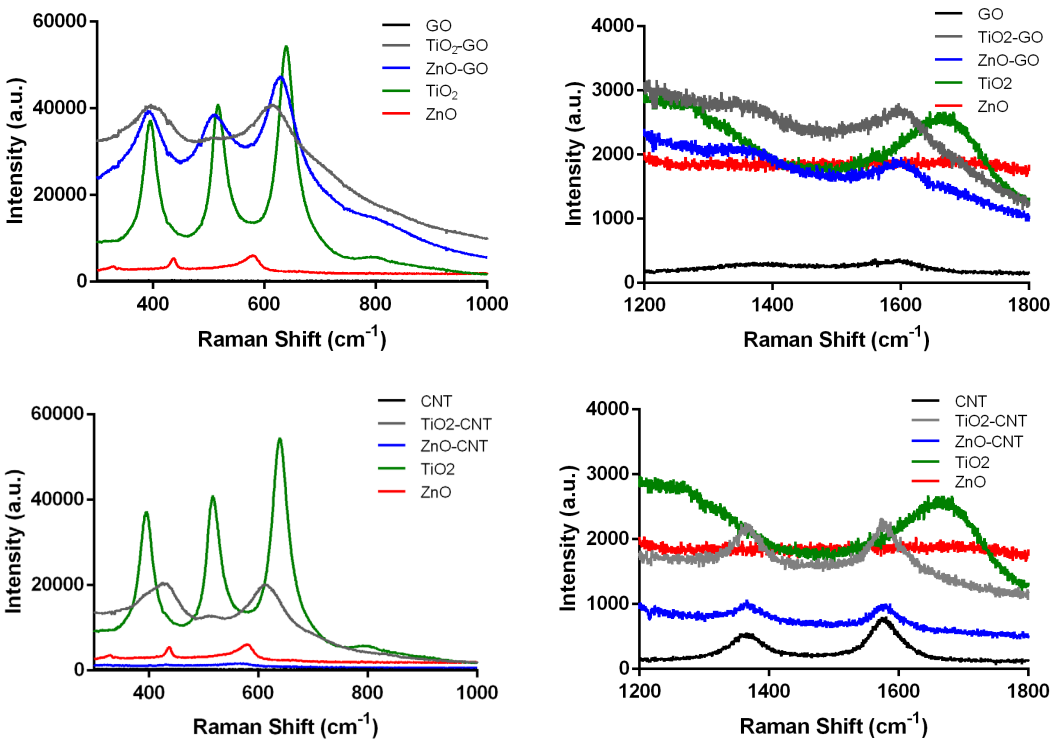
GO
TiO2-GO
ZnO-GO
TiO2
ZnO
CNT
TiO2-CNT
ZnO-CNT
Intensity (a.u.)
Raman Shift (cm-1)

(C)

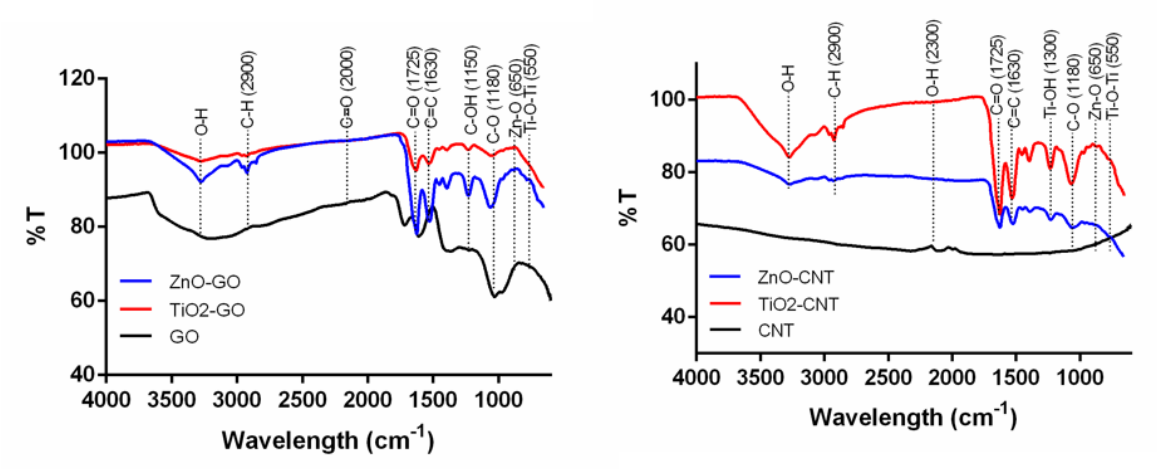

Figure 6.1. Physicochemical properties of nanohybrids. (A) SEM and TEM images, (B) Raman analysis of four types of nanohybrids, and (C) FT-IR analysis of four different types of NHs [Baek et al., 2018].

6.3.2. Analysis of Raman spectra

The G band at 580 cm^{-1} displayed on the Raman spectrum of graphene-based materials indicates the C–C vibrational mode, and the D band peak at 1,350 cm^{-1} suggests that carbon is disordered or a graphitic structure is flawed (François Perreault 2015, Karaolia, Michael-Kordatou et al. 2018). The peaks of the D band in CNT-based NHs exhibit more significance compared to that of the D band in the GO-based material, indicating better stability in the structure of GO-based NHs compared to that of CNT-based nanocomposites (Karaolia et al., 2018). The presence of the anatase TiO_2 polymorph was confirmed with peaks at 398 cm^{-1}, 519 cm^{-1} and 641 cm^{-1}, and E2 and E1 (LO) modes of the wurtzite ZnO structure were verified at 430 cm^{-1} and 580 cm^{-1} peaks (François Perreault 2015, Karaolia, Michael-Kordatou et al. 2018).

6.3.3. Analysis of FT-IR spectroscopy

Fourier transform-infrared (FT-IR) spectra of bare GO, ZnO–GO, TiO_2–GO, bare CNT, ZnO–CNT, and TiO_2–CNT NHs were examined to characterize the compounds' functional groups (Fig. 6.1). In Fig. 6.1A, the IR peaks at 1,725 cm^{-1}, 1,150 cm^{-1}, and 1,180 cm^{-1} are associated with oxygen-containing functional groups on C=O, C–OH, and C–O stretching vibrations, respectively. The C=C bond is indicated in the peak at 1,630 cm^{-1}, and the IR peak around 650 cm^{-1} is associated with the Zn–O structure. The oxygen functional groups confer high hydrophilicity on GO, which produces its solubility and potentially high mobility in water. The significant decrease in the intensity of the O–H peak for GO in ZnO–GO and remarkable elimination of oxygen functional groups in TiO_2–GO composites were consistent with those in the literatures (Liu, Yang et al. 2017, Rajeswari and Prabu 2017). The GO was further reduced as indicated by the lower peaks in ZnO–GO because of the attachment of ZnO NPs onto the GO nanosheet (Rajaura, Sharma et al. 2017). The stretching vibration of Ti–O–Ti and Ti–O–C bonds was found from the dramatic peaks at 500–900 cm^{-1} (Karaolia, Michael-Kordatou et al. 2018). However, as revealed in Fig. 6.1B, no distinct peaks were found in the CNT spectrum at 500–4,000 cm^{-1}(Nguyen and Shim 2015)(Nguyen and Shim 2015) (Nguyen and Shim 2015). There were several peaks (O–H, C–H, C=O, C=C, and C–O) from the spectrum of ZnO–CNT to TiO_2–CNT, with the peaks at 1,300 cm^{-1} (Ti–OH) and 550 cm^{-1} (Ti–O–Ti) (Upasani, Sreekumar et al. 2017, Yuan, Hung et al. 2017, Karaolia, Michael-Kordatou et al. 2018) .

6.3.4. Antibacterial effects of NHs on *T.pseudonana*

Figure. 6.2 illustrates the growth inhibition of the *T. pseudonana* algae when the marine diatomic algae were exposed to four types of NHs at two different concentrations of NHs (50 and 100 mg/L) over 24 h, 48 h, and 72 h. The growth inhibition was estimated based on the following (Galletti et al., 2016):

$$\text{Growth inhibition (\%)} = \left(1 - \frac{UV \cdot abs_{concentration\ at\ 6h}}{UV \cdot abs_{control}}\right) \times 100 \qquad \text{[Eq. 1].}$$

(A)

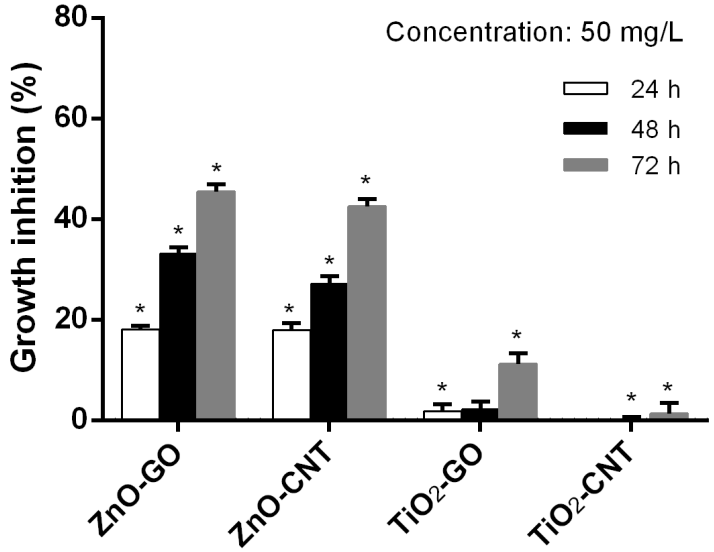

(B)

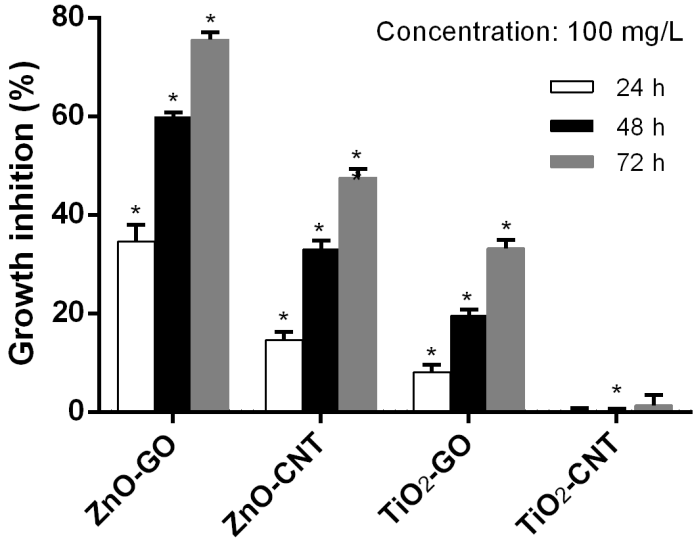

Figure 6.2. Toxicity effect of four different types of NHs on *T. pseudonana* (A) growth inhibition at 50 mg/L and (B) growth inhibition at 100 mg/L over 72 h.

The mortality of *T. pseudonana* increased over increasing exposure time from 24 to 72 h, and the extent of mortality was more apparent at the high concentration of NHs and dependent on the types of NHs. For instance, the growth inhibition rate of *T. pseudonana* was in the order ZnO–GO (45.5%) > ZnO–CNT (42.5%) > TiO_2–GO (11.2%) > TiO_2–CNT (1.3%). In regard to the concentration effect of NHs on the growth inhibition of *T. pseudonana*, the highest inhibition rate of 45.5% NHs was observed with ZnO–GO at 50 mg/L, and at a higher concentration of NHs at 100 mg/L, the growth inhibition rate of *T. pseudonana* increased, especially for the ZnO--based NH-exposed suspensions (e.g., ZnO–GO; ZnO–CNT; TiO_2–GO), in the order ZnO–GO (75.5%), ZnO–CNT (47.5%), TiO_2–GO (33.2%), and TiO_2–CNT (1.3%), respectively.

Several studies have noted that ZnO NPs are more toxic than TiO_2 NPs because of the higher solubility of ZnO NPs than that of TiO_2 NPs (Adams, Lyon et al. 2006, Aruoja,

Dubourguier et al. 2009, Dasari, Pathakoti et al. 2013). The primary attribute of toxicity appears to be due to the production of ROS from NPs, which is responsible for cell damage by such oxidative stress (Hou, Wu et al. 2018, Morelli, Gabellieri et al. 2018, Rajput, Minkina et al. 2018). Researchers reported ROS generation from NPs to be increased as NP concentration increased and size decreased. The correlation between the toxicity of NPs on algal cells and reduced cell viability by a nanoparticle concentration increase was noted in several studies (Bhuvaneshwari, Iswarya et al. 2015, Li, Liang et al. 2015, Suman, Radhika Rajasree et al. 2015, Xia, Chen et al. 2015), with proposed mechanisms including physical interaction between algae and NPs, ROS generation, and the shading effect (aggregation). NPs can damage or enter the cell wall by passing through or attaching to cells.

As surface area increases, nanoparticle attachment on cell membranes can be increased by electrostatic force, thereby causing damage to the cell membranes (Hou, Wang et al. 2018). The shading effect reduces light availability for photosynthesis of algae, so that aggregation of NPs can affect the shading by blocking or attaching to the surface of the cells (Li, Liang et al. 2015). Thus, the size of aggregation can also be a key factor in determining the effect of NPs on cells due to NPs' surface area and reactivity (Hu, Wang et al. 2018). Notably, ZnO- and TiO_2-cojugated GO (i.e., ZnO–GO and TiO_2–GO) exhibited higher mortality than ZnO- and TiO_2-combined CNT (e.g., ZnO–CNT and TiO_2–CNT) at both concentrations of NHs, with no toxicity effect on algae at both concentrations of 50 mg/L and 100 mg/L from the TiO_2–CNT nanohybrid.

A similar observation when there was more toxicity of GO on algal cells compared to CNT was observed in a recent study by Zhao et al. (2017), possibly due to GO's hydrophilic

surface and strong electrostatic repulsion between GO sheets. Lv, Yang et al. (2018) reported that GO could be more toxic than other carbon nanomaterials due to its enhanced dispersibility and high hydrophilicity, whereas carbon nanotubes are hydrophobic nanomaterials that are likely to form more aggregates. A study by Lv et al. (2018) revealed the toxicity mechanism of GO on *Daphnia magna* as oxidative stress from GO accumulation after 24 h exposure of *Daphnia magna* to GO NPs. Other suggested explanations were high hydrophilicity of GO and faster GO uptake/depuration that occurred in daphnia than those in other carbon nanomaterials, thereby preventing aggregation by dispersion of NPs on GO, with a subsequent increase in NP surface and reactivity. A study by Hu et al. (2018) reported that the aggregation and the following sedimentation of TiO_2 NPs reduced their adverse effect on microalgae and suggested that other factors such as ionic strength and NP concentration influenced aggregation and sedimentation rates.

The toxicity effect of single metal oxide NPs (ZnO, or TiO_2) on *T. pseudonana* was compared with toxicity effects from GO-conjugated TiO_2 or ZnO NPs. The results suggest higher toxicity on exposure of *T. pseudonana* to metal oxide NPs (either ZnO or TiO_2)-conjugated with GO in comparison to the toxicity, when *T. pseudonana* is exposed to single type of NPs. This is possibly due to dispersion effect by GO, rendering NPs to have high surface area and to increase the ROS generation. For instance, the growth inhibition rate of *T. pseudonana* was in the order of ZnO-GO (77%) > ZnO (42%) > TiO_2-GO (23.4%) > TiO_2 (4.3%). Notably, ZnO-based NHs showed higher toxicity than TiO_2-conjugated NHs, because of higher solubility of ZnO NPs than that of TiO_2 NPs, influencing the ROS generation. Soluble ZnO NPs was more efficient than insoluble TiO_2

6.3.5. Assessment of ROS generation

When nanocomposites absorb light energy, charge seperation is induced, and nanocomposites produce pairs of e^- and h^+. The excited electrons are transferred from the valence band (VB) to the conduction band (CB), and leave holes in the VB. This is followed by the generation of ROS by oxidation and reduction reactions of facilitated pairs of e^- and h^+ (Yuan Yao 2008). When metal-oxide NPs are combined with other nanocomposites (GO and CNT), the separated charges are transferred to each other, thereby enhancing suppression of the recombination of electron–hole pairs and increasing photocatalytic activity of nanocomposites by adsorption of NHs (Qi, Cheng et al. 2017). The ROS generation measured by the fluorescence intensity rate (%) after exposure of algae to four types of NHs was in the ascending order ZnO–GO > ZnO–CNT > TiO_2–GO > TiO_2–CNT, which was consistent with observation in the toxicity effect of algae (Fig. 6.3). The generation of ROS from ZnO–GO-exposed algae was significantly higher than that of the other types (i.e. CNT, TiO_2–GO, and TiO_2–CNT) of nanohybrid-exposed algal cells. A previous study suggested that the distribution of metal oxide on GO can enhance ROS generation because the distribution of NPs on GO can increase the surface area of NHs(Zhao, Cao et al. 2017). Thus, hydroxyl radicals were generated even under the absence of ultraviolet light by metal-oxide NPs (Adams et al., 2006). Wang, Zhang et al. (2017) reported that the toxicity of graphene and ionic liquids may be driven by few mechanisms, such as adsorption, stability, and oxidative stress. Especially, the physicochemical interaction of graphene by the liquids' sharp edges was important to toxicity on algae in aquatic environments.

As illustrated in Fig. 6.3, the increase of ROS correlated to the concentration of NHs and exposure time. However, there was a slight decrease in ROS generation observed over 72 h exposure to algae at 50 mg/L of ZnO–GO, possibly due to reduced photoactivity from aggregation and the shading effect over long-term exposure of NHs to algae at a low ZnO–GO concentration (50 mg/L). It appears that reduced surface area and reactivity from aggregation of NHs decreased the photoactivity of NHs. A study by Ko et al. (2018) revealed that the exposure of Ag–GO nanocomposites to algae resulted in the inhibition of microorganism activities through oxidative stress and cell-membrane damage induced from GO and Ag–GO. In this study, 80% of ROS was generated by GO within 1 h, whereas ROS was not detected in 24 h and 48 h because of aggregation and precipitation of GO. Applying a scavenger (NAC) suppressed the ROS generation and the extent of suppression was increased with higher concentration of NAC (0.5 mM versus 2 mM), indicating that the ROS generation was a primary toxicity mechanism and the maximum capacity of NAC increased with increasing NAC concentrations(Ma, Wallis et al. 2014)(Ma, Wallis et al. 2014) . Different types of nanomaterials (ZnO NPs, TiO_2 NPs, GO, and CNTs) may induce oxidative stress by producing ROS, causing DNA damage and attaching to cell surfaces, which leads to toxic effects in the cells by disrupting metabolic biomolecules (Nogueira, Nakabayashi et al. 2015). Several studies reported that NHs, which are a combination of metal-oxide NPs and carbon-based nanomaterials, have more photocatalytic activity than single-NP types of NPs (Chen, Zhang et al. 2013, Wang, Cao et al. 2014). This is because the long distance of Shuttling electrons between metal-oxide NPs and carbon-based nanomaterials leads to blocking of the recombination of photo-generated e^- and h^+ pairs by electron transfer to each other (Zhang, Zhang et al. 2011).

Results on the ROS generations from single type of NPs versus ZnO or TiO_2-conjugated GO NHs were consistent with the toxicity effect of four types of NPs (ZnO, ZnO-GO, TiO_2, TiO_2-GO) on *T. pseudonana*, in which the ROS generation was in the ascending order of ZnO-GO > ZnO > TiO_2-GO > TiO_2. Results suggest the dispersion effect by GO increases the active surface area of NPs (Chen, Zhang et al. 2013), and a recent study (Hu et al., 2012) indicated higher ROS production from TiO_2-GO than that from TiO_2 NPs, which is consistent with results presented in this study. Overall, results of the fluorescence intensity test exhibited that toxicity of NHs combined with ZnO NPs is higher than that of TiO_2 NP-based NHs. These results are consistent with those obtained by other researchers (Adams, Lyon et al. 2006, Aruoja, Dubourguier et al. 2009, Kumar, Pandey et al. 2011). Compared to ZnO NPs, suspensions of TiO_2 NPs were of remarkably lower toxicity to algae. Several studies reported that the kinetics and aggregation of ZnO NPs and TiO_2 NPs on algae were highly dependent on pH and ionic strength (Pagnout, Jomini et al. 2012, Krol, Pomastowski et al. 2017). As observed in the present study, no influence of TiO_2–CNT on both cell growth inhibition and ROS intensity was observed over 72 h exposure of TiO_2–CNT to algae, which was attributed to the aggregation of the CNT due to its hydrophobic nature, thereby promoting self-association and aggregation, as noted by other studies (Koh and Cheng 2014).

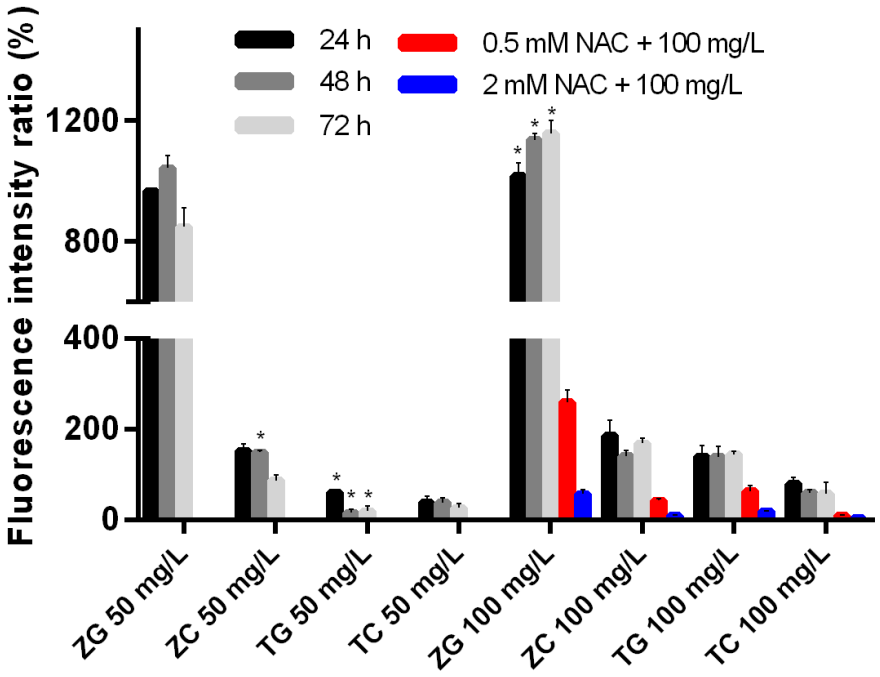

Figure. 6.3. The fluorescence intensity of *T. pseudonana* exposed to four different types of NHs of two concentrations for 72 h.

6.3.6. SEM analysis of algae and NHs

The interaction between algae and four types of NHs was assessed using SEM image analysis. As illustrated in Fig. 6.4, the SEM images of NHs after exposure to *T. pseudonana* for 72 h indicate that algal cells were directly clumped and attached to NHs. GO sheets formed aggregation and attachment to the algae and exhibited significant catalytic effects (Zhang, Meng et al. 2018), through the interaction of nanocomposites with algal cells, disrupting the algal cell wall by oxidative degradation of lipids resulting in cell damage (Souza, Venturini et al. 2018). A recent study by Zhao et al. (2017) indicated that there were direct physical damages to algal cells with sharp edges and corners induced by GO, although GO did not penetrate into algal cells because of the protection of cell walls. Other studies that employed SEM images to analyze the interaction between algal cells and

CNTs reported severely aggregated CNTs (Rhiem, Riding et al. 2015, Zhang, Lei et al. 2015, Pikula, Zakharenko et al. 2018), which visualized the CNTs' exposure to algal suspension—interaction of CNTs with algal cells by attacthing to the outer cell wall of algae. As revelaed in Fig. 6.4, significant morphology changes with algal cell structure were observed, and aggregated NHs were attached to the surface of cells when NHs were exposed to algae. Shading effects of GO or the CNT and the resultant reduction of light for algal photosynthesis were reported in several studies (Wang, Zhang et al. 2008, Wei, Thakkar et al. 2010) in which GO or CNT agglomeration was around the algal cells, and such shading effects resulted in decreasing chlorophyll to algal cells due to nanocompsites' adsorption on cell surfaces. According to these studies (Wei et al., 2010; Aruoja et al., 2009), the growth inhibition was correlated with the shading due to carbon nanomaterials and their agglomeration around algal cells.

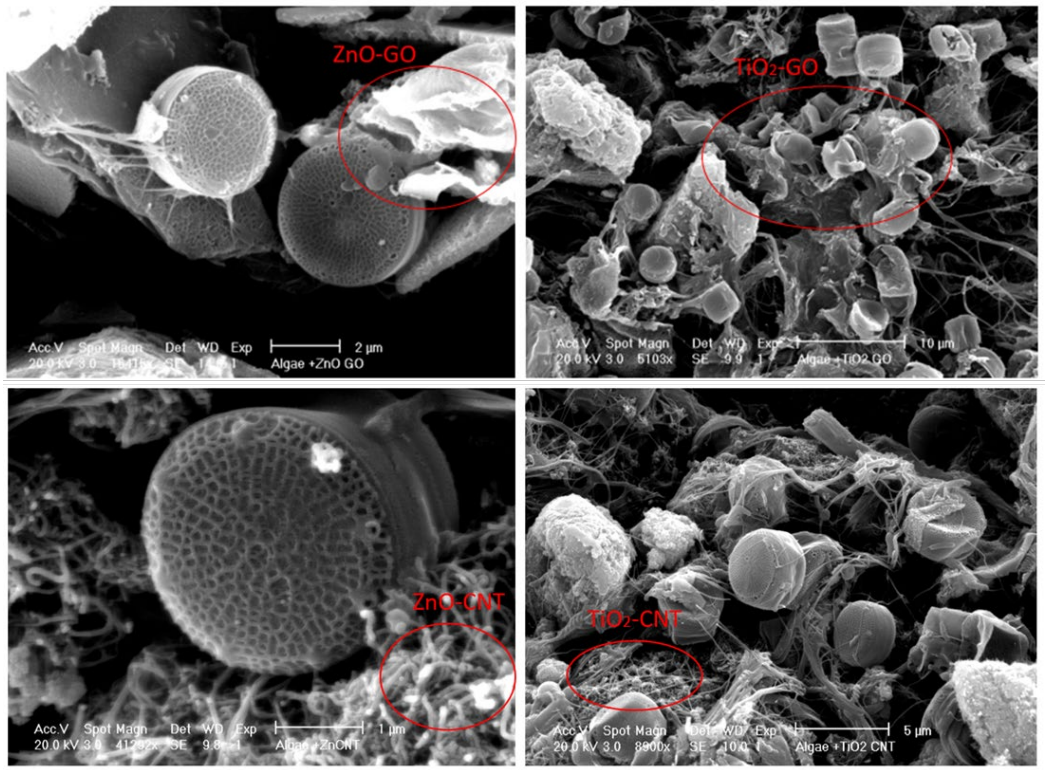

Figure 6.4. SEM images of four different types of NHs after exposure to *T. pseudonana* for 72 h.

According to a study by Schwab et al. (2011), well-dispersed CNTs also had a stronger shading effect than high CNT concentration, and they affected ROS generation (Schwab, Bucheli et al. 2011). In this study, experimental results indicated that well-dispersed CNTs absorbed over six times more light than agglomerated CNTs. Consequently, both shading and agglomeration of algal cells with GO and CNTs could cause the toxicity effects and ROS generation. Another study reported that the toxicity of algae was not influeced by photocatalytic activity of GO, whereas algal growth inhibition was correlated with the shading effect due to carbon nanomaterials and their agglomeration with agal cells (Nogueira, Nakabayashi et al. 2015). As discussed earlier, the shading effect that was related to NP aggregation could reduce a specific area and active sites of the NP surface, so that this aggregation may prevent chlorophyll from absorbing light and inhibit algae growth (Li, Liang et al. 2015).

6.3.7. Comparison of NPs and NHs on antibacterial effect

To compare the toxicity effect of single types of NPs and GO based NHs, algae was exposed to ZnO NPs, ZnO-GO, TiO_2 NPs, and TiO_2-GO. Figure 6.5A shows growth inhibition rate of *T.speudonana* after exposure to 4 types of nanomaterials for 72 h at 100 mg/L of concentration. Inhibition rate on *T.speudonana* after exposure to ZnO NPs and ZnO-GO NHs indicated 75% and 42.6%, respectively. Inhibition rate on *T.speudonana* after exposure to TiO_2 NPs and TiO_2-GO NHs indicated 16% and 1%, respectively. This experimental data is consistent with the hypothesis that toxicity of single type of metal

oxide NPs increase when it is combined with GO due to the dispersion of metal oxide NPs on GO. High surface area and morphology of GO sheets promotes effective dispersion of metal oxides on GO, so that surface area of metal oxide NPs increase resulting in the increase of ROS generation.

ZnO-based nanomaterials were more toxic than TiO_2-based nanomaterials, possibly because of higher solubility of ZnO NPs than that of TiO_2 NPs. This is because solubility of metal oxide NPs also can affect to their ROS generation. Kocbek et al. (2010) showed that partially soluble ZnO NPs stimulated the ROS production more than did insoluble TiO_2 (Kocbek, Teskac et al. 2010). Thus, solubility can also affect to their dispersion on GO. From the SEM images of ZnO-GO and TiO_2-GO, it was observed that the aggregated size of TiO_2 onto GO was larger with less dispersion compared to that onto ZnO–GO.

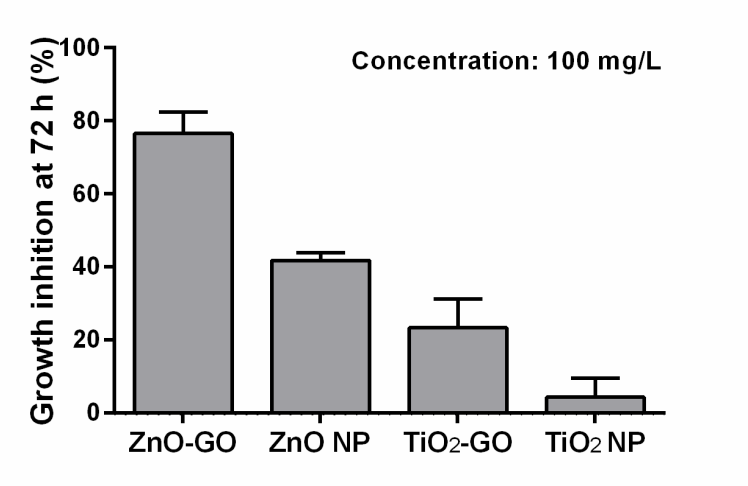

(A)

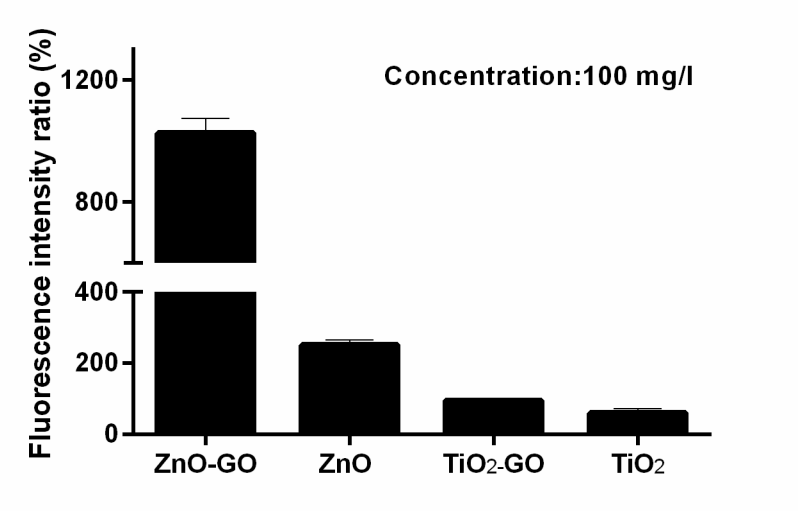

(B)

Figure 6.5. Growth inhibition of algae by a single type of NPs (ZnO or TiO_2) versus nanohybrids (A) and the fluorescence intensity of *T. pseudonana* exposed to nanomaterials for 72 h (B).

6.4. Conclusions

The antibacterial properties of 4 synthesized NHs composites were investigated on SH*E. coli* bacterial cells. ZnO-GO, ZnO-CNT, TiO_2-GO, and TiO_2-CNT NHs were successfully synthesized and their formation was confirmed with TEM, SEM, and FT-IR results. The presence of GO was shown to increase dispersion of metal oxide onto GO due to its large surface area with sheet shape morphology. FT-IR analysis confirmed the formation of considerable amounts of functional groups on surface of NHs, as compared to the bare carbon materials. Antibacterial activities of synthesized NHs were dose and exposure time dependent, and growth inhibitions of 4 NHs on cells were consistent with ROS generation. ZnO nanocomposites has higher toxicity to *E. coli* than TiO_2 nanocomposites when ZnO and TiO_2 NPs are synthesized with GO or CNT. Thus, GO and CNT increased the dispersion of metal oxide NPs, because synthesized nanocomposites

intensified ROS generation by suppressing the recombination of electron-hole pairs. SEM and TEM images presented GO based nanocomposites attached on the surface of cells while CNT nanocomposites were aggregated each other without interaction with cells. This indicates that GO nanocomposites had a batter interaction with ZnO with dispersion and significantly enhanced antibacterial effect compared to CNT.

The results of our study provide a fundamental understanding of toxicity effect of NHs on cells and its antibacterial mechanisms when NPs are present in combined form. ZnO-GO composites exhibited significant antibacterial properties not only for the ROS generation, but also attachment on cells due to its increased surface area and its sharp morphology shape which can damage cell membranes. This finding has implications to the toxicity activity of NHs on microorganisms. NHs potentially could be used as substantial materials to treat bacteria present in water by their enhanced photocatalytic effect. Thus, NHs materials can be developed for point-of-use water treatment purification for the removal of microbes especially under solar energy by facilitating the photocatalysis properties of nanomaterials.

Second, the antibacterial properties of 4 synthesized NHs composites were investigated on *T.peudonana.* The toxicity significance was also in the order ZnO–GO > ZnO–CNT > TiO_2–GO > TiO_2–CNT. The generation of ROS by NHs following the induction of electron–hole pairs appears to be a primary toxicity mechanism. Cell membrane damage caused by NH attachment may also contribute to the toxicity of NHs, especially ZnO NP-conjugated NHs. Last, the shading effect of NHs by preventing the photosynthesis of algae is one of toxicity mechanisms.

As revealed in the SEM images, there were aggregated NHs attached to or around the algae surfaces, thus causing shading effects which reduce light availability for photosynthesis of algae. These key findings on the toxicity kinetics and underlining mechanisms of the NH toxicity are encouraging in that designing and manufacturing NHs in a safe and eco-friendly manner can not only minimize harm to the marine environments but also improve understanding of the ultimate fate and transport of NPs, since scant information is available on the NH toxicity and toxicity mechanisms of a marine aquatic species.

CHAPTER 7:

NANOCOMPOSITES FOR THE REMOVAL OF ANTIBIOTIC-RESISTANT BACTERIA IN WATER BY NANOPARTICLES-ALGINATE BEADS[5]

[5] Baek, S., Joo, S. H., Toborek, M. (2018) Novel treatment of antibiotic-resistant bacteria by encapsulation of ZnO nanoparticles in an alginate biopolymer: Insights into treatment mechanisms. *Journal of Hazardous Materials*. (under review)

7.1. Application of nanoparticles for the water treatment

Considering the unique antibacterial properties of NPs as discussed in Chapter 3-6, NPs seem to be used as a material which inactivates harmful bacteria in environmental applications. *E. coli* and *P. aeruginosa* are the antibiotic-resistant bacteria present in wastewater, and a pathogen that known to cause urinary tract infections, respiratory system infections, dermatitis, and a variety of systemic infections, particularly in patients. For example, *P. aeruginosa* resists high concentrations of salt, dyes, weak antiseptics, and many commonly used antibiotics (Shrivastava, Upreti et al. 2004, Jahani, Saeidi et al. 2016). Generally, chlorine, UV, and the ozone process are commonly used to deactivate pathogenic microorganisms including antibiotic-resistant bacteria in water (Zheng, Su et al. 2017). However, studies show that chlorine is not very effective for the removal of antibiotic-resistant bacteria present in water (Shrivastava, Upreti et al. 2004). A study was conducted on the effect of chlorine, ozone, and TiO_2 photocatalytic processes on the removal of antibiotic-resistant bacteria, and results showed TiO_2 NPs induced more damage than chlorine in cell DNA (Öncü, Menceloğlu et al. 2011). Other studies have applied UV and ozone processes for inactivation of microbial pollutants, but high treatment expense and dosages were demanded to disinfect microbial with these methods (Johnson 2010, Jager, Alexander et al. 2018). It is also reported that chlorine used in water and sewage can selectively promote the survival of antibiotic-resistant bacteria (Shrivastava, Upreti et al. 2004). For instance, sewage treatment facilities using chlorine may have the unintended consequences of encouraging the formation of other antibiotics in the discharged water drinking water, by selectively supporting the survival of antibiotic-resistant bacteria. Since the problem of antibiotic resistance in water is being worsened

worldwide, and superbugs have been found in water treatment plants (Ahmed, Zhou et al. 2015), there is a need to come up with alternative disinfectants to provide safe and clean water.

Nanomaterials can be incorporated to develop small scale cost-effective pathogenic bacteria control systems due to their antibacterial properties (i.e., large surface area and ROS generation) even in a small amount of NPs. Thus, NPs require less processing, no DBPs, and reusable materials. Among many NMs, ZnO NPs show strong antibacterial effect with other chemical stability properties and high surface area; thus it is inexpensive and easy to prepare. However, the use of NPs for the removal of bacteria has not been studied well enough because it is related to retention of particles and reusability of NPs for application. Therefore, the use of polymers where the NPs can be contained can be considered because adding NPs in a polymeric matrix can immobilize NPs and be utilized for controlling microbial activity.

In this chapter 7, the application of NPs was developed by using a polymeric material to immobilize NPs, and utilized as a water treatment material to inactivate antibiotic-resistant bacteria in water. Among many different types of NPs, ZnO NPs were selected to synthesize nanocomposite-alginate beads based on chapter 3-6 studies because they have great antibacterial properties in small quantities and are inexpensive. Thus, sodium alginate was selected as coating materials to encapsulate and disperse ZnO NPs in the nanocomposite beads.

7.2. Novel treatment of antibiotic-resistant bacteria by encapsulation of ZnO nanoparticles in an alginate biopolymer: Insights into treatment mechanisms

7.2.1. Background

The presence of antibiotic-resistant bacteria in water is a major concern worldwide because of its negative health effects. Recently, antibiotic-resistant bacteria, otherwise known as superbugs, have been detected in drinking water across many nations (Ahmed, Zhou et al. 2015). Superbugs are known to cause serious illness and are responsible for at least 2 million infections and 23,000 deaths each year in the United States (CDC 2013). Conventional disinfection technologies, such as ultraviolet, ozone, and chlorine disinfection, are currently used to inactivate the antibiotic-resistant bacteria in water(Öncü, Menceloğlu et al. 2011). However, these processes are not very effective for the removal of antibiotic-resistant bacteria present in water because they not only require high dosages and long contact time to inactivate the antibiotic-resistant bacteria but also produce byproducts (Shrivastava, Upreti et al. 2004).

Several studies applied conventional treatment processes for the removal of antibiotic-resistant bacteria (Johnson 2010, Öncü, Menceloğlu et al. 2011, Jager, Alexander et al. 2018). Among chlorine, ozone, and TiO_2 photocatalytic processes, TiO_2 nanoparticles (NPs) induced more damage than chlorine in cell DNA(Öncü, Menceloğlu et al. 2011). NPs, even in a small number, have potential benefits as novel materials in terms of inactivating pathogenic bacteria due to their strong antibacterial effect (Batley 2012, Lin, Li et al. 2014, Baek, Joo et al. 2017, Baek, Joo et al. 2018). NPs are considered to be relatively more efficient, more affordable (if reusable), and free from any toxic disinfection

byproducts compared to conventional disinfectants(Rasalingam, Peng et al. 2014, Karaolia, Michael-Kordatou et al. 2018, Sarkar, Mandal et al. 2018). However, the use of NPs for the removal of bacteria has not been studied well enough because of concerns about leaching of NPs into water, which results in the difficulty of water reuse (Dimapilis, Hsu et al. 2018). Overcoming these obstacles could make NPs an affordable alternative material. Therefore, the current study investigated the application of ZnO NPs encapsulated in an alginate biopolymer solution, resulting in the production of ZnO–alginate beads that prevent leaching of NPs and reuse of beads.

Recently, polymeric materials such as alginate and chitosan have been used as a host for impregnation of NPs (Motshekga, Ray et al. 2015, Chatterjee, Ghangrekar et al. 2017, Motshekga, Sinha Ray et al. 2018, Salama, Diab et al. 2018), particularly alginate composite beads, for increasing adsorption capacity for the removal of contaminants. Having NPs (especially those with antibacterial properties) encapsulated in alginate could offer increasing surface area through dispersion and immobilization of NPs. Lin et al. (Lin, Huang et al. 2013) investigated the antibacterial effect of silver NP–alginate beads using various filter materials for point-of-use drinking water disinfection. A recent study that applied chitosan nanocomposites with silver and ZnO NPs to inactivate bacteria in water (Motshekga, Sinha Ray et al. 2018) indicated that the antibacterial effect was improved with a large number of nanocomposites and longer contact time at a low concentration of bacteria (200 CFU mL^{-1}), while the inactivation at high concentrations of bacteria exhibited less efficiency. Other researchers demonstrated the efficient removal of *E. coli, P. aeruginosa*, and *S. aureus* using silver NP–coated beads and observed no

adsorption/adhesion of bacterial cells on the synthesized beads (Gangadharan, Harshvardan et al. 2010).

Despite ongoing development of water treatment methods using nanocomposite beads, little is known regarding disinfection mechanisms of nanocomposite beads, reusability of spent nanocomposite beads, and the application of nanocomposite beads for treating high concentrations of antibiotic-resistant bacteria. This study aims to (1) explore the antibacterial effect of ZnO NP–alginate beads on two model antibiotic-resistant bacteria (*E. coli* DH-5α and *P. aeruginosa*), (2) identify antibacterial mechanisms and reusability of the beads, and (3) recommend optimum conditions in a more cost-effective manner compared to conventional disinfectants along with future research directions.

7.2.2. Materials and methods

7.2.2.1. Materials

Industrial ZnO NPs (>97% purity, <50 ± 5 nm nominal size, and >10.8 m^2/g surface area) and sodium alginate powder (medium viscosity: 600–900 cps) were purchased from Sigma-Aldrich (St. Louis, MO). The antibiotic-resistant bacteria strains used to investigate the antibacterial activity were *E. coli* with MAX Efficiency DH5α Competent Cells (Invitrogen, CA) and *P. aeruginosa* (Schroeter) Migula (ATCC®, VA, USA).

7.2.2.2. Synthesis of nanocomposite–alginate beads

The sodium alginate solution was prepared by dissolving 10 g of sodium alginate powder in 1 L deionized (DI) water and stirred until a clear solution was obtained. A calcium chloride ($CaCl_2$) solution (2%) was dissolved in DI water, and this mixture was purged with N_2 gas for 20 min to remove air bubbles. To create the beads, 50 mL of the

sodium alginate solution was mixed with different amounts of ZnO NPs (0.2, 0.5, and 1 g) under a stirrer at 600 rpm to get a homogenous mixture. The ZnO NP–alginate mixture was pumped dropwise using a peristaltic pump (model Easy-load® II, Cole-Parmer Instrument Co., USA) and tubing (Masterflex Tygon Lab tubing, L/S 13). The mixture drop through tubing was added into 50 mL of deoxygenated $CaCl_2$ solution from 12 cm above the surface. Upon the mixture touching the $CaCl_2$ solution under the stirrer, ZnO NP–alginate beads were formed and left in the solution for 24 h to harden. Afterwards, the $CaCl_2$ solution was decanted, and the beads were washed several times with DI water.

7.2.2.3. Characterization of ZnO NP–alginate beads

The morphologies and elemental analysis of synthesized ZnO NP–alginate beads were characterized with Field Emission Scanning Electron Microscopy (SEM, Philips XL-30 FEG) and Energy Dispersive Spectroscopy (EDS). During their SEM analysis, the beads were coated with a thin (20 nm) coating of Pd in a Cressington Sputter coater. The samples were then placed in an FEI XL-30 Field Emission SEM and imaged at several magnifications. EDS in SEM particulate samples was examined at various magnifications, and X rays were collected at a scan speed of 2 and a working distance of 10 mm.

7.2.2.4. Inactivation of *E. coli* and *P. aeruginosa*

To determine the inactivating effect of the synthesized beads, model bacteria (i.e. *E. coli* and *P. aeruginosa*) were cultured, and a batch test was conducted. Incubated *E. coli* and *P. aeruginosa* were spread on Luria-Bertani (LB) agar plates containing ampicillin and incubated overnight at 37 °C. The colonies from each agar plate were cultured in an LB broth (3 mL) for 12–14 h in an incubator (MaxQ 4000, Thermo Scientific, NY) at 37 °C

under continuous shaking at 225 rpm. A 100 µL of cultures was incubated in 100 mL of the LB broth in a sterilized flask, and the cultivation of bacteria was performed for 12–16 h until the absorbance value reached 0.09 (10^8 cells mL^{-1}) by OD_{600}. The cultivated cells were exposed to different ZnO NP dosages of alginate beads under 37 °C for 6 h under room light. The concentrations of bacterial cells mixed with ZnO NP–alginate beads were measured using OD_{600} every 2 h, and all reported values were averaged from duplicate experiments.

7.2.2.5. ROS detection from ZnO NP–alginate beads

The generation of reactive oxygen species (ROS) from bacteria cells exposed to ZnO NP–alginate beads was measured by fluorescence intensity with Spectramax Gemini EM Microplate Reader (Molecular Devices, CA). The DCF-DA (2',7'–dichlorofluorescin diacetate) cellular ROS detection assay kit (Abcam Inc, Toronto, ON, Canada) was used to dye ROS such as hydroxyl and peroxyl radicals within *E. coli* and *P. aeruginosa* cells. After cells were exposed to ZnO NP–alginate beads (initial, 2 h, 4 h, and 6 h), cells were collected in a conical tube and washed by centrifugation in phosphate buffered saline (PBS). Washed cells were suspended in the DCF-DA solution and incubated at 37 °C for 30 min in the dark. Then, cells were transferred into a clear bottom black 96-well microplate after being washed through centrifugation with the PBS buffer. The DCF was detected by fluorescence spectroscopy with maximum excitation and emission spectra of 485 nm and 535 nm in the presence of the buffer. The photocatalytic activity of NPs was examined with antioxidant *N*-acetyl cysteine (NAC) (Sarkar, Mandal et al. 2018). The NAC, a ROS scavenger, was used to verify the antibacterial effect of ROS, since NAC prevents toxicity caused by ROS through directly scavenging ROS or promoting production of antioxidant

enzymes (Schrand, Rahman et al. 2010). As such, cells were pretreated with 0.5 and 2 mM of NAC, and fluorescence intensity was measured at 6 h in duplicate.

7.2.2.6. Leaching analysis

The release of Zn ions from the ZnO NP–alginate beads was quantified. Monitoring and quantification of the release of Zn ions involved mixing 10 g of beads with 100 mL of DI water, shaking at 37 ℃ for 6 h at 225 rpm, taking samples every 2 h and measuring the leaching amount of ZnO NPs from the beads using ICP-OES (Perkin Elmer Optima 5300 DV ICP-OES, Waltham, MA, USA).

7.2.3. Results and discussion

7.2.3.1. Characterization of ZnO NPs-alginate beads

The morphology of ZnO NP-alginate beads, dispersion of ZnO NPs on the beads, and surface characteristics of synthesized ZnO NP–alginate beads were examined using an SEM analysis. Fig. 7.1 presents SEM images of a half-cut section of alginate beads (control) and ZnO NP–alginate beads. The microscopic analysis revealed that diameters of alginate beads were around 2 mm. The SEM images of control beads exhibited a uniform plain morphology (Fig. 7.1A). The surface of the half-cut section of the ZnO NP–alginate beads appears irregular and bumpy because of ZnO NPs attached or coated on the alginate beads (Fig. 7.1B). Thus, ZnO NPs attached on the surface of beads aggregated with one another. These images indicate that ZnO NPs were coated not only on the surface of the beads but also inside the beads. The uneven distribution of metal-oxide NPs on polymer beads could be due to the chemical reduction route employed to have metal-oxide NPs on the beads (Gangadharan, Harshvardan et al. 2010).

Similar surface morphology of ZnO NP–chitosan beads was reported in a recent study (Chatterjee, Ghangrekar et al. 2017). In this study, some wrinkles and many irregularities on the surface of the ZnO NP–chitosan beads were observed, and a laminar morphology was observed on the chitosan beads that did not contain ZnO NPs. The elemental composition of ZnO NP–alginate beads was determined using EDS (Fig. 7.1A). The EDS analysis confirmed clear peaks of Zn as the primary element, and other compounds, such as Ca and Cl, presented by the beads during synthesis. The size of aggregated ZnO NPs on the surface of the ZnO NP–alginate beads indicates an irregular spherical shape of ZnO NPs, with sizes ranging from 120 to 236 nm, coated on the surface of alginate beads (Fig. 7.1B). The agglomeration of the particles may be attributed to the aggregation behavior of NPs or the viscosities of the solutions (Motshekga, Ray et al. 2015). The sizes of the NPs have a considerable effect on their antibacterial activity, as they determine the surface area of NPs, which is important for NPs' reactivity (Barnes, Molina et al. 2013, Jahani, Saeidi et al. 2016).

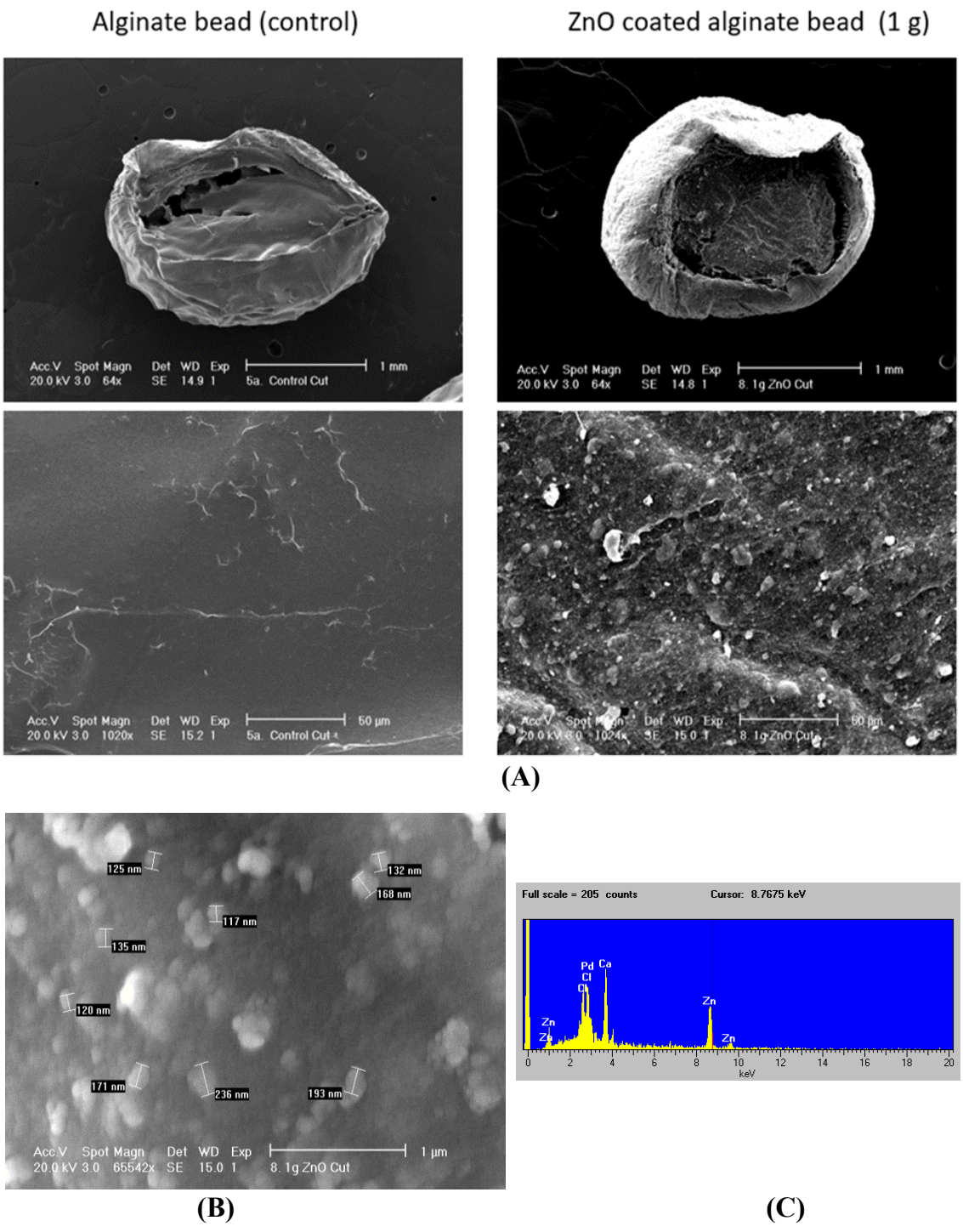

Figure 7.1. SEM images of (A) half cut section of alginate beads (control) and ZnO-alginate bead, (B) the size measurement of ZnO NPs on the surface of ZnO-alginate beads, and (C) EDS analysis of ZnO NP–alginate beads.

7.2.3.2. Antibacterial effect of ZnO NPs-alginate beads on antibiotic-resistant bacteria

The antibacterial effect of ZnO NP–alginate beads was investigated on antibiotic-resistant bacteria (*E. coli* and *P. aeruginosa*). A batch test was conducted against antibiotic-resistant bacteria with different concentrations of ZnO NPs-alginate beads (control without ZnO NPs and ZnO NPs at 0.2, 0.5, and 1 g in 50 mL of alginate mixture) at the initial bacteria concentration of 10^8 cells mL^{-1}. Fig. 7.2A illustrates the growth curve and growth inhibition rate of *E. coli* after exposure to different concentrations of ZnO NP–alginate beads. It was observed that bacterial growth inhibition increased with an increase in contact time and the amount of ZnO NPs present in ZnO NP–alginate beads (96.8 % at 0.5 g ZnO NPs to 97.4 % at 1 g ZnO NPs). The initial rapid growth inhibition of the antibiotic-resistant bacteria at 0.5 g ZnO NPs appears to depend on the type of bacteria. For instance, the growth curve and growth inhibition rate of *P. aeruginosa* bacteria exposed to 0.5 g of ZnO NPs present in ZnO NP–alginate beads exhibited only 25.3 % growth inhibition of *P. aeruginosa*. However, the growth inhibition rate abruptly increased to 88% when the concentration of ZnO NPs in the alginate solution increased to 1 g (Fig. 7.2B). Several studies suggested that *P. aeruginosa* are more resistant to antibiotics than *E. coli* because of *P. aeruginosa*'s extracellular polymeric substance (also sometimes abbreviated EPS) which has high-molecular-weight polymers surrounding microorganisms (Kumar, Pandey et al. 2011, Xue, Hessler et al. 2013). EPSs produced by *P. aeruginosa* provide a protective role for bacterial cells against disinfectant or limit access to reactive sites on a cell membrane (Jiang, Zhang et al. 2016).

Figure 7.2C illustrates the growth and the growth inhibition rate of different concentrations of ZnO NP–alginate beads on mixed-species antibiotic-resistant bacteria (*P. aeruginosa* and *E. coli*). The inhibition rate of mixed bacteria in water was 38.5% for 0.2 g, 93.3% for 0.5 g, and 97.7% for 1 g of ZnO NPs in ZnO NP–alginate beads, respectively. The data exhibits the enhanced inhibition rate of *P. aeruginosa* when *P. aeruginosa* was mixed with *E. coli*, whereas a decreasing inhibition rate of *E. coli* was found when *E. coli* was treated with *P. aeruginosa*, suggesting synergistic effects when mixed bacteria are treated with ZnO NP–alginate beads in water. Given that the occurrence and the spread of antibiotic-resistant bacteria in water are pressing public health problems worldwide, the application of ZnO NP–alginate beads seems to be highly effective in the inactivation of mixed antibiotic-resistant bacteria in water. Overall, the inactivation of bacteria by ZnO NP–alginate beads increased with an increasing amount of ZnO NPs, which is due to more active sites and larger surface area for the antibacterial effect on bacteria on increasing concentrations of NPs (Suganthi and Rajan 2012, Venkatesan, Lee et al. 2017).

While the inactivation kinetics may depend on the concentration of NPs, the initial bacterial concentration and contact time also influence the antibacterial effect of ZnO NP–alginate beads on bacteria as demonstrated in a study where no bacteria were present in water after 70 min of contact time with initial bacteria (*S. aureus*) concentration of 200 CFU mL^{-1} (Motshekga, Sinha Ray et al. 2018). Similarly, another study found the inactivation of *E. coli* and *S. aureus* by chitosan–alginate biosynthesized silver, and the extent of antibacterial effect due to the addition of silver NPs to the biopolymer was significant (Fatehah, Aziz et al. 2014). Chatterjee et al. (Chatterjee, Ghangrekar et al. 2017) revealed that treating total suspended solid concentrations (50–100 mg L^{-1}) in the sewage by ZnO–Ag NPs in chitosan

beads resulted in a 10–20 % disinfection efficiency decrease through the mechanism of ROS generation. In the combined ZnO and Ag NPs in chitosan beads, bacterial inactivation was influenced by factors including pH, particle size and surface area (Motshekga, Ray et al. 2015).

There are four possible antibacterial mechanisms that could contribute to the inactivation of hazardous bacteria. Specifically, bacterial cells can be damaged through the release of metal ions, injury to the cell membrane by direct contact, or the generation of ROS. Given that ZnO NPs are encapsulated in an alginate solution, direct interaction between ZnO NPs and cells may be excluded as one of the antibacterial mechanisms. However, the generation of ROS can likely be one of the mechanisms, since the ROS can destroy bacterial cells, as illustrated in our previous studies (Baek, Joo et al. 2017, Baek, Joo et al. 2018). In addition, the electro-steric effect by dispersants used to coat NPs may be involved, especially when coating materials are present where molecular weight or viscosity of the polymer influences the antibacterial effect of nanocomposite–alginate beads.

Regiel et al. (Padmavathy and Vijayaraghavan 2016) evaluated the antibacterial effect of a silver NP–chitosan nanocomposite film. The study revealed the antibacterial effect influenced by the polymer molecular weight at a medium molecular weight of chitosan in which a larger surface area was prone to oxidation with optimum viscosity. The electro-steric repulsion effect from dispersants (polymer coating materials) may prevent aggregation of NPs and maintain or increase the surface area of NPs, thereby enhancing their antibacterial effect. The release of metal ions could also influence the antibacterial effect. However, in the present study, pH levels of cell suspension with ZnO NP–alginate

beads remained 7.2–7.4, suggesting the release of Zn ion is unlikely to happen since the point of zero charge (PZC) of ZnO NPs occurs at pH 7.1–9.4 (Tso, Zhung et al. 2010, WHO 2011, Leung, Xu et al. 2016). Thus, the primary antibacterial mechanism of ZnO NP–alginate beads could be linked to ROS generation, which results in more rapid growth inhibition of cells (Barnes, Molina et al. 2013, Regiel, Irusta et al. 2013).

(A)

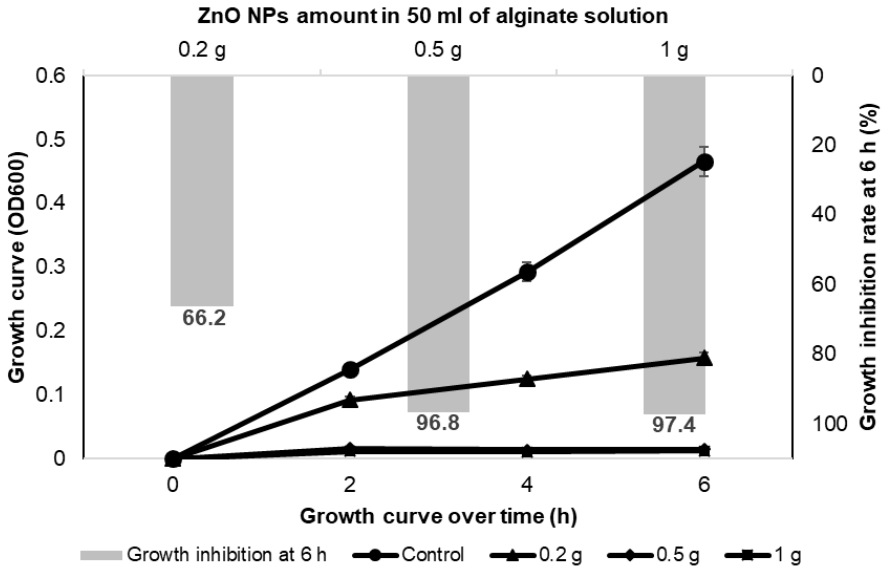

(B)

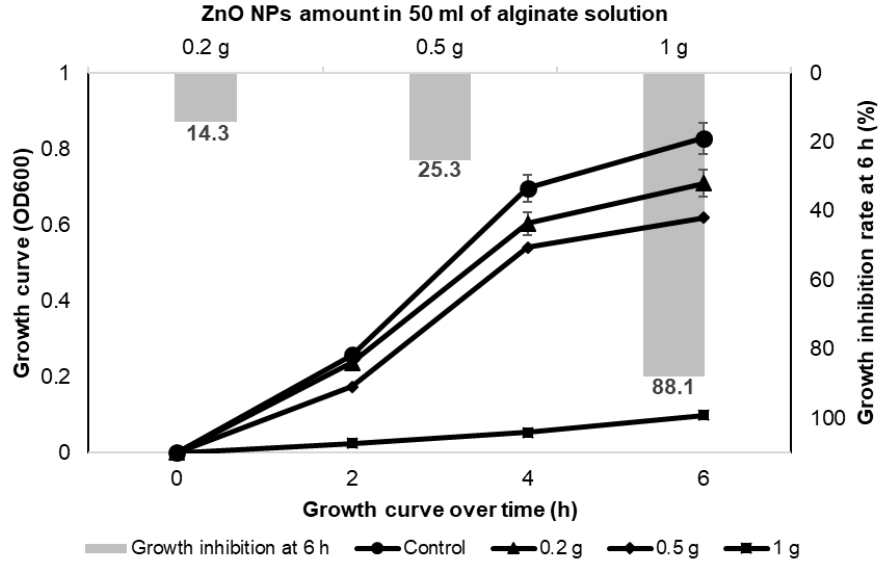

(C)

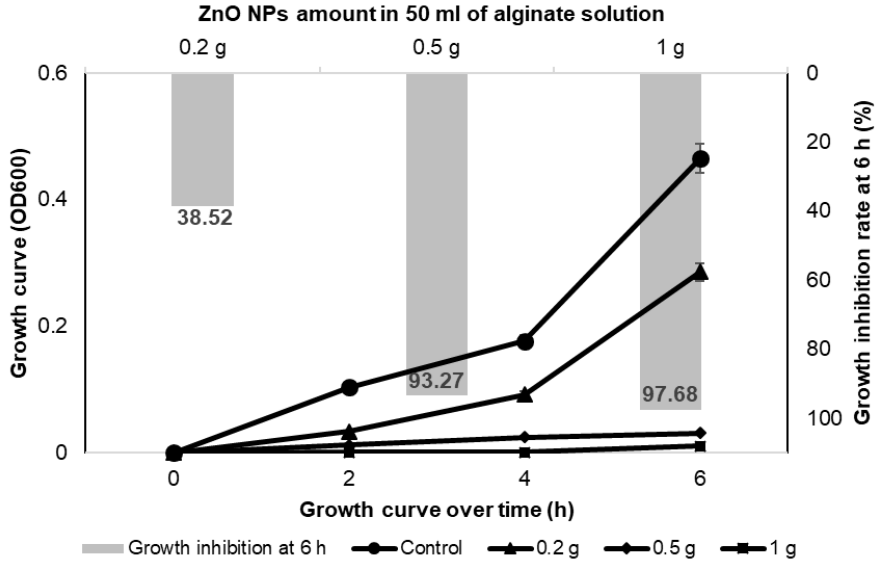

Figure 7.2. Growth rate and growth inhibition rate of antibiotic-resistant bacteria of (A) *E. coli*, (B) *P. aeruginosa*, and (C) mixed bacteria with *E. coli* and *P. aeruginosa* after being exposed for 6 h to different concentrations of ZnO NP–alginate beads.

7.2.3.3. Release behavior and antibacterial activity of ZnO NPs-alginate beads

Zinc is known to be toxic on cells at elevated concentrations, and this has limited the concentration allowable for safe use in water to 3–5 mg L^{-1} Zn^{2+} in drinking water (Wong, Leung et al. 2010, Motshekga, Ray et al. 2015). The release of metal ions from NPs could have adverse effects when their concentration is above the standard levels (Motshekga, Ray et al. 2015). Moreover, the release of metal ions could lead to the perforation of the bacteria cells, resulting in cell death (Li, Lin et al. 2013, Baker, Tyler et al. 2014). As one of potential antibacterial mechanisms, the release of Zn^{2+} from ZnO NP–alginate beads was measured through an ICP-AES analysis. As illustrated in Fig. 7.3, the amount of Zn ions released from ZnO NP–alginate beads was ≤ 0.4 mg L^{-1} over 6 h, which is significantly less than the maximum allowable Zn^{2+} concentration in water. Given that the pH level of

the water solution was around PZC of ZnO NPs, dissolved Zn^{2+} effects might not be significant, and particles would be present with aggregation or partial disaggregation (Godymchuk, Karepina et al. 2015). Thus, the amount of released zinc ions from ZnO NP–alginate beads had not increased after 2 h exposure, indicating the least antibacterial effect by the release of zinc ions.

At the neutral pH level (7.2–7.4) maintained throughout the experiments, the maximum amount of released Zn^{2+} from the ZnO NP–alginate beads were 0.4 mg L^{-1}. The released amount of Zn^{2+} remained stable within the alginate matrix, which is even within acceptable limits for drinking water. A similar observation was made in another study (Padmavathy and Vijayaraghavan 2016), in which the strong attachment of NPs on chitosan reduced leaching rate of NPs, which was related to the molecular mass of the chitosan. A study by Motshekga et al. (Motshekga, Ray et al. 2015, Motshekga, Sinha Ray et al. 2018)suggested that zinc-ion leaching may be attributed to the quantity of NPs within beads or partially exposed NPs on the surface of beads. Another study by Li et al. (Song, Zhang et al. 2010) reported that the toxicity of ZnO NPs to *E. coli* depended on zinc-ion concentration, demonstrating that 0.4–0.8 mg/L of Zn^{2+} on bacteria was in accordance with 10–40% of bacterial mortality. The Zn ions have been found to associate with damaged cells and stimulate oxygen radical generation by cells (Shalumon, Anulekha et al. 2011, Mohd Omar, Abdul Aziz et al. 2014). Thus, the toxicity of Zn^{2+} is a dose-dependent response, indicating that increasing the ZnO dissolution rate could increase the toxicity of ZnO NPs on cells. However, given that the release of metal ions is also influenced by pH, an increase in zinc ions could cause higher toxicity by attaching ions onto the surface of bacterial cells (Jassby, Farner Budarz et al. 2012). Nonetheless, in the present study, the antibacterial effect by the

release of Zn ions is unlikely because of the pH within the PZC ranges.

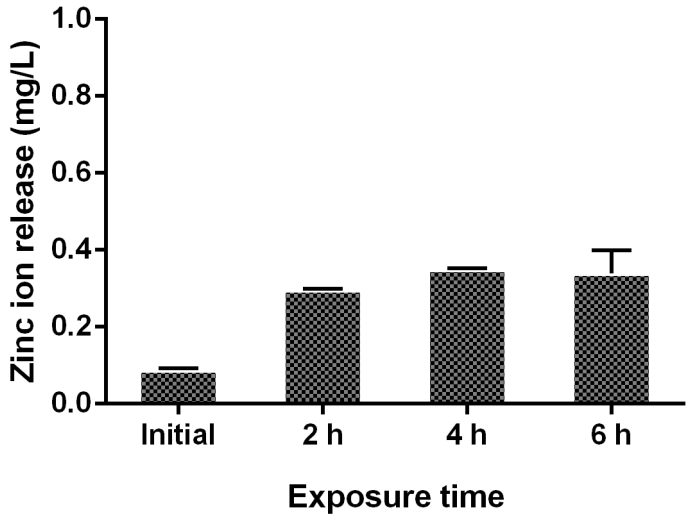

Figure 7.3. The amount of zinc-ion release from synthesized ZnO NP–alginate beads (1 g of ZnO NPs in 50 ml of alginate solution) over 6 h

The ROS generation of ZnO NPs has played an important role in many types of bacterial cell damage, which can result in cell death and DNA damage (Sharma, Anderson et al. 2012, Dasari, Pathakoti et al. 2013, Regiel, Irusta et al. 2013). ROS, such as H_2O_2, $^{\bullet}OH$, and $O_2^{\bullet-}$, from ZnO NP suspensions are formed through the following processes (Xue, Liu et al. 2011, Avalos, Haza et al. 2014):

$$\text{ZnO NPs} \bullet \longrightarrow e^- \qquad O_2 + e^- \rightarrow O_2^{\bullet-}$$

$$O_2^{\bullet-} + H_2O \rightarrow {}^{\bullet}HO_2 + OH^- \qquad {}^{\bullet}HO_2 + {}^{\bullet}HO_2 \rightarrow H_2O_2 + O_2$$

$$H_2O_2 + O_2^{\bullet-} \rightarrow O_2 + {}^{\bullet}OH + OH^-$$

When ZnO NPs are excited by light energy, the electrons and holes react with adjacent molecules (O_2, H_2O, and OH^-) and result in the formation of ROS. To understand the effect of ZnO NP–alginate beads on oxidative stress to antibiotic-resistant bacterial cells, ROS generation was evaluated using the DCF-DA assay. Fig. 7.4 illustrates fluorescence

intensity of ZnO NP–alginate beads after exposure over 6 hours to *E. coli* and *P. aeruginosa*. To probe the antibacterial mechanism by the generation of ROS, N-acetyl-L-cysteine (NAC), which is known as a scavenger of ROS, was pretreated with cells at concentrations of 0.5 and 2 mM.

As illustrated in Fig. 7.4, no significant difference in the ROS generation was observed during the initial exposure to *E. coli* cells (Fig. 7.4A). However, as time passed, the bacterial cells exposed to the ZnO NP–alginate beads exhibited higher ROS generation than those exposed to control alginate beads. The control beads and ZnO NP–alginate beads containing less than 1 g of ZnO NPs exhibited similar ROS generations in cells, whereas alginate beads with 1 g of ZnO NPs produced relatively high ROS generation. The results indicate increasing generation of ROS with the increasing amount of ZnO NPs in alginate beads, but upon the addition of NAC, the amount of ROS generation decreased, in which the extent of decrease depended on the concentration of NAC (0.5 and 2 mM). For instance, when *E. coli* cells were pre-treated with 0.5 mM of NAC after exposure to 1 g of ZnO NP–alginate beads, they produced less ROS compared to cells without NAC. Further, cells with a higher concentration of NAC at 2 mM produced much lower fluorescence intensity compared to cells without NAC. As NAC concentration increased, ROS generation from cells pre-treated with NAC decreased. This suggests the maximum capacity of NAC as a ROS scavenger was limited as the amount of NAC decreased (Schrand, Rahman et al. 2010).

Fig. 7.4B illustrates fluorescence intensity of *P. aeruginosa* after exposure to ZnO NP–alginate beads. A similar observation was made in that fluorescence intensity was increased as exposure time and the amount of ZnO NPs in alginate beads were increased. The ROS

levels increased significantly with respect to control after a 6 h treatment at the highest concentration (1 g of ZnO NPs in alginate beads), indicating the generation of ROS dependent on the amount of ZnO NPs after 6 h. Similarly, to the *E. coli* cells, the addition of ZnO NP–alginate beads to *P. aeruginosa* cells that were pre-treated with NAC indicated a reduction in the fluorescence intensity compared to cells without NAC. In both antibiotic-resistant cells, ROS generation was largely prevented by NAC. These results suggest that oxidative stress is primarily responsible for the antibacterial effect of ZnO NP–alginate beads. Several studies suggest that since NAC has the ability to directly decrease cell oxidative stress, ROS levels and cell damage are reduced after NAC treatment (Adams, Lyon et al. 2006, Farzana and Meenakshi 2015).

A study by Chatterjee et al. (Chatterjee, Ghangrekar et al. 2017) reported that ROS generation from Ag- and ZnO NP-coated chitosan beads was a primary bacterial inactivation mechanism. In this study, while the role of silver ions was suggested, negligible release of silver ions was observed in which ROS was concluded to be a main antibacterial mechanism. Farzana and Meenakshi (Hirota, Sugimoto et al. 2010) found that ZnO NP-impregnated biopolymer (chitosan) beads used to decompose textile dyes took the photocatalytic activity of ZnO NPs that oxidized dye molecules with enhanced treatment effectiveness under UV-vis. In the study, a polymer solution, such as chitosan, was suggested to make the surface modification of ZnO NPs promote more photocatalytic activity by absorbing visible light.

Since UV-vis excites more electron–hole pairs in ZnO, ZnO NP–alginate beads under UV-vis may cause more ROS generation for the inactivation of bacteria. Several studies have reported that the creation of ROS including superoxide species can occur under room light or even at dark condition (Heinlaan, Ivask et al. 2008, Jones, Ray et al. 2008, Brayner, Dahoumane et al. 2010), which is a consistent observation with the present study. As stated earlier, the bacterial inactivation may occur through the release of metal ions, damage of cell membrane with direct contact, or the generation of ROS from NPs. In the following section, another possible mechanism, other than the generation of ROS and the release of Zn ions, is explored.

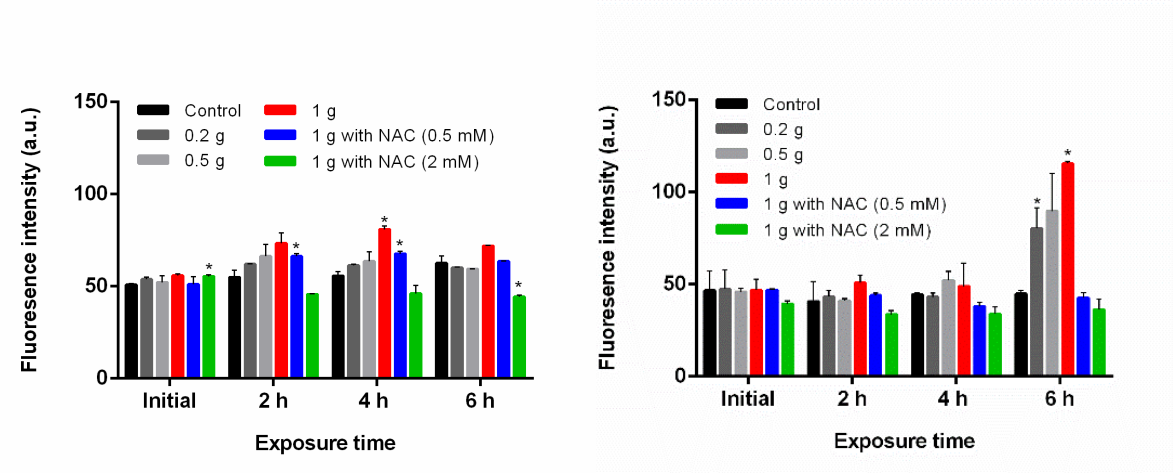

Figure 7.4. ROS generation of ZnO NP–alginate beads after exposure to (A) *E. coli* and (B) *P. aeruginosa* over 6 hours. NAC treated bacterial cells were pre-treated with 0.5 and 2 mM NAC for 2 hours. The results were analyzed using the two-way ANOVA. *Significantly different as compared to control at $p<0.05$.

7.2.3.4. Cell morphology after exposure to ZnO NP–alginate beads

The interaction between bacteria cells after exposure to ZnO NP–alginate beads was examined using SEM analysis to probe one of the antibacterial mechanisms. As indicated by the SEM images, the ZnO NPs were completely encapsulated in alginate beads

and dispersed or attached inside the beads. Fig. 7.5A presents SEM images of *E. coli* cells that were exposed to alginate control beads and ZnO NP–alginate beads for 6 h. Compared to the cells exposed to alginate control beads (beads without ZnO NPs), more significant deformation and morphological changes of bacterial cells were observed after exposure to ZnO NPs (1 g) –alginate beads. The majority of bacterial cells were not in contact with ZnO NPs; however, a few bacterial cells were in contact with ZnO NPs or were surrounded by aggregated ZnO NPs. These aggregated NPs may be leached from ZnO NP–alginate beads and attached on the cell surface.

Figure 7.5B presented SEM images of *P. aeruginosa* cells after exposure to ZnO NP–alginate beads for 6 h. Similarly, to the images for *E. coli* exposed to ZnO NP–alginate beads, cell disruption of *P. aeruginosa* was found, but fewer cell damages were observed in *P. aeruginosa* compared to *E. coli* cells when they were exposed to the same amount of ZnO NP–alginate beads; this is in agreement with results of antibacterial activity. SEM images indicate that cells treated with ZnO NP–alginate beads were damaged without direct interaction with the particles. These observations may suggest that the inactivation of bacterial cells does not occur through direct contact with ZnO NPs, rather cell damages still arise from ROS generation irrespective of direct contact with NPs (Wang, Lin et al. 2016). In the perspectives of proposed antibacterial mechanisms , antibacterial mechanisms of NPs seem to be related with their high surface-to-volume ratio and unique physicochemical properties (Barnes, Molina et al. 2013, Tan and Wang 2017). These antibacterial mechanisms are related factors including but not limited to particle sizes, NP concentrations, bacterial species, coating materials, pH, and surface charges. As an example, when the solution pH increases, more negative surface charge becomes available

as zinc ions are released (Kao, Chen et al. 2012). As negative surface charge increases in NPs, the electrostatic repulsion between metal cations and particles increases, causing the dispersion of NPs.

As per the electro-steric effect, alginate beads may serve as a platform for dispersion of NPs, resulting in steric effects that enhance the antibacterial effects of ZnO NPs on bacteria. The carboxylic group present in the alginate polymer (Fig, 7.5B) can enhance the adsorption of metal ions released from NPs, and the free carboxylic functional groups are also available as metal-binding sites when the alginate solution combines with metal oxide NPs (Kao, Chen et al. 2012). When the carboxylate group of alginate induces the electrostatic interaction with metal oxide NPs, NPs can be dispersed or distributed on the alginate beads (Fatehah, Aziz et al. 2014), and this stabilizing function of the carboxyl group on particles depends on the pH of suspensions (Cabral 2010). This binding may induce the dispersion of ZnO NPs on alginate composites and increase NPs' surface area, which enhances the photocatalytic activity (Daemi and Barikani 2012). Similarly, several studies (Kao, Chen et al. 2012, Fatehah, Aziz et al. 2014, Motshekga, Ray et al. 2015, Motshekga, Sinha Ray et al. 2018) reported that synthesis of polymer beads, such as chitosan and alginate with metal-oxide NPs, is stable because of their high percentage of cross-linking. Such an example includes ZnO incorporated into alginate fibers in which the formation of covalent bonds and carboxylate bonds was found between ZnO NPs and alginate composites (Liu, Hu et al. 2012).

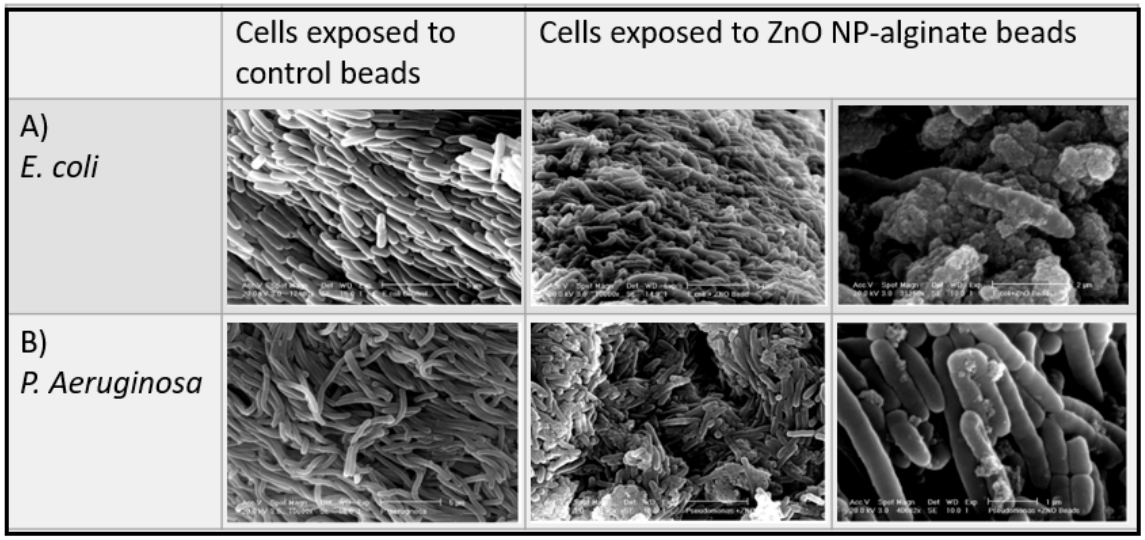

Figure 7.5. SEM images of (A) *E. coli* and (B) *P. aeruginosa* after being exposed to control alginate beads and ZnO NP (1 g)–alginate beads for 6 h

(A)

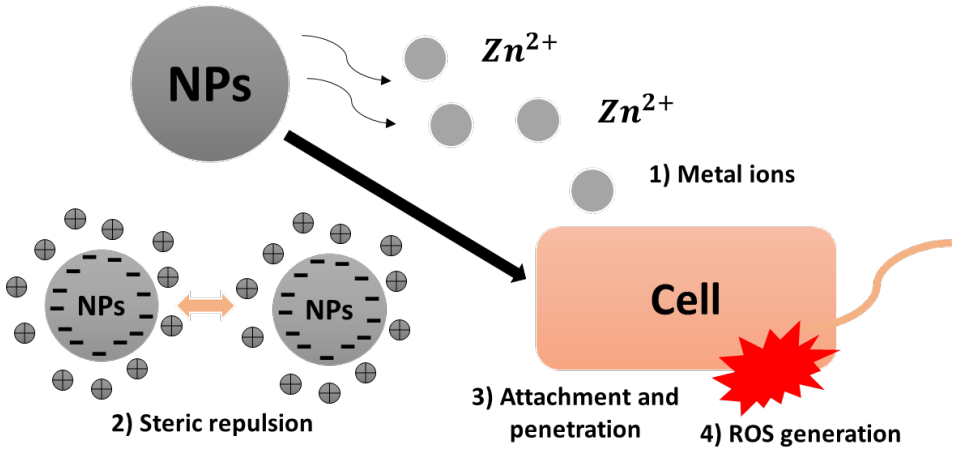

(B)

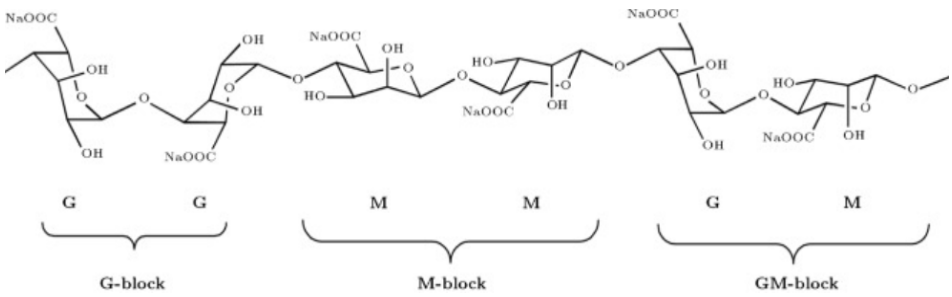

Figure 7.6. A: Schematics for the antibacterial mechanisms of ZnO NPs on bacteria cells; B: Chemical structure of alginate

7.2.3.5. Reusability of the ZnO NP–alginate beads

The reusability of ZnO NP–alginate beads was measured by sequential batch experiments. Subsequent to each batch test, 50 ZnO NP–alginate beads (concentration: 1 g of ZnO NPs in 50 mL of alginate solution) were exposed to 10^8 cells (*E. coli* and *P. aeruginosa*) for 6 h. The reusability of spent ZnO NP–alginate beads was examined through continuous treatment of incoming water contaminated with the model bacteria (*E. coli* DH5-α and *P. aeruginosa*) under five consecutive cycles. Fig. 7.7A indicates almost 99.7% inactivation rate of *E. coli* at the first operation cycle and similar inactivation rate as 97.5% until the third operational cycle, indicating efficacy of the used ZnO NP–alginate beads, although the efficiency gradually decreased to approximately 60% and further to 27%. However, although the overall inactivation rate of *P. aeruginosa* by the spent ZnO NP–alginate beads was lower compared to that of *E. coli*, an inactivation rate higher than 50% was observed in four operation cycles. Considering the significantly large accumulated amount of bacterial cells (CFU mL^{-1}), the used ZnO NP–alginate beads were reusable without replacement with new beads or addition of additional beads into the treatment system (Fig. 7.7B). Overall, for treating 10^8 cells per milliliter of antibiotic-resistant bacteria, only 50 beads (ZnO NP–alginate beads) were used. Given that typical concentrations of bacteria in raw and treated domestic wastewater are approximately 10^1–10^4 cells mL^{-1}, the application of ZnO NP–alginate beads for treating water contaminated with antibiotic-resistant bacteria is promising in terms of cost-effectiveness, rapid

treatment, being an environmentally friendly method, no byproducts formed after being used in treatment systems and ease of operation for field applications.

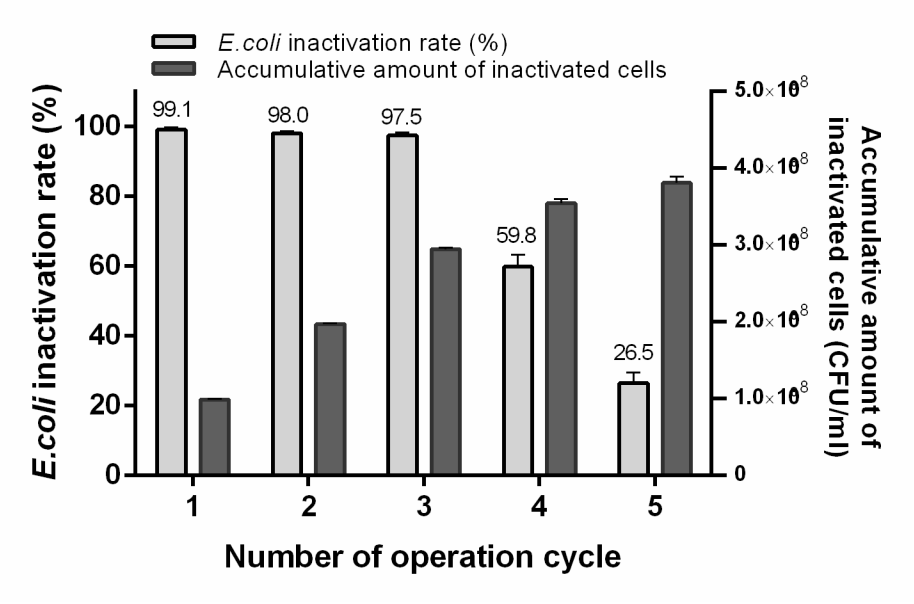

(A)

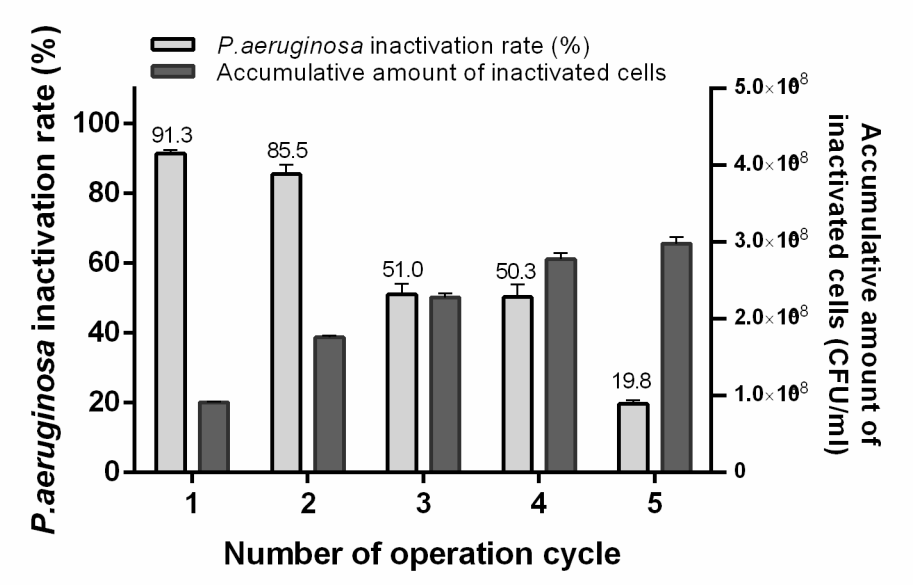

(B)

Figure 7.7. Reusability of ZnO NP–alginate beads for antibiotic-resistant bacteria over the accumulated amount of inactivated cells (CFU mL^{-1}): (A) *E. coli* and (B) *P. aeruginosa*

7.2.3.6. Comparison of the effectiveness of the chlorine and ZnO NP–alginate beads for the removal of antibiotic-resistant bacteria

The effectiveness of the chlorine and ZnO NPs-alginate beads was compared for the removal of antibiotic-resistant bacteria. Figure 7.8(A) show the antibacterial effects of chlorine and on *P.aeruginosa* and *E.coli* during repeated batch test with 5 consecutive cycles under same conditions. Subsequent to each batch test, chlorine (conc.:5 ml/L (10-15%)) were exposed to 10^8 cells of mixed bacteria which consist of *P.aeruginosa* and *E.coli* for 6 h. When antibiotic-resistant bacteria cells were treated with 5 ml/L of chlorine, bacteria inactivation rate showed 100% for both *P.aeruginosa* and *E.coli*. Then, effect of chlorine for bacteria inactivation gradually decreased for 5 continuous batch test, and inactivation of *P.aeruginosa* cells were not as effective as *E.coli* cells.

The comparison of the effectiveness of chlorine and ZnO NPs-alginate on antibiotic-resistant bacteria is shown in Figure 7.8(B) and revealsthe antibacterial effects of ZnO NPs-alginate beads on antibiotic-resistant bacteria for 5 consecutive cycles. It shows that bacterial inactivation rate of chlorine is higher than that of ZnO NPs-alginate beads at first operation, showing that 100 % of inactivation rate for both bacterial cells, while ZnO NPs-alginate beads showed 99.1% and 91.3% for *E.coli* and *P.aeruginosa* respectively. However, the inactivation effect of ZnO NPs-alginate beads is higher than that of chlorine from 2^{nd} operation cycle, showing that 98.0% and 85.5% of inactivation rate on *E.coli* and *P.aeruginosa* respectively. This results indicate that ZnO NPs-alginate beads are more reusable compared to chlorine, although the inactivation rate of chlorine at first batch operation was 100 %. Thus, ZnO NPs-alginate beads are more stable than chlorine because there is no release any byproduct from ZnO NPs-alginate beads while chlorine produce

byproducts, such as Halogenated trihalomethanes (THMs) and haloacetic acids (HAAs), which are harmful to human health.

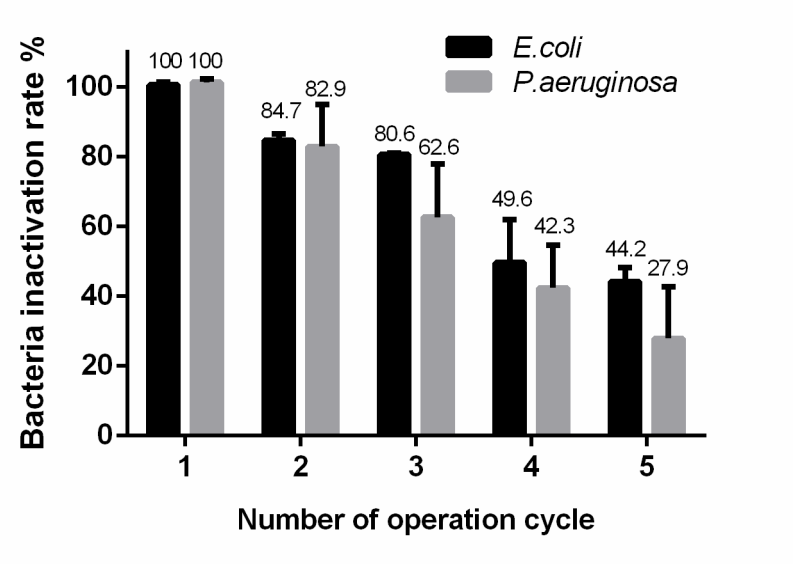

(A)

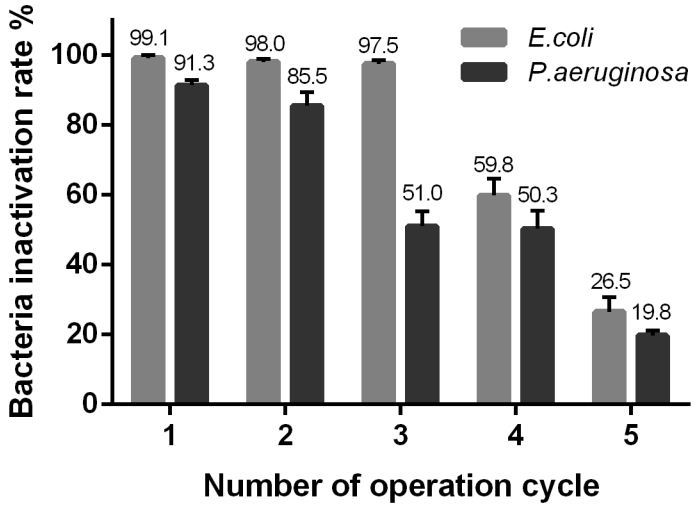

(B)

Figure 7.8. Antibacterial effect of (A) chlorine (conc.:5 ml/L) and (B) ZnO NPs-alginate beads for antibiotic-resistant bacteria inactivation

Table 2 shows the cost analysis of chlorine and ZnO NPs-alginate beads for the inactivation of antibiotic-resistant bacteria. The reusability of ZnO NP–alginate beads was measured

by sequential batch experiments. Subsequent to each batch test, 50 ZnO NP–alginate beads (concentration: 1 g of ZnO NPs in 50 mL of alginate solution) and chlorine (conc.:5 ml/L (10-15%)) were exposed to 10^8 cells (*E. coli* and *P. aeruginosa*) for 6 h. The reusability of spent ZnO NP–alginate beads was examined through continuous treatment of incoming water contaminated with the model bacteria (*E. coli* DH5-α and *P. aeruginosa*) under five consecutive cycles as shown in Figure 7.8. The operational cost analysis is one of the very important parameters for water treatment study. It is a combination of direct cost items (cost of the used materials and electrical energy) and indirect cost items (labor, maintenance etc.). As later cost items are independent of direct cost items, only direct cost items were considered.

$$C=C_{materials}+C_{electrical}$$

Costs per batch test by using chlorine and ZnO NPs-alginate beads were 0.185US$ for chlorine and 0.0638US$ for ZnO NPs-alginate beads. This indicates that using ZnO NPs-alginate beads were economical for the removal of antibiotic-resistant bacteria from water. The application of ZnO NP–alginate beads for treating water contaminated with antibiotic-resistant bacteria is promising in terms of cost-effectiveness, rapid treatment, being an environmentally friendly method, no byproducts formed.

Table 2. Cost analysis of chlorine and ZnO NPs-alginate beads for the inactivation of antibiotic-resistant bacteria

	Method	Removal efficiency (%)		Reusability	Removal capacity 5 consecutive cycles	By products	Removal cost ($)
		E.coli	*P.aeruginosa*				
Chlorine	Batch test for 6 h at 37 ℃ (Initial bacteria concentration: 10^8 cells/ml)	100	100	Y	3.8×10^8 (cells/ml)	Y	0.185
ZnO NPs-alginate beads		99.1	91.3	Y	3.59×10^8 (cells/ml)	N	0.0638

7.2.4. Conclusions

In this work, alginate nanocomposites were prepared and characterized to develop a new antibacterial material for bacteria contaminated water. The application of synthesized ZnO NP–alginate beads for the inactivation of antibiotic-resistant bacteria revealed efficacy with no products formed in the treatment process and proved cost-effectiveness and reusability of the spent beads for continuous treatment of incoming water contaminated with antibiotic-resistant bacteria. While the use of NPs for environmental remediation has been widely investigated, few studies have addressed issues of nanoparticle leaching and the resultant mobility. In the present study, possible antibacterial mechanisms were unveiled with experimental approaches. In general, the antibacterial effects of ZnO NP–alginate beads were dependent on factors including but not limited to initial bacterial concentration, exposure time, solution pH, dispersant, and the amount of ZnO NP–alginate beads. Among four possible antibacterial mechanisms (ROS, electrostatic repulsion, changes in physicochemical properties, and release of Zn ions), the generation of ROS and resultant cell-membrane damage by extracellular ROS primarily contributed to the inactivation of the two model antibiotic bacteria (*E. coli* and *P. aeruginosa*). It is well

known that the generation of ROS by NPs is influenced by UV light. Thus, the antibacterial effect of ZnO NP–alginate beads could be enhanced under UV with increasing generation of ROS from ZnO NPs.

The release of Zn^{2+} ions from NPs examined indicated minimum leaching with relatively low levels (below the accepted WaHO standards), which was then excluded from four potential antibacterial mechanisms. The role of the alginate biopolymer acting as a dispersant led to inactivation of the bacteria to some degree since the dispersant can enhance electro-steric repulsion, thereby preventing aggregation of NPs and maintaining large surface area (small particle size). As illustrated in the SEM images and the corresponding inactivation rate of bacteria, NPs do not necessarily appear to enter or interact with cells to cause toxicity. Rather, the ROS generation causes cell damage regardless of contact between bacterial cells and NPs.

As demonstrated in the reusability investigation of the used beads, even a difficult-to-treat contaminant of concern (*P. aeruginosa*) was easily treatable over continuously incoming water contaminated with antibiotic-resistant bacteria. The encapsulation of ZnO NPs into alginate beads serves as a promising antibacterial material without NP leaching into water and resultant environmental impacts. Considering the conventional chlorine disinfectant, which has recently been reported to be ineffective and to even promote antibiotic resistance, our results are significant in terms of water treatment, especially the inactivation of antibiotic-resistant bacteria to protect the environment and public health, and its effectiveness in terms of combined filtration and disinfection in a given condition on antibiotic-resistant bacteria.

CHAPTER 8:

CONCLUSIONS AND FUTURE RESEARCH

8.1. Conclusions

The prime goals of the present work were to examine the antibacterial effect and toxicity mechanisms of different types of NPs and to develop the applications of NPs for the removal of antibiotic-resistant bacteria in water. To sum up, the following conclusions are derived.

1. The physical and chemical characteristics of NPs extracted from a consumer product were different from the industrial-grade NPs. The presence of coating materials such as CMC, PVP, and silica was found to change NPs' physicochemical properties resulting in different aggregation sizes. The aggregation size and surface area of particle affected ROS generation of NPs, and ROS generation was the primary factor in causing the antibacterial effect on microorganisms other than metal ion release and physical contact. TiO_2 NPs extracted from sunscreen products were coated with silica, and the presence of silica increased the reactivity of TiO_2 NPs due to stabilization by increased hydrophobic properties of NPs. This hydrophobic property is considered from the strong repulsive force by coating media around the NPs.

- Different physicochemical properties of ZnO influenced on antibacterial effect.
- Toxicity effect of ZnO enhanced through ROS generation and smaller particle sizes.
- The coating with CMC, PVP, or SiO_2 enhanced toxicity of TiO_2 NPs on *E. coli*.
- Toxicity of CMC or PVP coating linked to size reduction of TiO_2 NPs.
- The presence of silica increased the generation of ROS from TiO_2 NPs.
- More ROS generation by silica correlated with TiO_2 NP toxicity.

2. The presence of other NPs such as GO and CNT increased the dispersion of metal-oxide NPs through increasing ROS generation by suppressing the recombination of electron-hole pairs. Among four synthesized nanohybrids (i.e. ZnO-conjugated graphene oxide (GO), ZnO-conjugated carbon nanotubes (CNTs), TiO_2-conjugated GO and TiO_2-conjugated CNT, ZnO-GO exhibited significant toxicity effects on bacteria and algae cells because of the high solubility of ZnO NPs in water and the hydrophilic affinity of GO, which increase dispersions of metal oxide NPs on their surface. A significant dispersion of metal-oxide NPs GO induces not only higher oxidation but also prevention of NPs aggregation. Thus, NHs induced the shading effect on algae by preventing the photosynthesis of algae which results in limited growth.

- The ZnO–GO NHs exhibited the most effective antibacterial effect on *E. coli* and inhibited algae cells.
- The GO-based NHs increased the generation of reactive oxygen species and the shading effects.
- Toxicity of NHs was significant with ZnO-conjugated nanohybrids.
- CNT-based NHs revealed unstable and deficient structures.

3. The antibacterial properties of NPs were developed to test the inactivation of antibiotic-resistant bacteria by encapsulating ZnO NPs in alginate beads. The generation of ROS and resultant cell-membrane damages by extracellular ROS primarily contributed to the inactivation of the two model antibiotic-resistant bacteria (*E. coli* and *P. aeruginosa*), regardless of contact between bacterial cells and NPs. This developed ZnO NPs-alginate beads revealed efficacy with no byproducts formed in the treatment process, while

conventional disinfectants produce byproduct formation (e.g. THMs, HAAs, etc). Thus, it proved cost-effectiveness and reusability of the spent beads for continuous treatment of water, which is contaminated with antibiotic-resistant bacteria. Only 50 beads (ZnO NP–alginate beads) were used for treating 10^8 cells/mL of antibiotic-resistant bacteria (with 99.1% of removal efficiency), which were reusable to remove high concentration of bacteria in water. Given that typical concentrations of bacteria in raw and treated domestic wastewater are approximately 10^1–10^4 cells mL^{-1}, the application of ZnO NP–alginate beads for treating water contaminated with antibiotic-resistant bacteria is promising. Thus, ZnO NPs-alginate beads represent a novel alternative antibacterial treatment offering multiple benefits. They are not only cost-effective, reusable, and efficient, but also environmental-friendly with no byproducts formation and easy to use in field applications, while conventional methods are requiring high doses, forming byproducts, and not-reusable.

- ZnO NP–alginate beads revealed significant antibacterial effects with 99.1% of removal efficiency without byproduct formation.
- The antibacterial mechanism involved the generation of reactive oxygen species.
- The beads exhibited inactivation of bacteria in several consecutive cycles (reusable up to 3rd cycle).
- ZnO NP–alginate beads resulted in the least leaching of zinc ions in water.

These findings and discovery of primary antibacterial mechanisms may contribute to defining the antibacterial effect of consumer products derived NPs and toxicity mechanisms for different types of NPs, and these results expanded the antibacterial

mechanisms of NPs. Also, these results will be useful for environment policymakers and regulation of the nanotechnology industry. Furthermore, the application of NPs as an antibacterial material offers new opportunities of NPs for the removal of antibiotic-resistant bacteria in the environment.

8.2. Future research directions

The results are significant regarding the design of new antibacterial treatment methods by using NPs, especially for the purpose of removing antibiotic-resistant bacteria detected in water which contribute to environmental protection and public health. The overall performance of the nanocomposite beads in this study showed that the ZnO NPs-alginate beads are promising as an alternative method for treating bacteria-contaminated water. The NPs-alginate beads could also be applied as an alternative or additional method to conventional chlorine disinfection technology, especially for controlling regrowth of persistent microorganisms in water. However, this technology needs to be further explored to enhance the performance of NPs as antimicrobial materials.

First, given that ROS generation was a primary mechanism of antibacterial effect on bacteria, further study should consider the use of light energy to maximize the performance of NPs. Since the photo activities of NPs are promoted under light condition, nanocomposites can perform better on their antibacterial effect.

Second, optimization studies for nanocomposites use (quantities of beads, coated amounts of NPs, optimized ratios between the contaminants and quantities of beads) are also necessary to achieve cost-effective operation. Thus, the application of nanocomposites beads needs to be examined while treating real wastewater in order to test the long-term

performance of NP-alginate beads. Based on the results obtained from the effect of NP-alginate beads on inactivating of the model bacteria, the ideal optimization of NPs should be examined through bead column test. For example, column experiments can be set up and performed. NPs-alginate beads can be filled in a column reactor, and bacteria-contaminated water can be passed through the column. Cost-effective preparation of nanocomposite beads and beads-column may allow for a large-scale production which could potentially be useful for point-of-use.

Lastly, other contaminants present in the untreated water (e.g., nitrate and perchlorate) can be treated by this NPs-alginate bead. Because NP's large surface area and high adsorbent qualities have thus been widely regarded as a possible solution to small-scale water treatment applications. To overcome technical, economic, and social barriers, NPs-alginate beads filtration prototypes need to be manufactured for a low cost and easy use, for the purposes of scaling-up and testing the efficiency of point-of-use systems.

REFERENCES

Adams, L. K., D. Y. Lyon and P. J. Alvarez (2006). "Comparative eco-toxicity of nanoscale TiO2, SiO2, and ZnO water suspensions." Water Res **40**(19): 3527-3532.

Ahmadi, M., H. Ramezani Motlagh, N. Jaafarzadeh, A. Mostoufi, R. Saeedi, G. Barzegar and S. Jorfi (2017). "Enhanced photocatalytic degradation of tetracycline and real pharmaceutical wastewater using MWCNT/TiO2 nano-composite." J Environ Manage **186**(Pt 1): 55-63.

Ahmed, M. B., J. L. Zhou, H. H. Ngo and W. Guo (2015). "Adsorptive removal of antibiotics from water and wastewater: Progress and challenges." Sci Total Environ **532**: 112-126.

Aimable, A., Tomasz Strachowski, Ewelina Wolska, Witold Lojkowski, and Paul Bowen. (2010). "Comparison of two innovative precipitation systems for ZnO and Al-doped ZnO nanoparticle synthesis." Processing and Application of Ceramics **4**: 107-114.

Akhavan, O., R. Azimirad and S. Safa (2011). "Functionalized carbon nanotubes in ZnO thin films for photoinactivation of bacteria." Materials Chemistry and Physics **130**(1-2): 598-602.

Alrousan, D. M., P. S. Dunlop, T. A. McMurray and J. A. Byrne (2009). "Photocatalytic inactivation of E. coli in surface water using immobilised nanoparticle TiO2 films." Water Res **43**(1): 47-54.

Angélique Simon-Deckers, S. L., Martine Mayne-L'hermite, Nathalie Herlin-Boime, Nicolas Menguy, Cécile Reynaud, Barbara Gouget, and Marie Carrière (2009). "Size-, composition- and shape-dependent toxicological impact of metal oxide nanoparticles and carbon nanotubes toward bacteria." Environmental Science & Technology **43**(21): 8423-8429.

Applerot, G., et al. (2009). "Enhanced antibacterial activity of nanocrystalline ZnO due to increased ROS-mediated cell injury." Advanced Functional Materials **19**(6): 842-852.

Arakha, M., S. Pal, D. Samantarrai, T. K. Panigrahi, B. C. Mallick, K. Pramanik, B. Mallick and S. Jha (2015). "Antimicrobial activity of iron oxide nanoparticle upon modulation of nanoparticle-bacteria interface." Sci Rep **5**: 14813.

Armbrust, E. V., Berges, J.A., Bowler, C., Green, B.R., Martinez, D., Putnam, N.H., Zhou, S., Allen, A.E., Apt, K.E., Bechner, M. and Brzezinski, M.A. (2004). "The genome of the diatom Thalassiosira pseudonana: ecology, evolution, and metabolism." Science **306**(5693): 79-86.

Aruoja, V., H. C. Dubourguier, K. Kasemets and A. Kahru (2009). "Toxicity of nanoparticles of CuO, ZnO and TiO2 to microalgae Pseudokirchneriella subcapitata." Sci Total Environ **407**(4): 1461-1468.

Auffan, M., J. Rose, J. Y. Bottero, G. V. Lowry, J. P. Jolivet and M. R. Wiesner (2009). "Towards a definition of inorganic nanoparticles from an environmental, health and safety perspective." Nat Nanotechnol **4**(10): 634-641.

Avalos, A., A. I. Haza, D. Mateo and P. Morales (2014). "Cytotoxicity and ROS production of manufactured silver nanoparticles of different sizes in hepatoma and leukemia cells." J Appl Toxicol **34**(4): 413-423.

Baek, S., S. H. Joo, P. Blackwelder and M. Toborek (2018). "Effects of coating materials on antibacterial properties of industrial and sunscreen-derived titanium-dioxide nanoparticles on Escherichia coli." Chemosphere **208**: 196-206.

Baek, S., S. H. Joo, N. Kumar and M. Toborek (2017). "Antibacterial effect and toxicity pathways of industrial and sunscreen ZnO nanoparticles on Escherichia coli." Journal of Environmental Chemical Engineering **5**(3): 3024-3032.

Baek, Y. W. and Y. J. An (2011). "Microbial toxicity of metal oxide nanoparticles (CuO, NiO, ZnO, and Sb2O3) to Escherichia coli, Bacillus subtilis, and Streptococcus aureus." Sci Total Environ **409**(8): 1603-1608.

Baker, T. J., C. R. Tyler and T. S. Galloway (2014). "Impacts of metal and metal oxide nanoparticles on marine organisms." Environ Pollut **186**: 257-271.

Bao, Q., D. Zhang and P. Qi (2011). "Synthesis and characterization of silver nanoparticle and graphene oxide nanosheet composites as a bactericidal agent for water disinfection." J Colloid Interface Sci **360**(2): 463-470.

Barnes, R. J., R. Molina, J. Xu, P. J. Dobson and I. P. Thompson (2013). "Comparison of TiO2 and ZnO nanoparticles for photocatalytic degradation of methylene blue and the correlated inactivation of gram-positive and gram-negative bacteria." Journal of Nanoparticle Research **15**(2).

Batley, G. E., Jason K. Kirby, and Michael J. McLaughlin (2012). "Fate and Risks of nanomaterials in aquatic and terrestrial environments." Accounts of chemical research **46**(3): 854-862.

Baun, A., N. B. Hartmann, K. Grieger and K. O. Kusk (2008). "Ecotoxicity of engineered nanoparticles to aquatic invertebrates: a brief review and recommendations for future toxicity testing." Ecotoxicology **17**(5): 387-395.

Bhuvaneshwari, M., V. Iswarya, S. Archanaa, G. M. Madhu, G. K. S. Kumar, R. Nagarajan, N. Chandrasekaran and A. Mukherjee (2015). "Cytotoxicity of ZnO NPs towards fresh water algae Scenedesmus obliquus at low exposure concentrations in UV-C, visible and dark conditions." Aquat Toxicol **162**: 29-38.

Bian, S. W., I. A. Mudunkotuwa, T. Rupasinghe and V. H. Grassian (2011). "Aggregation and dissolution of 4 nm ZnO nanoparticles in aqueous environments: influence of pH, ionic strength, size, and adsorption of humic acid." Langmuir **27**(10): 6059-6068.

Biswas, P. and R. Bandyopadhyaya (2016). "Water disinfection using silver nanoparticle impregnated activated carbon: Escherichia coli cell-killing in batch and continuous packed column operation over a long duration." Water Res **100**: 105-115.

Bondarenko, O., K. Juganson, A. Ivask, K. Kasemets, M. Mortimer and A. Kahru (2013). "Toxicity of Ag, CuO and ZnO nanoparticles to selected environmentally relevant test organisms and mammalian cells in vitro: a critical review." Arch Toxicol **87**(7): 1181-1200.

Brayner, R. (2008). "The toxicological impact of nanoparticles." Nano Today **3**(1-2): 48-55.

Brayner, R., S. A. Dahoumane, C. Yepremian, C. Djediat, M. Meyer, A. Coute and F. Fievet (2010). "ZnO nanoparticles: synthesis, characterization, and ecotoxicological studies." Langmuir **26**(9): 6522-6528.

Brayner, R., et al. (2006). "Toxicological impact studies based on Escherichia coli bacteria in ultrafine ZnO nanoparticles colloidal medium." Nano letters **6**(4): 866-870.

Byrappa, K., A. S. Dayananda, C. P. Sajan, B. Basavalingu, M. B. Shayan, K. Soga and M. Yoshimura (2008). "Hydrothermal preparation of ZnO:CNT and TiO2:CNT composites and their photocatalytic applications." Journal of Materials Science **43**(7): 2348-2355.

Cabral, J. P. (2010). "Water microbiology. Bacterial pathogens and water." Int J Environ Res Public Health **7**(10): 3657-3703.

Cai, Y., M. Liu, X. Song, J. Zhang, Q. Wei and L. Zhang (2015). "A form-stable phase change material made with a cellulose acetate nanofibrous mat from bicomponent electrospinning and incorporated capric–myristic–stearic acid ternary eutectic mixture for thermal energy storage/retrieval." RSC Adv. **5**(102): 84245-84251.

Cardinale, B. J. (2011). "Biodiversity improves water quality through niche partitioning." Nature **472**(7341): 86-89.

Carlotti, M. E., E. Ugazio, S. Sapino, I. Fenoglio, G. Greco and B. Fubini (2009). "Role of particle coating in controlling skin damage photoinduced by titania nanoparticles." Free Radic Res **43**(3): 312-322.

CDC (2013). " Centers for diseases control and prevention, threat report." CDC.

Chatterjee, P., M. M. Ghangrekar and S. Rao (2017). "Disinfection of secondary treated sewage using chitosan beads coated with ZnO-Ag nanoparticles to facilitate reuse of treated water." Journal of Chemical Technology & Biotechnology **92**(9): 2334-2341.

Chen, M., S. Zhou, Y. Zhu, Y. Sun, G. Zeng, C. Yang, P. Xu, M. Yan, Z. Liu and W. Zhang (2018). "Toxicity of carbon nanomaterials to plants, animals and microbes: Recent progress from 2015-present." Chemosphere **206**: 255-264.

Chen, T. H., C. C. Lin and P. J. Meng (2014). "Zinc oxide nanoparticles alter hatching and larval locomotor activity in zebrafish (Danio rerio)." J Hazard Mater **277**: 134-140.

Chen, Y.-L., C.-E. Zhang, C. Deng, P. Fei, M. Zhong and B.-T. Su (2013). "Preparation of ZnO/GO composite material with highly photocatalytic performance via an improved two-step method." Chinese Chemical Letters **24**(6): 518-520.

Choi, Y., H. A. Kim, K. W. Kim and B. T. Lee (2018). "Comparative toxicity of silver nanoparticles and silver ions to Escherichia coli." J Environ Sci (China) **66**: 50-60.

Chowdhury, I., D. M. Cwiertny and S. L. Walker (2012). "Combined factors influencing the aggregation and deposition of nano-TiO2 in the presence of humic acid and bacteria." Environ Sci Technol **46**(13): 6968-6976.

Crane, R. A. and T. B. Scott (2012). "Nanoscale zero-valent iron: future prospects for an emerging water treatment technology." J Hazard Mater **211-212**: 112-125.

Daemi, H. and M. Barikani (2012). "Synthesis and characterization of calcium alginate nanoparticles, sodium homopolymannuronate salt and its calcium nanoparticles." Scientia Iranica **19**(6): 2023-2028.

Dalai, S., S. Pakrashi, R. S. S. Kumar, N. Chandrasekaran and A. Mukherjee (2012). "A comparative cytotoxicity study of TiO2 nanoparticles under light and dark conditions at low exposure concentrations." Toxicology Research **1**(2): 116.

Das, R., S. B. Abd Hamid, M. E. Ali, A. F. Ismail, M. S. M. Annuar and S. Ramakrishna (2014). "Multifunctional carbon nanotubes in water treatment: The present, past and future." Desalination **354**: 160-179.

Dasari, T. P., K. Pathakoti and H.-M. Hwang (2013). "Determination of the mechanism of photoinduced toxicity of selected metal oxide nanoparticles (ZnO, CuO, Co3O4 and TiO2) to E. coli bacteria." Journal of Environmental Sciences **25**(5): 882-888.

De Angelis, I., F. Barone, A. Zijno, L. Bizzarri, M. T. Russo, R. Pozzi, F. Franchini, G. Giudetti, C. Uboldi, J. Ponti, F. Rossi and B. De Berardis (2013). "Comparative study of ZnO and TiO(2) nanoparticles: physicochemical characterisation and toxicological effects on human colon carcinoma cells." Nanotoxicology **7**(8): 1361-1372.

Dimapilis, E. A. S., C.-S. Hsu, R. M. O. Mendoza and M.-C. Lu (2018). "Zinc oxide nanoparticles for water disinfection." Sustainable Environment Research **28**(2): 47-56.

Dizaj, S. M., F. Lotfipour, M. Barzegar-Jalali, M. H. Zarrintan and K. Adibkia (2014). "Antimicrobial activity of the metals and metal oxide nanoparticles." Mater Sci Eng C Mater Biol Appl **44**: 278-284.

Espitia, P. J. P., N. d. F. F. Soares, J. S. d. R. Coimbra, N. J. de Andrade, R. S. Cruz and E. A. A. Medeiros (2012). "Zinc oxide nanoparticles: synthesis, antimicrobial activity and food packaging applications." Food and Bioprocess Technology **5**(5): 1447-1464.

Farzana, M. H. and S. Meenakshi (2015). "Visible light-driven photoactivity of zinc oxide impregnated chitosan beads for the detoxification of textile dyes." Applied Catalysis A: General **503**: 124-134.

Fatehah, M. O., H. A. Aziz and S. Stoll (2014). "Stability of ZnO nanoparticles in solution. Influence of pH, dissolution, aggregation and disaggregation effects." Journal of Colloid Science and Biotechnology **3**(1): 75-84.

Feng, X., S. Zhang, H. Wu and X. Lou (2015). "A novel folic acid-conjugated TiO(2)-SiO(2) photosensitizer for cancer targeting in photodynamic therapy." Colloids Surf B Biointerfaces **125**: 197-205.

François Perreault, A. F. d. F., Siamak Nejati, and Menachem Elimelech (2015). "Antimicrobial properties of graphene oxide nanosheets: why size matters." ACS Nano **9**(7): 7726-7236.

Freixa, A., V. Acuna, J. Sanchis, M. Farre, D. Barcelo and S. Sabater (2018). "Ecotoxicological effects of carbon based nanomaterials in aquatic organisms." Sci Total Environ **619-620**: 328-337.

French, R. A., Astrid R. Jacobson, Bojeong Kim, Sara L. Isley, R. Lee Penn, and Philippe C. Baveye (2009). "Influence of ionic strength, pH, and cation valence on aggregation kinetics of titanium dioxide nanoparticles." Environmental Science & Technology Letters **43**(5): 1354-1359.

Fu, H., Y. Jiang, J. Ding, J. Zhang, M. Zhang, Y. Zhu and H. Li (2018). "Zinc oxide nanoparticle incorporated graphene oxide as sensing coating for interferometric optical microfiber for ammonia gas detection." Sensors and Actuators B: Chemical **254**: 239-247.

Fu, L., M. Hamzeh, S. Dodard, Y. H. Zhao and G. I. Sunahara (2015). "Effects of TiO2 nanoparticles on ROS production and growth inhibition using freshwater green algae pre-exposed to UV irradiation." Environ Toxicol Pharmacol **39**(3): 1074-1080.

Fujishima, A., Rao, T.N. and Tryk, D.A. (2000). " Titanium dioxide photocatalysis." Journal of Photochemistry and Photobiology C: Photochemistry Reviews **1**(1): 1-21.

Galletti, A., S. Seo, S. H. Joo, C. Su and P. Blackwelder (2016). "Effects of titanium dioxide nanoparticles derived from consumer products on the marine diatom Thalassiosira pseudonana." Environ Sci Pollut Res Int **23**(20): 21113-21122.

Gangadharan, D., K. Harshvardan, G. Gnanasekar, D. Dixit, K. M. Popat and P. S. Anand (2010). "Polymeric microspheres containing silver nanoparticles as a bactericidal agent for water disinfection." Water Res **44**(18): 5481-5487.

Godymchuk, A., E. Karepina, E. Yunda, G. Lyamina, N. Kosova and D. Kuznetsov (2015). "Stability study of ZnO nanoparticles in aqueous solutions of carboxylate anions." Journal of Nanoparticle Research **17**(3).

Gomez, E., M. Bachelot, C. Boillot, D. Munaron, S. Chiron, C. Casellas and H. Fenet (2011). "Bioconcentration of two pharmaceuticals (benzodiazepines) and two personal care products (UV filters) in marine mussels (Mytilus galloprovincialis) under controlled laboratory conditions." Environ Sci Pollut Res Int **19**(7): 2561-2569.

Guillard, R. R. (1975). Culture of phytoplankton for feeding marine invertebrates. Springer, Boston, MA.

Guo, H., W. Wang, L. Liu, Y. He, C. Li and Y. Wang (2013). "Shape-controlled synthesis of Ag@TiO2 cage-bell hybrid structure with enhanced photocatalytic activity and superior lithium storage." Green Chemistry **15**(10).

Gupta, S. M. and M. Tripathi (2011). "A review of TiO2 nanoparticles." Chinese Science Bulletin **56**(16): 1639-1657.

Hajipour, M. J., K. M. Fromm, A. A. Ashkarran, D. Jimenez de Aberasturi, I. R. de Larramendi, T. Rojo, V. Serpooshan, W. J. Parak and M. Mahmoudi (2012). "Antibacterial properties of nanoparticles." Trends Biotechnol **30**(10): 499-511.

Hariharan, C. (2006). "Photocatalytic degradation of organic contaminants in water by ZnO nanoparticles: Revisited." Applied Catalysis A: General **304**: 55-61.

Hegde, K., S. K. Brar, M. Verma and R. Y. Surampalli (2016). "Current understandings of toxicity, risks and regulations of engineered nanoparticles with respect to environmental microorganisms." Nanotechnology for Environmental Engineering **1**(5).

Heinlaan, M., A. Ivask, I. Blinova, H. C. Dubourguier and A. Kahru (2008). "Toxicity of nanosized and bulk ZnO, CuO and TiO2 to bacteria Vibrio fischeri and crustaceans Daphnia magna and Thamnocephalus platyurus." Chemosphere **71**(7): 1308-1316.

Hirota, K., M. Sugimoto, M. Kato, K. Tsukagoshi, T. Tanigawa and H. Sugimoto (2010). "Preparation of zinc oxide ceramics with a sustainable antibacterial activity under dark conditions." Ceramics International **36**(2): 497-506.

Hotze, E. M., T. Phenrat and G. V. Lowry (2010). "Nanoparticle aggregation: challenges to understanding transport and reactivity in the environment." Journal of Environment Quality **39**(6): 1909.

Hou, J., L. Wang, C. Wang, S. Zhang, H. Liu, S. Li and X. Wang (2018). "Toxicity and mechanisms of action of titanium dioxide nanoparticles in living organisms." Journal of Environmental Sciences.

Hou, J., Y. Wu, X. Li, B. Wei, S. Li and X. Wang (2018). "Toxic effects of different types of zinc oxide nanoparticles on algae, plants, invertebrates, vertebrates and microorganisms." Chemosphere **193**: 852-860.

Hsiao, M. C., C. C. Ma, J. C. Chiang, K. K. Ho, T. Y. Chou, X. Xie, C. H. Tsai, L. H. Chang and C. K. Hsieh (2013). "Thermally conductive and electrically insulating epoxy nanocomposites with thermally reduced graphene oxide-silica hybrid nanosheets." Nanoscale **5**(13): 5863-5871.

Hu, J., J. Wang, S. Liu, Z. Zhang, H. Zhang, X. Cai, J. Pan and J. Liu (2018). "Effect of TiO2 nanoparticle aggregation on marine microalgae Isochrysis galbana." J Environ Sci (China) **66**: 208-215.

Hu, Z., Y. Huang, S. Sun, W. Guan, Y. Yao, P. Tang and C. Li (2012). "Visible light driven photodynamic anticancer activity of graphene oxide/TiO2 hybrid." Carbon **50**(3): 994-1004.

Huang, J., J. Zang, Y. Zhao, L. Dong and Y. Wang (2014). "One-step synthesis of nanocrystalline TiO2-coated carbon nanotube support for Pt electrocatalyst in direct methanol fuel cell." Materials Letters **137**: 335-338.

Huang, Y., T. Wang, X. Zhao, X. Wang, L. Zhou, Y. Yang, F. Liao and Y. Ju (2015). "Poly(lactic acid)/graphene oxide-ZnO nanocomposite films with good mechanical, dynamic mechanical, anti-UV and antibacterial properties." Journal of Chemical Technology & Biotechnology **90**(9): 1677-1684.

Hui, L., J. G. Piao, J. Auletta, K. Hu, Y. Zhu, T. Meyer, H. Liu and L. Yang (2014). "Availability of the basal planes of graphene oxide determines whether it is antibacterial." ACS Appl Mater Interfaces **6**(15): 13183-13190.

Huynh, K. A. and K. L. Chen (2011). "Aggregation kinetics of citrate and polyvinylpyrrolidone coated silver nanoparticles in monovalent and divalent electrolyte solutions." Environ Sci Technol **45**(13): 5564-5571.

Jafry, H. R., M. V. Liga, Q. Li and A. R. Barron (2011). "Simple route to enhanced photocatalytic activity of p25 titanium dioxide nanoparticles by silica addition." Environ Sci Technol **45**(4): 1563-1568.

Jager, T., J. Alexander, S. Kirchen, A. Dotsch, A. Wieland, C. Hiller and T. Schwartz (2018). "Live-dead discrimination analysis, qPCR assessment for opportunistic pathogens, and population analysis at ozone wastewater treatment plants." Environ Pollut **232**: 571-579.

Jahani, S., S. Saeidi, F. Javadian, Z. Akbarizadeh and A. Sobhanizade (2016). "Investigating the antibacterial effects of plant extracts on Pseudomonas aeruginosa and Escherichia coli." International Journal of Infection **3**(2).

Jaroenworaluck, A., W. Sunsaneeyametha, N. Kosachan and R. Stevens (2006). "Characteristics of silica-coated TiO2 and its UV absorption for sunscreen cosmetic applications." Surface and Interface Analysis **38**(4): 473-477.

Jassby, D., J. Farner Budarz and M. Wiesner (2012). "Impact of aggregate size and structure on the photocatalytic properties of TiO2 and ZnO nanoparticles." Environ Sci Technol **46**(13): 6934-6941.

Jeon, S.-k., E.-j. Kim, J. Lee and S. Lee (2016). "Potential risks of TiO2 and ZnO nanoparticles released from sunscreens into outdoor swimming pools." Journal of Hazardous Materials **317**: 312-318.

Jiang, Y., L. Zhang, D. Wen and Y. Ding (2016). "Role of physical and chemical interactions in the antibacterial behavior of ZnO nanoparticles against E. coli." Materials Science and Engineering: C **69**: 1361-1366.

Johnson, K. M., Kumar, M. A., Ponmurugan, P., & Gananamangai, B. M. (2010). "Ultraviolet radiation and its germicidal effect in drinking water purification." Journal of Phytology.

Jones, N., B. Ray, K. T. Ranjit and A. C. Manna (2008). "Antibacterial activity of ZnO nanoparticle suspensions on a broad spectrum of microorganisms." FEMS Microbiol Lett **279**(1): 71-76.

Joo, S. H., M. Knecht, C. Su, S. Seo and R. Lawrence (2016). "Influence of siloxane on the transport of ZnO nanoparticles from different release pathways in saturated sand." RSC Adv. **6**(102): 100494-100503.

Jung, J. H., G. B. Hwang, J. E. Lee and G. N. Bae (2011). "Preparation of airborne Ag/CNT hybrid nanoparticles using an aerosol process and their application to antimicrobial air filtration." Langmuir **27**(16): 10256-10264.

Kanakaraju, D., S. Ravichandar and Y. C. Lim (2017). "Combined effects of adsorption and photocatalysis by hybrid TiO2/ZnO-calcium alginate beads for the removal of copper." J Environ Sci (China) **55**: 214-223.

Kanel, S. R. and S. R. Al-Abed (2011). "Influence of pH on the transport of nanoscale zinc oxide in saturated porous media." Journal of Nanoparticle Research **13**(9): 4035-4047.

Kao, Y. Y., Y. C. Chen, T. J. Cheng, Y. M. Chiung and P. S. Liu (2012). "Zinc oxide nanoparticles interfere with zinc ion homeostasis to cause cytotoxicity." Toxicol Sci **125**(2): 462-472.

Karaolia, P., I. Michael-Kordatou, E. Hapeshi, C. Drosou, Y. Bertakis, D. Christofilos, G. S. Armatas, L. Sygellou, T. Schwartz, N. P. Xekoukoulotakis and D. Fatta-Kassinos (2018). "Removal of antibiotics, antibiotic-resistant bacteria and their associated genes by graphene-based TiO 2 composite photocatalysts under solar radiation in urban wastewaters." Applied Catalysis B: Environmental **224**: 810-824.

Karimi, M., R. Sadeghi and J. Kokini (2018). "Human exposure to nanoparticles through trophic transfer and the biosafety concerns that nanoparticle-contaminated foods pose to consumers." Trends in Food Science & Technology **75**: 129-145.

Kim, H.-J., Y.-G. Shul and H. Han (2005). "Photocatalytic properties of silica-supported TiO2." Topics in Catalysis **35**(3-4): 287-293.

Kiwi, J. and V. Nadtochenko (2005). "Evidence for the mechanism of photocatalytic degradation of the bacterial wall membrane at the TiO2 interface by ATR-FTIR and laser kinetic spectroscopy." Langmuir **21**(10): 4631-4641.

Klaine, S. J., Pedro JJ Alvarez, Graeme E. Batley, Teresa F. Fernandes, Richard D. Handy, Delina Y. Lyon, Shaily Mahendra, Michael J. McLaughlin, and Jamie R. Lead (2008). "Nanomaterials in the environment: behavior, fate, bioavailability, and effects." Environmental toxicology and chemistry **27**(9): 1825-1851.

Kocbek, P., K. Teskac, M. E. Kreft and J. Kristl (2010). "Toxicological aspects of long-term treatment of keratinocytes with ZnO and TiO2 nanoparticles." Small **6**(17): 1908-1917.

Koh, B. and W. Cheng (2014). "Mechanisms of carbon nanotube aggregation and the reversion of carbon nanotube aggregates in aqueous medium." Langmuir **30**(36): 10899-10909

Krasner, S. W., Howard S. Weinberg, Susan D. Richardson, Salvador J. Pastor, Russell Chinn, Michael J. Sclimenti, Gretchen D. Onstad, and Alfred D. Thruston (2006). "Occurrence of a new generation of disinfection byproducts." Environmental Science & Technology Letters **40**(23): 7175-7185.

Krol, A., P. Pomastowski, K. Rafinska, V. Railean-Plugaru and B. Buszewski (2017). "Zinc oxide nanoparticles: synthesis, antiseptic activity and toxicity mechanism." Adv Colloid Interface Sci **249**: 37-52.

Kumar, A., A. K. Pandey, S. S. Singh, R. Shanker and A. Dhawan (2011). "Engineered ZnO and TiO2 nanoparticles induce oxidative stress and DNA damage leading to reduced viability of Escherichia coli." Free Radic Biol Med **51**(10): 1872-1881.

Kumar, R. V. and G. Raza (2008). "Photocatalytic disinfection of water with Ag–TiO2 nanocrystalline composite." Ionics **15**(5): 579-587.

Labille, J., J. Feng, C. Botta, D. Borschneck, M. Sammut, M. Cabie, M. Auffan, J. Rose and J. Y. Bottero (2010). "Aging of TiO2 nanocomposites used in sunscreen. Dispersion and fate of the degradation products in aqueous environment." Environ Pollut **158**(12): 3482-3489.

Lee, W., K. J. Kim and D. G. Lee (2014). "A novel mechanism for the antibacterial effect of silver nanoparticles on Escherichia coli." Biometals **27**(6): 1191-1201.

Lee, W. A., N. Pernodet, B. Li, C. H. Lin, E. Hatchwell and M. H. Rafailovich (2007). "Multicomponent polymer coating to block photocatalytic activity of TiO2 nanoparticles." Chem Commun (Camb)(45): 4815-4817.

Leung, Y. H., A. M. Ng, X. Xu, Z. Shen, L. A. Gethings, M. T. Wong, C. M. Chan, M. Y. Guo, Y. H. Ng, A. B. Djurisic, P. K. Lee, W. K. Chan, L. H. Yu, D. L. Phillips, A. P. Ma and F. C. Leung (2014). "Mechanisms of antibacterial activity of MgO: non-ROS mediated toxicity of MgO nanoparticles towards Escherichia coli." Small **10**(6): 1171-1183.

Leung, Y. H., X. Xu, A. P. Ma, F. Liu, A. M. Ng, Z. Shen, L. A. Gethings, M. Y. Guo, A. B. Djurisic, P. K. Lee, H. K. Lee, W. K. Chan and F. C. Leung (2016). "Toxicity of ZnO and TiO2 to Escherichia coli cells." Sci Rep **6**: 35243.

Lewicka, Z. A., A. F. Benedetto, D. N. Benoit, W. W. Yu, J. D. Fortner and V. L. Colvin (2011). "The structure, composition, and dimensions of TiO2 and ZnO nanomaterials in commercial sunscreens." Journal of Nanoparticle Research **13**(9): 3607-3617.

Li, F., Z. Liang, X. Zheng, W. Zhao, M. Wu and Z. Wang (2015). "Toxicity of nano-TiO2 on algae and the site of reactive oxygen species production." Aquat Toxicol **158**: 1-13.

Li, J.-H., Y.-Y. Xu, L.-P. Zhu, J.-H. Wang and C.-H. Du (2009). "Fabrication and characterization of a novel TiO2 nanoparticle self-assembly membrane with improved fouling resistance." Journal of Membrane Science **326**(2): 659-666.

Li, M., D. Lin and L. Zhu (2013). "Effects of water chemistry on the dissolution of ZnO nanoparticles and their toxicity to Escherichia coli." Environ Pollut **173**: 97-102.

Li, M., Pokhrel, S., Jin, X., Mädler, L., Damoiseaux, R., & Hoek, E. M. (2010). "Stability, bioavailability, and bacterial toxicity of ZnO and iron-doped ZnO nanoparticles in aquatic media." Environmental science & technology **45**(2): 755-761.

Li, M., L. Zhu and D. Lin (2011). "Toxicity of ZnO nanoparticles to Escherichia coli: mechanism and the influence of medium components." Environ Sci Technol **45**(5): 1977-1983.

Li, Q., S. Mahendra, D. Y. Lyon, L. Brunet, M. V. Liga, D. Li and P. J. Alvarez (2008). "Antimicrobial nanomaterials for water disinfection and microbial control: potential applications and implications." Water Res **42**(18): 4591-4602.

Li, X., et al. (2014). "Functional gold nanoparticles as potent antimicrobial agents against multi-drug-resistant bacteria." American Chemical Society **8**(10):10682-10686.

Li, Y., J. Niu, W. Zhang, L. Zhang and E. Shang (2014). "Influence of aqueous media on the ROS-mediated toxicity of ZnO nanoparticles toward green fluorescent protein-expressing Escherichia coli under UV-365 irradiation." Langmuir **30**(10): 2852-2862.

Li, Z. (2011). "Mechanistic insight into the effect of polymer and NOM coatings on Adhesion and nteractions between nanoparticles and bacteria." (Doctoral dissertation). Carnegie Mellon University, Pittsburgh, PA.

Lin, S., R. Huang, Y. Cheng, J. Liu, B. L. Lau and M. R. Wiesner (2013). "Silver nanoparticle-alginate composite beads for point-of-use drinking water disinfection." Water Res **47**(12): 3959-3965.

Lin, X., et al (2014). "Toxicity of TiO 2 nanoparticles to Escherichia coli: effects of particle size, crystal phase and water chemistry." PloS one **9**(10): e110247.

Lin, X., J. Li, S. Ma, G. Liu, K. Yang, M. Tong and D. Lin (2014). "Toxicity of TiO 2 nanoparticles to Escherichia coli: effects of particle size, crystal phase and water chemistry." PloS one **9**(10): e110247.

Lipovsky, A., Tzitrinovich, Z., Friedmann, H., Applerot, G., Gedanken, A., & Lubart, R. (2009). "EPR study of visible light-induced ROS generation by nanoparticles of ZnO." The Journal of Physical Chemistry C **113**(36): 15997-16001.

Liu, J., L. Liu, H. Bai, Y. Wang and D. D. Sun (2011). "Gram-scale production of graphene oxide–TiO2 nanorod composites: Towards high-activity photocatalytic materials." Applied Catalysis B: Environmental.

Liu, L. P., X. N. Yang, L. Ye, D. D. Xue, M. Liu, S. R. Jia, Y. Hou, L. Q. Chu and C. Zhong (2017). "Preparation and characterization of a photocatalytic antibacterial material: Graphene oxide/TiO2/bacterial cellulose nanocomposite." Carbohydr Polym **174**: 1078-1086.

Liu, S., M. Hu, T. H. Zeng, R. Wu, R. Jiang, J. Wei, L. Wang, J. Kong and Y. Chen (2012). "Lateral dimension-dependent antibacterial activity of graphene oxide sheets." Langmuir **28**(33): 12364-12372.

Liu, Y., L. He, A. Mustapha, H. Li, Z. Q. Hu and M. Lin (2009). "Antibacterial activities of zinc oxide nanoparticles against Escherichia coli O157:H7." J Appl Microbiol **107**(4): 1193-1201.

Liu, Y., Y. Hu, M. Zhou, H. Qian and X. Hu (2012). "Microwave-assisted non-aqueous route to deposit well-dispersed ZnO nanocrystals on reduced graphene oxide sheets with improved photoactivity for the decolorization of dyes under visible light." Applied Catalysis B: Environmental **125**: 425-431.

Liufu, S., H. Xiao and Y. Li (2005). "Adsorption of poly(acrylic acid) onto the surface of titanium dioxide and the colloidal stability of aqueous suspension." J Colloid Interface Sci **281**(1): 155-163.

Love, S. A., M. A. Maurer-Jones, J. W. Thompson, Y. S. Lin and C. L. Haynes (2012). "Assessing nanoparticle toxicity." Annu Rev Anal Chem (Palo Alto Calif) **5**: 181-205.

Lupan, I., R. Carpa, A. Oltean, B. S. Kelemen and O. Popescu (2017). "Release of antibiotic resistant bacteria by a waste treatment plant from Romania." Microbes Environ **32**(3): 219-225.

Lv, X., Y. Yang, Y. Tao, Y. Jiang, B. Chen, X. Zhu, Z. Cai and B. Li (2018). "A mechanism study on toxicity of graphene oxide to Daphnia magna: Direct link between bioaccumulation and oxidative stress." Environ Pollut **234**: 953-959.

Ma, H., L. K. Wallis, S. Diamond, S. Li, J. Canas-Carrell and A. Parra (2014). "Impact of solar UV radiation on toxicity of ZnO nanoparticles through photocatalytic reactive oxygen species (ROS) generation and photo-induced dissolution." Environ Pollut **193**: 165-172.

Ma, H., P. L. Williams and S. A. Diamond (2013). "Ecotoxicity of manufactured ZnO nanoparticles--a review." Environ Pollut **172**: 76-85.

MamathaKumari, M., D. Praveen Kumar, P. Haridoss, V. DurgaKumari and M. V. Shankar (2015). "Nanohybrid of titania/carbon nanotubes – nanohorns: a promising photocatalyst for enhanced hydrogen production under solar irradiation." International Journal of Hydrogen Energy **40**(4): 1665-1674.

Maness, P. C., Smolinski, S., Blake, D. M., Huang, Z., Wolfrum, E. J., & Jacoby, W. A. (1999). "Bactericidal activity of photocatalytic TiO2 reaction: toward an understanding of its killing mechanism." Applied and environmental microbiology **65**(9): 4094-4098.

Mangadlao, J. D., C. M. Santos, M. J. Felipe, A. C. de Leon, D. F. Rodrigues and R. C. Advincula (2015). "On the antibacterial mechanism of graphene oxide (GO) Langmuir-Blodgett films." Chem Commun (Camb) **51**(14): 2886-2889.

Manzo, S., M. L. Miglietta, G. Rametta, S. Buono and G. Di Francia (2013). "Toxic effects of ZnO nanoparticles towards marine algae Dunaliella tertiolecta." Sci Total Environ **445-446**: 371-376.

Mao, J., R. Guo and L. T. Yan (2014). "Simulation and analysis of cellular internalization pathways and membrane perturbation for graphene nanosheets." Biomaterials **35**(23): 6069-6077.

Metzler, D. M., M. Li, A. Erdem and C. P. Huang (2011). "Responses of algae to photocatalytic nano-TiO2 particles with an emphasis on the effect of particle size." Chemical Engineering Journal **170**(2-3): 538-546.

Middepogu, A., J. Hou, X. Gao and D. Lin (2018). "Effect and mechanism of TiO2 nanoparticles on the photosynthesis of Chlorella pyrenoidosa." Ecotoxicol Environ Saf **161**: 497-506.

Minetto, D., A. Volpi Ghirardini and G. Libralato (2016). "Saltwater ecotoxicology of Ag, Au, CuO, TiO2, ZnO and C60 engineered nanoparticles: An overview." Environ Int **92-93**: 189-201.

Mirabedini, A., S. M. Mirabedini, A. A. Babalou and S. Pazokifard (2011). "Synthesis, characterization and enhanced photocatalytic activity of TiO2/SiO2 nanocomposite in an aqueous solution and acrylic-based coatings." Progress in Organic Coatings **72**(3): 453-460.

Mohd Omar, F., H. Abdul Aziz and S. Stoll (2014). "Aggregation and disaggregation of ZnO nanoparticles: influence of pH and adsorption of Suwannee River humic acid." Sci Total Environ **468-469**: 195-201.

Morelli, E., E. Gabellieri, A. Bonomini, D. Tognotti, G. Grassi and I. Corsi (2018). "TiO2 nanoparticles in seawater: aggregation and interactions with the green alga Dunaliella tertiolecta." Ecotoxicol Environ Saf **148**: 184-193.

Motshekga, S. C., S. S. Ray, M. S. Onyango and M. N. B. Momba (2015). "Preparation and antibacterial activity of chitosan-based nanocomposites containing bentonite-supported silver and zinc oxide nanoparticles for water disinfection." Applied Clay Science **114**: 330-339.

Motshekga, S. C., S. Sinha Ray and A. Maity (2018). "Synthesis and characterization of alginate beads encapsulated zinc oxide nanoparticles for bacteria disinfection in water." J Colloid Interface Sci **512**: 686-692.

Mottier, A., F. Mouchet, E. Pinelli, L. Gauthier and E. Flahaut (2017). "Environmental impact of engineered carbon nanoparticles: from releases to effects on the aquatic biota." Curr Opin Biotechnol **46**: 1-6.

Nangmenyi, G., X. Li, S. Mehrabi, E. Mintz and J. Economy (2011). "Silver-modified iron oxide nanoparticle impregnated fiberglass for disinfection of bacteria and viruses in water." Materials Letters **65**(8): 1191-1193.

Nguyen, V. H. and J.-J. Shim (2015). "Green synthesis and characterization of carbon nanotubes/polyaniline nanocomposites." Journal of Spectroscopy **2015**: 1-9.

Nischwitz, V. and H. Goenaga-Infante (2012). "Improved sample preparation and quality control for the characterisation of titanium dioxide nanoparticles in sunscreens using flow field flow fractionation on-line with inductively coupled plasma mass spectrometry." Journal of Analytical Atomic Spectrometry **27**(7): 1084.

Nogueira, P. F., D. Nakabayashi and V. Zucolotto (2015). "The effects of graphene oxide on green algae Raphidocelis subcapitata." Aquat Toxicol **166**: 29-35.

Nosrati, R., A. Olad and S. Shakoori (2017). "Preparation of an antibacterial, hydrophilic and photocatalytically active polyacrylic coating using TiO2 nanoparticles sensitized by graphene oxide." Mater Sci Eng C Mater Biol Appl **80**: 642-651.

Nur, H. (2006). "Modification of titanium surface species of titania by attachment of silica nanoparticles." Materials Science and Engineering: B **133**(1-3): 49-54.

Öncü, N. B., Y. Z. Menceloğlu and I. Akmehmet Balcıoğlu (2011). "Comparison of the effectiveness of chlorine, ozone, and photocatalytic disinfection in reducing the risk of antibiotic resistance pollution." Journal of Advanced Oxidation Technologies **14**(2).

Othman, S. H., S. Abdul Rashid, T. I. Mohd Ghazi and N. Abdullah (2012). "Dispersion and stabilization of photocatalytic TiO2 nanoparticles in aqueous suspension for coatings applications." Journal of Nanomaterials **2012**: 1-10.

Padmavathy, N. and R. Vijayaraghavan (2016). "Enhanced bioactivity of ZnO nanoparticles—an antimicrobial study." Science and Technology of Advanced Materials **9**(3): 035004.

Pagnout, C., S. Jomini, M. Dadhwal, C. Caillet, F. Thomas and P. Bauda (2012). "Role of electrostatic interactions in the toxicity of titanium dioxide nanoparticles toward Escherichia coli." Colloids Surf B Biointerfaces **92**: 315-321.

Pal, S., Y. K. Tak and J. M. Song (2007). "Does the antibacterial activity of silver nanoparticles depend on the shape of the nanoparticle? A study of the Gram-negative bacterium Escherichia coli." Appl Environ Microbiol **73**(6): 1712-1720.

Park, O. K. and Y. S. Kang (2005). "Preparation and characterization of silica-coated TiO2 nanoparticle." Colloids and Surfaces A: Physicochemical and Engineering Aspects **257-258**: 261-265.

Park, Y. H., H. C. Bae, Y. Jang, S. H. Jeong, H. N. Lee, W.-I. Ryu, M. G. Yoo, Y. R. Kim, M. K. Kim, J. K. Lee, J. Jeong and S. W. Son (2013). "Effect of the size and surface charge of silica nanoparticles on cutaneous toxicity." Molecular & Cellular Toxicology **9**(1): 67-74.

Pasquet, J., Y. Chevalier, E. Couval, D. Bouvier, G. Noizet, C. Morliere and M. A. Bolzinger (2014). "Antimicrobial activity of zinc oxide particles on five micro-organisms of the challenge tests related to their physicochemical properties." Int J Pharm **460**(1-2): 92-100.

Peng, X., S. Palma, N. S. Fisher and S. S. Wong (2011). "Effect of morphology of ZnO nanostructures on their toxicity to marine algae." Aquat Toxicol **102**(3-4): 186-196.

Petros, R. A. and J. M. DeSimone (2010). "Strategies in the design of nanoparticles for therapeutic applications." Nat Rev Drug Discov **9**(8): 615-627.

Piccinno, F., F. Gottschalk, S. Seeger and B. Nowack (2012). "Industrial production quantities and uses of ten engineered nanomaterials in Europe and the world." Journal of Nanoparticle Research **14**(9): 1109.

Pikula, K. S., A. M. Zakharenko, V. V. Chaika, A. A. Vedyagin, T. Y. Orlova, I. V. Mishakov, V. L. Kuznetsov, S. Park, E. A. Renieri, A. Kahru, A. M. Tsatsakis and K. S. Golokhvast (2018). "Effects of carbon and silicon nanotubes and carbon nanofibers on marine microalgae Heterosigma akashiwo." Environ Res **166**: 473-480.

Planchon, M., R. Ferrari, F. Guyot, A. Gelabert, N. Menguy, C. Chaneac, A. Thill, M. F. Benedetti and O. Spalla (2013). "Interaction between Escherichia coli and TiO2 nanoparticles in natural and artificial waters." Colloids Surf B Biointerfaces **102**: 158-164.

Qi, K., B. Cheng, J. Yu and W. Ho (2017). "Review on the improvement of the photocatalytic and antibacterial activities of ZnO." Journal of Alloys and Compounds **727**: 792-820.

Raghupathi, K. R., R. T. Koodali and A. C. Manna (2011). "Size-dependent bacterial growth inhibition and mechanism of antibacterial activity of zinc oxide nanoparticles." Langmuir **27**(7): 4020-4028.

Rajaura, R. S., V. Sharma, R. S. Ronin, D. K. Gupta, S. Srivastava, K. Agrawal and Y. K. Vijay (2017). "Synthesis, characterization and enhanced antimicrobial activity of reduced graphene oxide–zinc oxide nanocomposite." Materials Research Express **4**(2): 025401.

Rajeswari, R. and H. G. Prabu (2017). "Synthesis characterization, antimicrobial, antioxidant, and cytotoxic activities of ZnO nanorods on reduced graphene oxide." Journal of Inorganic and Organometallic Polymers and Materials **28**(3): 679-693.

Rajput, V. D., T. M. Minkina, A. Behal, S. N. Sushkova, S. Mandzhieva, R. Singh, A. Gorovtsov, V. S. Tsitsuashvili, W. O. Purvis, K. A. Ghazaryan and H. S. Movsesyan (2018). "Effects of zinc-oxide nanoparticles on soil, plants, animals and soil organisms: A review." Environmental Nanotechnology, Monitoring & Management **9**: 76-84.

Ramani, M., S. Ponnusamy, C. Muthamizhchelvan, J. Cullen, S. Krishnamurthy and E. Marsili (2013). "Morphology-directed synthesis of ZnO nanostructures and their antibacterial activity." Colloids Surf B Biointerfaces **105**: 24-30.

Rasalingam, S., R. Peng and R. T. Koodali (2014). "Removal of hazardous pollutants from wastewaters: applications of TiO2-SiO2 mixed oxide materials." Journal of Nanomaterials **2014**: 1-42.

Regiel, A., S. Irusta, A. Kyziol, M. Arruebo and J. Santamaria (2013). "Preparation and characterization of chitosan-silver nanocomposite films and their antibacterial activity against Staphylococcus aureus." Nanotechnology **24**(1): 015101.

Rhiem, S., M. J. Riding, W. Baumgartner, F. L. Martin, K. T. Semple, K. C. Jones, A. Schaffer and H. M. Maes (2015). "Interactions of multiwalled carbon nanotubes with algal cells: quantification of association, visualization of uptake, and measurement of alterations in the composition of cells." Environ Pollut **196**: 431-439.

Rizzo, L., C. Manaia, C. Merlin, T. Schwartz, C. Dagot, M. C. Ploy, I. Michael and D. Fatta-Kassinos (2013). "Urban wastewater treatment plants as hotspots for antibiotic resistant bacteria and genes spread into the environment: a review." Sci Total Environ **447**: 345-360.

Romero-Vargas Castrillón, S., F. Perreault, A. F. de Faria and M. Elimelech (2015). "Interaction of graphene oxide with bacterial cell membranes: insights from force spectroscopy." Environmental Science & Technology Letters **2**(4): 112-117.

Salama, A., M. A. Diab, R. E. Abou-Zeid, H. A. Aljohani and K. R. Shoueir (2018). "Crosslinked alginate/silica/zinc oxide nanocomposite: A sustainable material with antibacterial properties." Composites Communications **7**: 7-11.

Sarkar, B., S. Mandal, Y. F. Tsang, P. Kumar, K. H. Kim and Y. S. Ok (2018). "Designer carbon nanotubes for contaminant removal in water and wastewater: A critical review." Sci Total Environ **612**: 561-581.

Sarwar, S., S. Chakraborti, S. Bera, I. A. Sheikh, K. M. Hoque and P. Chakrabarti (2016). "The antimicrobial activity of ZnO nanoparticles against Vibrio cholerae: Variation in response depends on biotype." Nanomedicine **12**(6): 1499-1509.

Schrand, A. M., M. F. Rahman, S. M. Hussain, J. J. Schlager, D. A. Smith and A. F. Syed (2010). "Metal-based nanoparticles and their toxicity assessment." Wiley Interdiscip Rev Nanomed Nanobiotechnol **2**(5): 544-568.

Schwab, F., T. D. Bucheli, L. P. Lukhele, A. Magrez, B. Nowack, L. Sigg and K. Knauer (2011). "Are carbon nanotube effects on green algae caused by shading and agglomeration?" Environ Sci Technol **45**(14): 6136-6144.

Shalumon, K. T., K. H. Anulekha, S. V. Nair, S. V. Nair, K. P. Chennazhi and R. Jayakumar (2011). "Sodium alginate/poly(vinyl alcohol)/nano ZnO composite nanofibers for antibacterial wound dressings." Int J Biol Macromol **49**(3): 247-254.

Shang, L., Nienhaus, K., & Nienhaus, G. U. (2014). "Engineered nanoparticles interacting with cells: size matters." Journal of Nanobiotechnology **12**(1): 5.

Sharma, V., D. Anderson and A. Dhawan (2012). "Zinc oxide nanoparticles induce oxidative DNA damage and ROS-triggered mitochondria mediated apoptosis in human liver cells (HepG2)." Apoptosis **17**(8): 852-870.

Shrivastava, R., R. K. Upreti, S. R. Jain, K. N. Prasad, P. K. Seth and U. C. Chaturvedi (2004). "Suboptimal chlorine treatment of drinking water leads to selection of multidrug-resistant Pseudomonas aeruginosa." Ecotoxicology and Environmental Safety **58**(2): 277-283.

Smijs, T. G. and S. Pavel (2011). "Titanium dioxide and zinc oxide nanoparticles in sunscreens: focus on their safety and effectiveness." Nanotechnol Sci Appl **4**: 95-112.

Sodano, V., M. T. Gorgitano, M. Quaglietta and F. Verneau (2016). "Regulating food nanotechnologies in the European Union: Open issues and political challenges." Trends in Food Science & Technology **54**: 216-226.

Song, C., P. Chen, C. Wang and L. Zhu (2012). "Photodegradation of perfluorooctanoic acid by synthesized TiO2-MWCNT composites under 365nm UV irradiation." Chemosphere **86**(8): 853-859.

Song, W., J. Zhang, J. Guo, J. Zhang, F. Ding, L. Li and Z. Sun (2010). "Role of the dissolved zinc ion and reactive oxygen species in cytotoxicity of ZnO nanoparticles." Toxicol Lett **199**(3): 389-397.

Souza, J. P., F. P. Venturini, F. Santos and V. Zucolotto (2018). "Chronic toxicity in Ceriodaphnia dubia induced by graphene oxide." Chemosphere **190**: 218-224.

Srivastava, S. and A. Kumar (2016). "Comparative cytotoxicity of nanoparticles and ions to Escherichia coli in binary mixtures." Journal of Environmental Sciences.

Stengl, V., S. Bakardjieva, T. M. Grygar, J. Bludska and M. Kormunda (2013). "TiO2-graphene oxide nanocomposite as advanced photocatalytic materials."

Stengl, V., S. Bakardjieva, T. M. Grygar, J. Bludska and M. Kormunda (2013). "TiO2-graphene oxide nanocomposite as advanced photocatalytic materials." Chem Cent J **7**(1): 41.

Stoimenov, P. K., Klinger, R. L., Marchin, G. L., & Klabunde, K. J. (2002). "Metal oxide nanoparticles as bactericidal agents." Langmuir **18**(17): 6679-6686.

Suganthi, K. S. and K. S. Rajan (2012). "Temperature induced changes in ZnO–water nanofluid: Zeta potential, size distribution and viscosity profiles." International Journal of Heat and Mass Transfer **55**(25-26): 7969-7980.

Sui, M., L. Zhang, L. Sheng, S. Huang and L. She (2013). "Synthesis of ZnO coated multi-walled carbon nanotubes and their antibacterial activities." Sci Total Environ **452-453**: 148-154.

Suman, T. Y., S. R. Radhika Rajasree and R. Kirubagaran (2015). "Evaluation of zinc oxide nanoparticles toxicity on marine algae chlorella vulgaris through flow cytometric, cytotoxicity and oxidative stress analysis." Ecotoxicol Environ Saf **113**: 23-30.

Suresh, A. K., D. A. Pelletier and M. J. Doktycz (2013). "Relating nanomaterial properties and microbial toxicity." Nanoscale **5**(2): 463-474.

Suwanboon, S., P. Amornpitoksuk, A. Haidoux and J. C. Tedenac (2008). "Structural and optical properties of undoped and aluminium doped zinc oxide nanoparticles via precipitation method at low temperature." Journal of Alloys and Compounds **462**(1-2): 335-339.

Tan, C. and W. X. Wang (2017). "Influences of TiO2 nanoparticles on dietary metal uptake in Daphnia magna." Environ Pollut **231**(Pt 1): 311-318.

Tejamaya, M., I. Romer, R. C. Merrifield and J. R. Lead (2012). "Stability of citrate, PVP, and PEG coated silver nanoparticles in ecotoxicology media." Environ Sci Technol **46**(13): 7011-7017.

Tso, C. P., C. M. Zhung, Y. H. Shih, Y. M. Tseng, S. C. Wu and R. A. Doong (2010). "Stability of metal oxide nanoparticles in aqueous solutions." Water Sci Technol **61**(1): 127-133.

Tu, Y., M. Lv, P. Xiu, T. Huynh, M. Zhang, M. Castelli, Z. Liu, Q. Huang, C. Fan, H. Fang and R. Zhou (2013). "Destructive extraction of phospholipids from Escherichia coli membranes by graphene nanosheets." Nat Nanotechnol **8**(8): 594-601.

Tuchina, E. S. and V. V. Tuchin (2010). "TiO2 nanoparticle enhanced photodynamic inhibition of pathogens." Laser Physics Letters **7**(8): 607-612.

Upasani, P., T. V. Sreekumar, V. G. Gaikar and N. Jha (2017). "Preparation of ZnO nanoribbon–MWCNT composite film and its application as antimicrobial bandage, antibacterial filter and thermal IR camouflage material." Bulletin of Materials Science **40**(4): 865-876.

van Elsas, J. D., A. V. Semenov, R. Costa and J. T. Trevors (2011). "Survival of Escherichia coli in the environment: fundamental and public health aspects." ISME J **5**(2): 173-183.

Venkatesan, J., J. Y. Lee, D. S. Kang, S. Anil, S. K. Kim, M. S. Shim and D. G. Kim (2017). "Antimicrobial and anticancer activities of porous chitosan-alginate biosynthesized silver nanoparticles." Int J Biol Macromol **98**: 515-525.

Wang, D., Z. Lin, T. Wang, Z. Yao, M. Qin, S. Zheng and W. Lu (2016). "Where does the toxicity of metal oxide nanoparticles come from: The nanoparticles, the ions, or a combination of both?" J Hazard Mater **308**: 328-334.

Wang, J. and Y. Fan (2014). "Lung injury induced by TiO2 nanoparticles depends on their structural features: size, shape, crystal phases, and surface coating." Int J Mol Sci **15**(12): 22258-22278.

Wang, J., X. Zhang, Y. Chen, M. Sommerfeld and Q. Hu (2008). "Toxicity assessment of manufactured nanomaterials using the unicellular green alga Chlamydomonas reinhardtii." Chemosphere **73**(7): 1121-1128.

Wang, X. and H. Chen (2015). "A new approach to preparation of TiO2@void@SiO2 rattle type core shell structure nanoparticles via titanyl oxalate complex." Colloids and Surfaces A: Physicochemical and Engineering Aspects **485**: 25-33.

Wang, X., B. Xia, X. Zhu, J. Chen, S. Qiu and J. Li (2008). "Controlled modification of multiwalled carbon nanotubes with Zno nanostructures." Journal of Solid State Chemistry **181**(4): 822-827.

Wang, Y., X. Zhu, Y. Lao, X. Lv, Y. Tao, B. Huang, J. Wang, J. Zhou and Z. Cai (2016). "TiO2 nanoparticles in the marine environment: Physical effects responsible for the toxicity on algae Phaeodactylum tricornutum." Sci Total Environ **565**: 818-826.

Wang, Y. W., A. Cao, Y. Jiang, X. Zhang, J. H. Liu, Y. Liu and H. Wang (2014). "Superior antibacterial activity of zinc oxide/graphene oxide composites originating from high zinc concentration localized around bacteria." ACS Appl Mater Interfaces **6**(4): 2791-2798.

Wang, Z., F. Zhang, S. Wang and W. Peijnenburg (2017). "Assessment and prediction of joint algal toxicity of binary mixtures of graphene and ionic liquids." Chemosphere **185**: 681-689.

Wei, L., M. Thakkar, Y. Chen, S. A. Ntim, S. Mitra and X. Zhang (2010). "Cytotoxicity effects of water dispersible oxidized multiwalled carbon nanotubes on marine alga, Dunaliella tertiolecta." Aquat Toxicol **100**(2): 194-201.

Weir, A., P. Westerhoff, L. Fabricius, K. Hristovski and N. von Goetz (2012). "Titanium dioxide nanoparticles in food and personal care products." Environ Sci Technol **46**(4): 2242-2250.

Wenbing Hu, C. P., Weijie Luo, Min Lv, Xiaoming Li, Di Li, Qing Huang, and Chunhai Fan (2010). "Graphene-based antibacterial paper." ACS Nano **4**(7): 4317-4323.

WHO (2011). "Guidelines for drinking-water quality." World Health Organization, Geneva, Switzerland Fourth ed.vol. 1.

Wilkie, A. C., and Walter W. Mulbry (2002). "Recovery of dairy manure nutrients by benthic freshwater algae." Bioresource technology **84**(1): 81-91.

Wong, S. W., P. T. Leung, A. B. Djurisic and K. M. Leung (2010). "Toxicities of nano zinc oxide to five marine organisms: influences of aggregate size and ion solubility." Anal Bioanal Chem **396**(2): 609-618.

Wu, Y., L.-D. Liao, H.-C. Pan, L. He, C.-T. Lin and M. C. Tan (2017). "Fabrication and interfacial characteristics of surface modified Ag nanoparticle based conductive composites." RSC Adv. **7**(47): 29702-29712.

Xia, B., B. Chen, X. Sun, K. Qu, F. Ma and M. Du (2015). "Interaction of TiO2 nanoparticles with the marine microalga Nitzschia closterium: growth inhibition, oxidative stress and internalization." Sci Total Environ **508**: 525-533.

Xiong, D., T. Fang, L. Yu, X. Sima and W. Zhu (2011). "Effects of nano-scale TiO2, ZnO and their bulk counterparts on zebrafish: acute toxicity, oxidative stress and oxidative damage." Sci Total Environ **409**(8): 1444-1452.

Xue, C., W. Liu, J. Wu, X. Yang and H. Xu (2011). "Chemoprotective effect of N-acetylcysteine (NAC) on cellular oxidative damages and apoptosis induced by nano titanium dioxide under UVA irradiation." Toxicol In Vitro **25**(1): 110-116.

Xue, Z., C. M. Hessler, W. Panmanee, D. J. Hassett and Y. Seo (2013). "Pseudomonas aeruginosa inactivation mechanism is affected by capsular extracellular polymeric substances reactivity with chlorine and monochloramine." FEMS Microbiol Ecol **83**(1): 101-111.

Yamamoto, O. (2001). "Influence of particle size on the antibacterial activity of zinc oxide." International Journal of Inorganic Materials **3**(7): 643-646.

Yang, C., J. Mamouni, Y. Tang and L. Yang (2010). "Antimicrobial activity of single-walled carbon nanotubes: length effect." Langmuir **26**(20): 16013-16019.

Yuan, C., C. H. Hung, C. S. Yuan and H. W. Li (2017). "Preparation and Application of Immobilized Surfactant-Modified PANi-CNT/TiO(2) under Visible-Light Irradiation." Materials (Basel) **10**(8).

Yuan Yao, G. L., Shannon Ciston, Richard M. Lueptow, and Kimberly A. Gray (2008). "Photoreactive TiO2/Carbon nanotube composites: synthesis and reactivity." Environmental Science & Technology **42**(13): 4952-4957.

Zamiri, R., A. Rebelo, G. Zamiri, A. Adnani, A. Kuashal, M. S. Belsley and J. M. F. Ferreira (2014). "Far-infrared optical constants of ZnO and ZnO/Ag nanostructures." RSC Adv. **4**(40): 20902-20908.

Zhang, K., F. J. Zhang, M. L. Chen and W. C. Oh (2011). "Comparison of catalytic activities for photocatalytic and sonocatalytic degradation of methylene blue in present of anatase TiO2-CNT catalysts." Ultrason Sonochem **18**(3): 765-772.

Zhang, L., Y. Jiang, Y. Ding, M. Povey and D. York (2006). "Investigation into the antibacterial behaviour of suspensions of ZnO nanoparticles (ZnO nanofluids)." Journal of Nanoparticle Research **9**(3): 479-489.

Zhang, L., C. Lei, J. Chen, K. Yang, L. Zhu and D. Lin (2015). "Effect of natural and synthetic surface coatings on the toxicity of multiwalled carbon nanotubes toward green algae." Carbon **83**: 198-207.

Zhang, M., L. Shi, S. Yuan, Y. Zhao and J. Fang (2009). "Synthesis and photocatalytic properties of highly stable and neutral TiO2/SiO2 hydrosol." J Colloid Interface Sci **330**(1): 113-118.

Zhang, W., J. Shi, X. Wang, Z. Jiang, X. Song and Q. Ai (2014). "Conferring an adhesion layer with mineralization-inducing capabilities for preparing organic–inorganic hybrid microcapsules." Journal of Materials Chemistry B **2**(10).

Zhang, Y., Y. Chen, P. Westerhoff and J. Crittenden (2009). "Impact of natural organic matter and divalent cations on the stability of aqueous nanoparticles." Water Res **43**(17): 4249-4257.

Zhang, Y., T. Meng, L. Shi, X. Guo, X. Si, R. Yang and X. Quan (2018). "The effects of humic acid on the toxicity of graphene oxide to Scenedesmus obliquus and Daphnia magna." Sci Total Environ **649**: 163-171.

Zhao, J., X. Cao, Z. Wang, Y. Dai and B. Xing (2017). "Mechanistic understanding toward the toxicity of graphene-family materials to freshwater algae." Water Res **111**: 18-27.

Zhao, X. and K. Drlica (2014). "Reactive oxygen species and the bacterial response to lethal stress." Curr Opin Microbiol **21**: 1-6.

Zheng, J., C. Su, J. Zhou, L. Xu, Y. Qian and H. Chen (2017). "Effects and mechanisms of ultraviolet, chlorination, and ozone disinfection on antibiotic resistance genes in secondary effluents of municipal wastewater treatment plants." Chemical Engineering Journal **317**: 309-316.

Zhou, D. and A. A. Keller (2010). "Role of morphology in the aggregation kinetics of ZnO nanoparticles." Water Res **44**(9): 2948-2956.

Zhu, X., Y. Chang and Y. Chen (2010). "Toxicity and bioaccumulation of TiO2 nanoparticle aggregates in Daphnia magna." Chemosphere **78**(3): 209-215.